

3-30-2021

Pharmacological Blockade of the 20-HETE Receptor Lowers Blood Pressure and Alters Vascular Function in Mice with Vascular Smooth Muscle- Specific Overexpression of CYP4a12-20-HETE Synthase

Kevin Agostinucci

Follow this and additional works at: https://touro scholar.touro.edu/nymc_students_theses

 Part of the [Medicinal and Pharmaceutical Chemistry Commons](#)

Recommended Citation

Agostinucci, Kevin, "Pharmacological Blockade of the 20-HETE Receptor Lowers Blood Pressure and Alters Vascular Function in Mice with Vascular Smooth Muscle- Specific Overexpression of CYP4a12-20-HETE Synthase" (2021). *NYMC Student Theses and Dissertations*. 27. https://touro scholar.touro.edu/nymc_students_theses/27

This Doctoral Dissertation - Open Access is brought to you for free and open access by the Students at Touro Scholar. It has been accepted for inclusion in NYMC Student Theses and Dissertations by an authorized administrator of Touro Scholar. For more information, please contact touro.scholar@touro.edu.

**Pharmacological Blockade of the 20-HETE Receptor
Lowers Blood Pressure and Alters Vascular
Function in Mice with Vascular Smooth Muscle-
Specific Overexpression of CYP4a12-20-HETE
Synthase**

Kevin James Agostinucci

A Doctoral Dissertation in the Program in Pharmacology
Submitted to the Faculty of the
Graduate School of Basic Medical Sciences
in Partial Fulfillment of the Requirements
for the Degree of Doctor of Philosophy
at New York Medical College

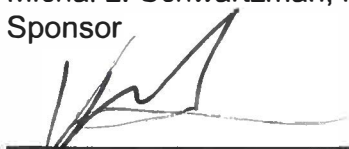
2021

Pharmacological Blockade of the 20-HETE Receptor Lowers Blood Pressure and Alters Vascular Function in Mice with Vascular Smooth Muscle-Specific Overexpression of CYP4a12-20-HETE Synthase

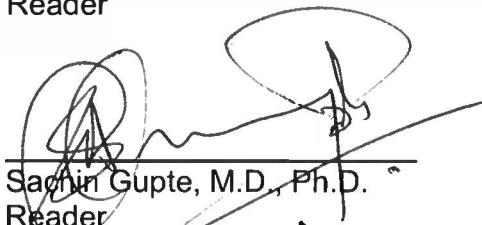
Kevin James Agostinucci

Michal Schwartzman

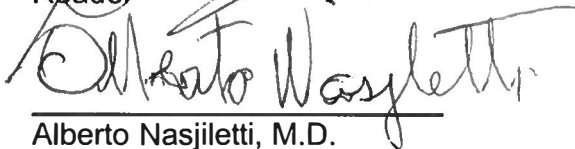
Michal L. Schwartzman, Ph.D.
Sponsor



Victor Garcia, Ph.D.
Reader



Sachin Gupte, M.D., Ph.D.
Reader



Alberto Nasjiletti, M.D.
Reader



Michael S. Wolin, Ph.D.
Reader

03/30/2021

Date of approval

Acknowledgements

The journey for the completion of my PhD at New York Medical College would not have been possible without the support of my colleagues, friends and family. First, I would like to thank Dr. Michal L. Schwartzman for the opportunity to complete my thesis under her mentorship. Dr. Schwartzman not only supported me throughout my time in her laboratory, but also challenged me, inspired me and facilitated me to be the best scientist I can be. I can't thank you enough for everything you have done for me. I would like to thank the members of my thesis committee: Drs. Victor Garcia, Sachin Gupte, Alberto Nasjiletti, and Michael Wolin. I appreciate all the guidance, input, and assistance with regards to the completion of my thesis. To the past and present members of Dr. Schwartzman's lab: Ankit Gilani, Sakib Hossain, Jonathan Pascale, Bibiana Iglesias, Elizabeth Villegas, Catherine D'addario, and Ghezal Froogh. Thank you for all the support you gave me throughout my time working in the lab. You all had valuable input that helped me complete some of my most difficult experiments. To all my friends I made during my time at NYMC: Juan Azcona, Roxanna Nahvi, Hannah Mulhall, Elizabeth Newman, Christina D'arco and Corey Gayletts. Thank you for all your support and encouragement. I will cherish all the moments we had together supporting each other in the lab and all the fun times we had at Captain Lawrence. To my parents, Karen and James and my sisters, Julie and Kristen, thank you for all your support throughout my academic career. You all have been there to give me the encouragement I need to help me push through the most difficult times. I love you all very much.

Table of Contents

Title page	i
Approval page	ii
Acknowledgements	iii
Table of contents	iv
List of figures	viii
List of Abbreviations	xi
Abstract.....	xii
Introduction and Background	1
Biosynthesis of 20-HETE	1
20-HETE effects on the vasculature	3
Actions on vascular endothelium	3
Actions on the vascular smooth muscle	5
Other actions of 20-HETE	8
The 20-HETE receptor, GPR75.....	9
20-HETE and hypertension.....	12

Hypothesis	16
Specific Aims	17
Materials and Methods	19
Animals	19
Blood Pressure Measurements	19
Wired Myography	20
Pressure Myography	21
Sodium Excretion Studies	22
Western Blot	23
Reverse Transcription Polymerase Chain Reaction	25
20-HETE Measurements.....	26
Statistics	27
Results	29
Aim 1: To determine if smooth muscle-specific overexpression of Cyp4a12- 20-HETE synthase causes hypertension and vascular dysfunction.....	29

<i>Myh11-Cre^(+/-)-Cyp4a12-Flox^(+/wt) (Myh11-4a12)</i> had significantly elevated Cyp4a12 levels in vessels that resulted in elevated 20-HETE	29
<i>Myh11-4a12</i> mice are hypertensive and have impaired vascular function	30
Markers of smooth muscle cell contraction and NO signaling were altered in <i>Myh11-4a12</i> mice.....	30
Aim 2: To determine if the vascular pathology in <i>Myh11-4a12</i> mice is 20-HETE-dependent.....	40
Administration of AAA decreased systolic blood pressure and improves vascular function in mice with smooth muscle specific <i>Cyp4a12</i> overexpression.	40
AAA administration improved media:lumen ratio but did not affect media thickness or cross-sectional area of RIA.	42
Markers of VSMC differentiation was elevated in <i>Myh11-4a12</i> mice	43
No differences in collagen synthesis was observed between <i>Myh11-4a12</i> and wild type mice.....	44
Aim 3: To explore cellular mechanisms underlying the increased contractility of arteries from mice with smooth muscle-specific overexpression of <i>Cyp4a12</i>	53

No changes were observed in ACE RNA expression between wild type and <i>Myh11-4a12</i> mice.....	53
<i>Myh11-4a12</i> mice had reductions in eNOS activation which was increased with AAA treatment.....	53
Administration of the 20-HETE receptor antagonist was able to reduce phosphorylation of myosin light chain.....	55
20-HETE was able to increase Rho-kinase activity which was attenuated with AAA.....	55
Discussion	65
Perspective and Significance	81
Reference:	82

List of Figures

Figure 1: <i>Myh11-4a12</i> mice display overexpression of Cyp4a12 in vessels.....	32
Figure 2: <i>Myh11-4a12</i> mice have elevated Cyp4a protein in vessels	33
Figure 3: <i>Myh11-4a12</i> mice display elevated 20-HETE.....	34
Figure 4: Mice with smooth muscle-specific overexpression of <i>Cyp4a12</i> are hypertensive.	35
Figure 5: Mice with smooth muscle-specific overexpression of <i>Cyp4a12</i> have impaired relaxation	36
Figure 6: Renal interlobar artery measurements of vascular remodeling are elevated in <i>Myh11-4a12</i> mice	37
Figure 7: Baseline expression of myosin light chain phosphorylation at serine 19 in mesenteric arteries were elevated in <i>Myh11-4a12</i> mice.....	38
Figure 8: Baseline expression of phosphorylated and total eNOS was reduced in aortas of <i>Myh11-4a12</i> mice.....	39
Figure 9: Administration of a 20-HETE receptor antagonist (AAA) was able to lower blood pressure after 12 days.....	45
Figure 10: Plasma 20-HETE levels were unchanged after 12-day AAA treatment	46
Figure 11: Urine volume and sodium excretion in WT and <i>Myh11-4a12</i> mice treated with and without AAA.....	47

Figure 12: Vascular activity was improved after 12 days of AAA treatment.....	48
Figure 13: <i>Myh11-4a12</i> mice had improved relaxation with AAA treatment ex <i>vivo</i>	49
Figure 14: <i>Myh11-4a12</i> mice have an elevated media:lumen ratio that was reduced with AAA treatment, however, AAA did not reduce the thickness of the vessel.....	50
Figure 15: Increases in markers of VSMC differentiation were observed in RIA of <i>Myh11-4a12</i> mice.....	51
Figure 16: No differences in collagen expression were observed between <i>Myh11- 4a12</i> and wild type mice.....	52
Figure 17: No differences in <i>ACE</i> expression were observed between <i>Myh11- 4a12</i> and wild type mice in mesenteric arteries.	58
Figure 18: Western blot analysis of eNOS and VASP phosphorylation in aorta.	59
Figure 19: Phosphorylation of eNOS at serine 1177 after 12 days of AAA treatment was reduced in mesenteric arteries of <i>Myh11-4a12</i> mice.....	60
Figure 20: <i>Myh11-4a12</i> mice have elevated phosphorylation of myosin light chain that was reduced with 12 day AAA treatment	61
Figure 21: ROCK1 protein expression was elevated in <i>Myh11-4a12</i> mice.....	62

Figure 22: Addition of AAA or Y-27632 prevented 20-HETE-mediated increase in myogenic tone of RIA from WT mice 63

Figure 23: Absolute internal diameter (ID) and percent myogenic tone values of WT RIA at 80mmHg and 100mmHg 64

List of Abbreviations

20-HETE	20-hydroxy-5,8,11,14-eicosatetraenoic acid
AAA	N-disodium succinate-20-hydroxyeicosa-6(Z),15(Z)-diencarboxamide
CYP	Cytochrome P450
VSMC	Vascular Smooth Muscle Cell
EC	Endothelial Cell
GPR75	G-protein couple receptor 75
SBP	Systolic blood pressure
NO	Nitric Oxide
SNP	Sodium Nitroprusside
ID/OD	Inner diameter/outer diameter
Myh11	Smooth muscle myosin heavy chain 11
eNOS	Endothelial specific nitric oxide synthase
MLC	Myosin light chain
Tagln	Transgelin/Sm22 α
Acta2	Smooth muscle actin 2
ROCK	Rho-kinase
ACE	Angiotensin converting enzyme
VASP	Vasodilator-stimulated phosphoprotein
RIA	Renal interlobar arteries
CSA	Cross-sectional area

Abstract

20-hydroxyeicosatetraenoic acid (20-HETE) is the ω -hydroxylation product of arachidonic acid catalyzed by CYP4A and 4F enzymes. 20-HETE is a vasoactive eicosanoid of the microcirculation exhibiting effects on both vascular smooth muscle cells (VSMC) and endothelial cells (EC). In VSMCs, 20-HETE's bioactions include the stimulation of contraction, migration, and growth. In ECs, elevated 20-HETE is associated with reduced nitric oxide (NO) bioavailability, increased angiotensin converting enzyme (ACE) expression, and the promotion of inflammation. Recently in our laboratory, we identified GPR75 as a novel target of 20-HETE that promotes changes in blood pressure and vascular function. The aim of this study is to assess the consequences of VSMC-targeted overexpression of *Cyp4a12*, the primary 20-HETE producing enzyme in mice, on blood pressure, vascular function, and vascular remodeling. Moreover, we looked to examine whether the administration of a 20-HETE receptor antagonist reverses the vascular phenotype associated with elevations in 20-HETE.

Mice with VSMC-specific overexpression of *Cyp4a12* (*Myh11-4a12*) and their littermate controls (WT) were generated by crossbreeding *Cyp4a12-flox* mice (gifted by Dr. Schunck) with *Myh11-Cre* mice. *Myh11-4a12* were administered AAA (10 mg.kg⁻¹.day⁻¹), a 20-HETE receptor antagonist, in the drinking water (vehicle). At the end of the experiments (12 days), renal interlobar arteries (RIA) and mesenteric arteries (MA) were harvested for the assessment of 20-HETE levels by LC-MS/MS, and vascular contractility, vasodilation, and remodeling using wire and pressure myography.

The *Myh11-4a12* mice showed higher Cyp4a levels in MA compared to WT mice (6.5 ± 0.71 vs 3.4 ± 0.70 ; Cyp4a/ β -actin $p < 0.05$). *Myh11-4a12* mice had increased 20-HETE levels in the MA (3334 ± 891 vs. 545 ± 197 pg/mg protein; $p < 0.05$) and RIA (1859 ± 376 vs 242 ± 62 pg/mg protein; $p < 0.05$), but, urine 20-HETE levels were not different (117 ± 9 vs. 93 ± 2 pg/mL; $p = 0.18$) when compared to WT. *Myh11-4a12* mice displayed higher SBP compared to WT mice (145 ± 2 vs. 127 ± 2 mmHg; $p < 0.05$). Administration of AAA for 12 days normalized BP in *Myh11-4a12* mice (124 ± 2 mmHg vs. 147 ± 4 mmHg, $p < 0.01$). RIA from vehicle treated *Myh11-4a12* mice displayed a higher media to lumen (M:L) ratio (0.277 ± 0.025 vs 0.163 ± 0.009 ; $p < 0.01$) and cross sectional area (CSA) (15114 ± 1871 vs 10560 ± 641 μm^2 ; $p < 0.01$) compared to WT mice on vehicle. Moreover, RIA from *Myh11-4a12* mice on AAA exhibit a lower M:L ratio compared to *Myh11-4a12* mice on vehicle (0.215 ± 0.013 , $p < 0.05$), but CSA was not different (14268 ± 1259 μm^2). Higher constrictor responsiveness to phenylephrine (EC_{50} : $1.63 \times 10^{-7} \pm 3.75 \times 10^{-8}$ vs $5.00 \times 10^{-7} \pm 0.7.85 \times 10^{-8}$ M, $p < 0.0001$) and an impaired relaxation response to acetylcholine (Maximum response at 10^{-4} M: 65 ± 1 vs 83 ± 2 % relaxation, $p < 0.001$) was observed in RIA from *Myh11-4a12* mice compared to WT. Treatment of *Myh11-4a12* mice with AAA diminished the constrictor responsiveness to phenylephrine (EC_{50} of $4.22 \times 10^{-7} \pm 4.55 \times 10^{-8}$ M, $p < 0.0001$) and improved the relaxation in response to acetylcholine (92 ± 2 % relaxation, $p < 0.001$). *Myh11-4a12* mice had elevated phosphorylation of myosin light chain compared to WT mice (1.60 ± 0.23 vs 1.00 ± 0.06 , Ser19 p-MLC/total MLC fold change, $p < 0.05$). *Myh11-4a12* mice on AAA

exhibited a decrease in myosin light chain phosphorylation compared to *Myh11-4a12* mice on vehicle (0.94 ± 0.11 , Ser19 p-MLC/total MLC fold change, $p < 0.05$). Upstream of myosin light chain is Rho kinase (ROCK). Expression of ROCK1 was assessed in RIA and *Myh11-4a12* mice had increased ROCK1 expression compared to WT mice (1.60 ± 0.21 vs 1.00 ± 0.18 , ROCK1/ β -tubulin fold change, $p < 0.05$) but AAA was unable to significantly reduce the expression (1.48 ± 0.20 , ROCK1/ β -tubulin fold change). Pressure myography was performed to assess 20-HETE receptor antagonism on ROCK activity. In RIA from WT mice, 20-HETE administration promoted a greater myogenic response and both AAA and ROCK inhibitor (Y-27632) inhibited the 20-HETE response in relation to the myogenic tone.

The results of this study suggest that VSMC specific overproduction of *Cyp4a12* and 20-HETE promotes increase in blood pressure and changes in vascular reactivity. 20-HETE receptor antagonism was capable of reversing the vascular pathology in mice with elevated 20-HETE presumably through inhibition of ROCK activity.

Introduction and Background

Biosynthesis 20-HETE

20-HETE is the ω -hydroxylation product of arachidonic acid catalyzed by cytochrome P450 enzymes (CYP4A/4F), with Cyp4a12 being the primary 20-HETE synthetase in mice. 20-HETE can be measured in tissue and in biological fluids. The vascular system is a primary site of 20-HETE production and it can be found in conduit arteries such as the aorta (Costa *et al.*, 2018; Soler *et al.*, 2018), and resistant arteries such as mesenteric arteries (Zhang *et al.*, 2001), renal microvessels (Croft *et al.*, 2000) and cerebral microvessels (Gebremedhin *et al.*, 1998, 2000). Within each vessel type, 20-HETE is generated in the vascular smooth muscle cells (VSMC) (Harder *et al.*, 1994; Gebremedhin *et al.*, 1998) and endothelial cells (EC) (Zhu *et al.*, 2002; Chen *et al.*, 2016; Joseph *et al.*, 2017). Circulating cells, such as endothelial progenitor cells, platelets, and myeloid cells, can also generate 20-HETE (Rosolowsky *et al.*, 1996; Christmas *et al.*, 2001; Wang *et al.*, 2006; Tsai *et al.*, 2011; Chen *et al.*, 2014). The kidney tubules is another site of 20-HETE production where it can be measured within the tissue and contribute to the amount present in the urine (Gilani *et al.*, 2020). Proximal tubules are the predominate sources of 20-HETE in the kidney tubules, with some production occurring in the thick ascending loop of henle (TALH), distal convoluted tubule and the collecting tubules (Carroll, M. A., Sala, A., Dunn, C.E., McGiff, J.C., 1991; Omata *et al.*, 1992). Heart, brain, lung and adipose tissue are more examples of tissues that can produce 20-HETE (Zhu *et al.*, 2002; Chuang *et al.*, 2004; Joseph *et al.*, 2017; Gilani *et al.*, 2018, 2021).

Several factors can play a role in either the increase or decrease production of 20-HETE. Androgens are well known for inducing *Cyp4a* expression and their administration has been established as a model for global overexpression of 20-HETE in mice and rats (Holla *et al.*, 2001; CC Wu *et al.*, 2013). PPAR γ agonists, such as Clofibrate, and parathyroid hormone can increase Cyp4 activity (Roman *et al.*, 1993; Ribeiro *et al.*, 1994; Silverstein *et al.*, 1998). Angiotensin II, norepinephrine and endothelin-1 all facilitate increase in 20-HETE by promoting increases in intracellular calcium which is necessary for cytosolic phospholipase A2 activity and arachidonic acid release from phospholipids (Muthalif *et al.*, 1996; Hercule and Oyekan, 2000; Parmentier *et al.*, 2001; Tsai *et al.*, 2011). Factors such as carbon monoxide or nitric oxide (NO) decrease 20-HETE production by binding to the heme moiety of Cyp4a enzyme to prevent its formation (Wang *et al.*, 2003; Kaide *et al.*, 2004).

Several cytochrome P450 enzymes have been shown to be involved in the production of 20-HETE across rodents and humans. In mice, Cyp4a10, Cyp4a12, and Cyp4a14 have some capacity to produce 20-HETE, with Cyp4a12 having the greatest capacity (Capdevila and Falck, 2000; Roman, 2002; Muller *et al.*, 2007). The 20-HETE-producing enzymes in rats include Cyp4a1, Cyp4a2 and Cyp4a3 (Nguyen *et al.*, 1999; Hardwick, 2008). The main 20-HETE-producing enzymes in humans are CYP4A11 and CYP4F2 (Powell *et al.*, 1998; Lasker *et al.*, 2000).

20-HETE effects on the vasculature

As indicated above, the vasculature is a significant source of 20-HETE production and a prime target of its actions. 20-HETE is a vasoactive lipid mediator affecting vascular tone and inflammation through actions on the vascular endothelium and the smooth muscle.

Actions on vascular endothelium

The vascular endothelium is a single layer of cells containing many factors that can diffuse to the smooth muscle to allow for changes in tension of vessels. 20-HETE overproduction has been shown to act in the endothelium to promote constriction. These actions include: 1) reduced NO bioavailability, 2) actions on renin-angiotensin-system, and 3) activation of endothelium inflammation processes.

NO is produced in the endothelium, by endothelial-specific nitric oxide synthase (eNOS), which is expelled to the VSMCs to exert its effect. 20-HETE can act on different parts of this signaling pathway to lower NO bioavailability. 20-HETE has a direct inhibitory effect on eNOS. Both *in vitro* and *in vivo*, 20-HETE has been shown to inhibit activation of eNOS by preventing phosphorylation at serine 1179 (Cheng *et al.*, 2008; Inoue *et al.*, 2009). Furthermore, 20-HETE has been shown to cause eNOS uncoupling with HSP90 via NF- κ B-IKK signaling pathway (Cheng *et al.*, 2010). 20-HETE also has indirect mechanisms which lower the bioavailability of NO. 20-HETE has been shown to increase superoxide production through NADPH oxidase-dependent and -independent mechanisms

(Guo *et al.*, 2007; Medhora *et al.*, 2008). The increase in superoxide shunts NO to produce peroxynitrite which prevents it from migrating to the VSMCs to cause dilation (Medhora *et al.*, 2008).

20-HETE has been shown to increase the expression and activity of angiotensin converting enzyme (ACE). Induction of 20-HETE production *in vivo* and *in vitro* has been shown to increase endothelial ACE expression via NF- κ B-IKK pathway (Cheng *et al.*, 2012; Garcia *et al.*, 2016). Increases in ACE expression were accompanied by increases in angiotensin II levels which can act on its own receptor to cause changes in vessel function (Sodhi *et al.*, 2010).

Vascular inflammation is another effect of 20-HETE in the endothelium. Reports have shown that 20-HETE can increase inflammatory markers such as IL-6 and IL-8 and adhesion molecules such as ICAM (Guo *et al.*, 2007; Ishizuka *et al.*, 2008). 20-HETE has been shown to increase NF- κ B and MAPK, which facilitate the production of inflammatory markers (Guo *et al.*, 2007; Ishizuka *et al.*, 2008). The inflammatory state of the vessels can be reversed with administration of 20-HETE synthase inhibitor.

Angiogenesis is the process of making new blood vessels from preexisting vessels. This process requires the coordinated action of the endothelium to branch out from the vessel, migrate away from the branch point and form a tube structure. 20-HETE *in vitro* has been shown to increase EC proliferation as a result of both increases in VEGF and HIF-1 α (Guo *et al.*, 2007, 2009). These actions relied on an increased oxidative environment which resulted in the activation of the NF- κ B pathway. Furthermore, 20-HETE *in vivo* has been shown

to upregulate angiogenesis by promoting endothelial progenitor cell homing and adhesion to the EC (Chen *et al.*, 2014, 2016).

Actions on vascular smooth muscle

The VSMC is the contractile unit within the vasculature. It is located in the tunica media adjacent to ECs. Contraction caused by VSMCs play a role in maintaining blood flow to tissues. 20-HETE has been documented to change the VSMC phenotype by either: 1) increased sensitivity to contractile stimuli and 2) increased vessel wall thickness. These changes in VSMC physiology ultimately reduces blood flow, reduce compliance and increases in blood pressure.

VSMCs are responsible for causing contraction to redirect blood flow to tissue with higher metabolic demand. It is important for VSMC to be sensitive to specific stimuli that can promote changes in lumen diameter so tissues can receive a consistent blood flow. Autoregulation is an intrinsic property of a vessel where blood flow is maintained despite changes in pressure in the system. Autoregulation relies on the ability of the vessel to contract when it senses increase transluminal pressure, defined as the myogenic response (Davis *et al.*, 1992). 20-HETE has been documented, in cerebral and renal circulation, to promote contraction which shift the autoregulation curve to the right so vessels maintain a constant flow at higher pressures (Zou *et al.*, 1994; Gebremedhin *et al.*, 2000). Inhibition of 20-HETE synthesis has been shown to cause dilation and prevent the vessel's autoregulatory ability.

20-HETE has been shown to promote contraction in VSMCs by 1) increasing intracellular calcium and 2) activating Rho kinase. Calcium signaling is important because it is the initial step to cause VSMCs contraction. Calcium enters the VSMC through the L-type calcium channel which increase intracellular calcium levels. The increase in intracellular calcium activates calmodulin which then activates myosin light chain kinase (Tansey *et al.*, 1994; Raina *et al.*, 2009). Myosin light chain kinase phosphorylates the myosin light chain which is the necessary signal in order to initiate excitation-contraction in the VSMCs (Driska *et al.*, 1981). The mechanisms by which 20-HETE affects intracellular calcium levels are through inhibition of the large-conductance Ca^{2+} -activated K^{+} -channel ($\text{BK}_{\text{Ca}^{2+}}$) (Zou *et al.*, 1996; Lauterbach *et al.*, 2002; Fan *et al.*, 2013; Toth *et al.*, 2013) and activation of L-type calcium channels (Gebremedhin *et al.*, 1998).

Mechanisms exist within the VSMC to terminate signaling for contraction. Myosin light chain phosphatase is the protein within the VSMC that can remove the phosphate group off of myosin light chain and inhibit contraction (Wang *et al.*, 2009). The activity of myosin phosphatase is regulated by Rho-kinase (ROCK). The activation of ROCK is initiated by GPCR-mediated mechanisms to activate Rho-GTP which removes the inhibitory subunit on ROCK (Swärd *et al.*, 2003). 20-HETE has been reported to increase the activity of ROCK and increase myosin light chain phosphorylation (Randriamboavonjy *et al.*, 2003). The inhibition of mechanisms to remove phosphate from myosin light chain sensitizes VSMCs to other constrictor stimuli.

The vascular wall is dynamic in that it can respond to external cues to change its architecture. In the normal state, the vessel is quiescent, but in the presence of certain stimuli, the vessel can undergo processes which allow it to thicken to compensate for the elevated pressure (Li *et al.*, 1994; Garcia, *et al.*, (2015b)). The consequences of remodeling in the vessels include decreases in compliance, reduced blood flow and ultimately even further increase in blood pressure. 20-HETE promotes changes in vascular wall remodeling without contribution to sympathetic nerve activation (Ding *et al.*, 2013), as well as increase in ACE (Garcia, *et al.*, (2015b)). Thus, 20-HETE displays its own signaling mechanism to promote thickening of the vascular wall. There are several signaling mechanisms which contribute to the mitogenic effect of 20-HETE. First, 20-HETE causes VSMC migration by activation of the MAP-kinase and PI3K/Akt signaling pathways (D Stec *et al.*, 2007). Proliferation is also increased with 20-HETE. *In vitro* experiments with norepinephrine stimulation suggests that 20-HETE promotes proliferation via MAP-kinase signaling (Uddin *et al.*, 1998; Kalyankrishna and Malik, 2003). 20-HETE has also been shown to cause proliferation *in vivo*. In an experiment by Orozco and colleagues (2013), they used a balloon injury model to promote carotid artery thickening which was prevented by administration of Cyp4a inhibitors (Orozco *et al.*, 2013).

Another contributor to the changes in vascular wall remodeling is through changes in the architecture of the extracellular matrix (ECM). The ECM is comprised of structural proteins that give the vessels its ability to withstand changes in wall tension. The actions of 20-HETE within the ECM includes

increased collagen IV deposition (Ding *et al.*, 2013) and elastin degradation (Soler *et al.*, 2018). 20-HETE can increase reactive oxygen species in VSMCs (Lakhkar *et al.*, 2016) which can act as a second messenger for the increased production of MMP12 that degrades elastin in conduit arteries (Soler *et al.*, 2018). These actions contribute to the reduction in compliances that result in elevated blood pressure.

Other actions of 20-HETE

The actions of 20-HETE are not limited to maintenance of vascular tone within the central circulation. 20-HETE has numerous actions within structures of the kidney that result in changes in plasma osmolality. In renal preglomerular vessels, 20-HETE has been shown to sensitize vessels to phenylephrine-induced constriction and impaired relaxation after acetylcholine administration (CC Wu *et al.*, 2013). Impairment in preglomerular microvessel activity resulted in reductions in glomerular filtration rate (Pandey *et al.*, 2017) and an increase in proteinuria (Inoue *et al.*, 2009). These changes resulted in an elevation in plasma osmolality and, ultimately, increases in blood volume. 20-HETE is produced and has actions within the kidney tubules (Omata *et al.*, 1992; Lin *et al.*, 1995). 20-HETE has been shown to act on different transporters in the nephron and, depending on the transporter, has a different effect on salt excretion. 20-HETE pro-natriuretic effect includes inhibition of Na⁺-K⁺-ATPase (Schwartzman *et al.*, 1985; Nowicki *et al.*, 1997) in the proximal tubule and sodium-potassium-chloride cotransporter (NKCC2) in the thick ascending limb (Amlal *et al.*, 1996, 1998). Furthermore, 20-

HETE also can increase the activity of the sodium chloride transporter resulting in an anti-natriuretic effect (Savas *et al.*, 2016; Gilani *et al.*, 2020).

20-HETE also has actions to promote increases in body weight gain and changes in insulin signaling. In human subjects, correlations have been shown between elevated 20-HETE in the urine and increased BMI. Mouse models of *Cyp4a12* overexpression have also shown that elevated 20-HETE promotes increases in body weight and insulin resistance when on a high-fat diet (Gilani *et al.*, 2018, 2021). These actions of global expression of *Cyp4a12* were reversed when mice were administered 20-SOLA (a 20-HETE antagonist) (Gilani *et al.*, 2018, 2021). The consequence of 20-HETE overproduction after a high-fat diet shows changes in insulin signaling and hyperglycemia. One report shows that overexpression of CYP4F2 promotes hyperglycemia on a normal diet (Lai *et al.*, 2012). Hyperglycemia can be contributed to changes in insulin signaling. Reports have shown that 20-HETE can affect activation of the insulin receptor and/or the ability of IRS-1 to dock on the insulin receptor (Li *et al.*, 2014; Gilani *et al.*, 2018, 2021). One report shows that 20-HETE can inhibit glucose-mediated insulin secretion through the FFAR1 receptor (Tunaru *et al.*, 2018).

The 20-HETE receptor, GPR75

The cellular mechanisms underlying the bioactions of 20-HETE have been extensively studied; however, what remains to be elucidated is the up-stream factors that result in the initiation of 20-HETE's signaling cascade. The first report to demonstrate 20-HETE's proximal signaling was published by Garcia and

colleagues (2017). They were the first to show that 20-HETE binds to a cell surface receptor, namely GPR75, and to report the proximal signaling mechanism through which 20-HETE causes hypertension and vascular dysfunction (Garcia *et al.*, 2017).

GPR75 is a 7-transmembrane G-protein coupled receptor (GPCR) that is classified as an orphan receptor (Garcia *et al.*, 2017). The gene for this receptor was identified on the 2p16 chromosome and translation of this gene results in a 540 amino acid GPCR with a molecular weight of 59 kDa (Tarttelin *et al.*, 1999). A unique feature of this receptor is its c-terminal tail that is 169 amino acids in length, which is longer than most GPCRs (Pease, 2006). The extended tail allows for docking of proteins to initiate complex signaling cascades. In several different cell models, GPR75 has been shown to complex with G_q, hic-5, c-Src and GIT-1 (Ignatov *et al.*, 2006; Garcia *et al.*, 2017).

The expression of GPR75 can be found in the retinal pigmented epithelium, brain and heart (Tarttelin *et al.*, 1999; Dedoni *et al.*, 2018; Gonzalez-Fernandez *et al.*, 2020). GPR75 expression is also detected in the vascular endothelium and smooth muscle (Garcia *et al.*, 2017; Gonzalez-Fernandez *et al.*, 2020), pancreatic islets (Liu *et al.*, 2013) and prostatic cancer cells (Cárdenas *et al.*, 2020). Within these cell types, it has been shown that activation of GPR75, mediated by G_q, increases intracellular calcium which then activates downstream signaling including phospho-ERK1/2 (Ignatov *et al.*, 2006; Garcia *et al.*, 2017; Dedoni *et al.*, 2018; Cárdenas *et al.*, 2020). Garcia *et al.* (2017), demonstrated that in VSMCs 20-HETE-GPR75 pairing results in a PKC- and c-Src-mediated

phosphorylation of BK_{Ca}²⁺ channels leading to their inactivation (Garcia *et al.*, 2017).

The effects of 20-HETE on the cardiovascular system through its binding to GPR75 is a new area of research. There is evidence that individuals with a permutation of the 2p chromosome (the site of GPR75 gene) are more likely to be non-responders to current hypertensive therapies (Padmanabhan *et al.*, 2006). Thus, exploring the effects of GPR75 on blood pressure can be useful. Garcia *et al.* (2017) showed that mice with overexpression of *Cyp4a12* were hypertensive and knocking down GPR75 with shRNA normalized blood pressure (Garcia *et al.*, 2017). Furthermore, pharmacological antagonism of the 20-HETE-GPR75 pairing has been shown to blunt 20-HETE-dependent actions in the cardiovascular system as well as in disease models (Pandey *et al.*, 2017; Gilani *et al.*, 2018, 2021; Soler *et al.*, 2018). In a report by Sedláková *et al.* (2018), they generated a rat model with elevated 20-HETE and angiotensin II that dramatically increased the blood pressure. They administered AAA (a novel 20-HETE receptor antagonist) which was able to lower the blood pressure of these rats (Sedláková *et al.*, 2018). In another report, AAA was shown to blunt the effects of 20-HETE on the metastatic features in a prostate cancer cell line (Cárdenas *et al.*, 2020). Thus, pharmacological antagonism may be a therapeutic strategy for the treatment of 20-HETE-related diseases.

20-HETE and hypertension

The link between 20-HETE and hypertension has been well established across numerous animal models. The use of animal models has been vital in understanding the actions of 20-HETE *in vivo*. Animal models have shown the consequences of elevated 20-HETE levels on vascular and renal function. Some examples of animal models include: 1) *Cyp4a12*-tg, 2) DHT-pellet-treated mice, 3) *Cyp4a14*^{-/-}, 4) spontaneously hypertensive rats, and 5) Dahl salt-sensitive hypertensive rats.

The *Cyp4a12*-tg mouse has elevated 20-HETE production in the presence of doxycycline (CC Wu *et al.*, 2013). This mouse was engineered to have *Cyp4a12* expression controlled by the tetracycline inducible promoter. This is advantageous in experiments where control of 20-HETE production is necessary. Administration of doxycycline (DOX) in these mice resulted in changes in blood pressure and vascular reactivity that are dependent on 20-HETE (CC Wu *et al.*, 2013; Ding *et al.*, 2013; Gilani *et al.*, 2021).

Androgens are a known inducer of *Cyp4a* expression and 20-HETE. Two animal models of androgen-inducible 20-HETE include the DHT-pellet-treated mouse and the *Cyp4a14*^{-/-} mouse. DHT-pellets are implanted subcutaneously in the mouse which allows for global overproduction of *Cyp4a12* and 20-HETE that can be observed in male and female mice (Singh *et al.*, 2007; CC Wu *et al.*, 2013; Garcia *et al.*, (2015a)). The *Cyp4a14*^{-/-} mouse also resulted in increased *Cyp4a12* and 20-HETE. The deletion of the *Cyp4a14* gene promotes androgen-driven *Cyp4a12* expression that is only observable in male mice (CC Wu *et al.*,

2013; Ding *et al.*, 2013; Pandey *et al.*, 2017). Both these experimental models are associated with elevation in blood pressure, altered vascular function and kidney function.

The Tie2-CYP4F2-Tr mouse is a genetically engineered mouse that displays overexpression of the human *CYP4F2* gene specifically in EC (Cheng *et al.*, 2014). These mice have elevated 20-HETE in EC of tissues including kidney, lung, liver, heart and aorta. The Tie2-CYP4F2-Tr displayed changes in the angiogenic phenotype but do not have any differences in blood pressure compared to wild type mice (Cheng *et al.*, 2014).

The spontaneously hypertensive rat (SHR) is documented to have elevated *Cyp4a1*, *Cyp4a2*, and *Cyp4a3* levels which all contribute to the elevation of 20-HETE (Sacerdoti *et al.*, 1989; Roman, 2002; Dunn *et al.*, 2008). This rat model has been documented to have increases in blood pressure, vascular reactivity and changes in cerebral and renal blood flow (Zhang *et al.*, 2001; Dunn *et al.*, 2008). The changes in cerebral circulation were associated with cerebral infarcts (Dunn *et al.*, 2008).

The Dahl salt-sensitive hypertensive rat is an example of an animal model where lower 20-HETE levels result in elevated blood pressure. In the medullary area of the kidney, *Cyp4a* expression was reduced (Stec *et al.*, 1996). Reductions in *Cyp4a* and 20-HETE were associated with changes in transmural voltage due to uninhibited activity of the NKCC2 cotransporter (Roman and Kaldunski, 1991; Ito and Roman, 1999). This increased salt and fluid

reabsorption which contribute to the elevation in blood pressure (J Wu *et al.*, 2013).

Hypertension is defined as the chronic elevation of blood pressure, >130/80mmhg (CDC, 2020). In the United States, nearly half of adults fit into this definition with men, African Americans and/or Hispanics having a greater risk of developing hypertension (CDC, 2020). Individuals with elevated blood pressure are at a greater risk of coronary heart disease, stroke, and renal failure (Gosmanova *et al.*, 2016). Current therapies, such as ACE inhibitions, diuretics, beta-blockers, and calcium channel blockers target their respective signaling mechanism to reduce blood pressure. However, approximately one-third of the population do not see a successful outcome from using hypertensive medications (Cushman *et al.*, 2002). Thus, new therapies are in need to improve the clinical outcome within these patients.

CYPs are well known to have genetic variations that are correlated with increasing blood pressure in humans (Rocic and Schwartzman, 2018). Genetic polymorphisms have been shown to change the catalytic activity of these enzymes. For example, the T8590C SNP for CYP4A11 and the V433M in CYP4F2 have been shown to be associated with hypertension (DE Stec *et al.*, 2007; Laffer *et al.*, 2008; Ward *et al.*, 2008; Huang *et al.*, 2020). Changes in catalytic activity of these enzymes may affect 20-HETE levels which drives the changes in blood pressure. 20-HETE has been shown to correlate with certain factors in hypertensive patients. 20-HETE has been shown to positively correlate

with blood pressure in patients with salt-sensitive hypertension (Laffer *et al.*, 2003), and negatively correlate with flow-dependent dilation (Ward *et al.*, 2004).

The effects of 20-HETE on blood pressure and sodium handling are complex. On one hand, it inhibits ion transport along the nephron leading to natriuresis thus contributing to anti-hypertensive mechanisms. For example, Dahl salt-sensitive hypertensive rats are known to have decreased Cyp4a expression and 20-HETE production which is associated with higher blood pressure (Stec *et al.*, 1996). 20-HETE in the kidney tubule has been shown to inhibit the NKCC2 co-transporter, which is occurring at a lower frequency in the Dahl salt-sensitive rat (Escalante *et al.*, 1991, 1994; Ito and Roman, 1999). On the other hand, global overexpression models of 20-HETE, including 5-dihydrotestosterone treated mice (Ding *et al.*, 2013), *Cyp4a12* transgenic mice (Garcia, *et al.*, (2015b)), and the *Cyp4a14*^{-/-}-knock out mouse (Holla *et al.*, 2001; CC Wu *et al.*, 2013) all have been shown to promote vasoconstriction and increases in peripheral vascular resistance and blood pressure due to systemic elevations of 20-HETE.

The proposed studies are aimed at identifying the cellular mechanism (GPR75-mediated) by which 20-HETE affects VSMC contractility and determining the role of VSMC-derived 20-HETE in the control of blood pressure. The influence of 20-HETE in the regulation of blood pressure makes it an attractive target for therapeutic intervention. The discovery of GPR75 as the 20-HETE receptor provides a specific therapeutic site to target 20-HETE bioactions.

Hypothesis

Smooth muscle-specific overexpression of Cyp4a12-20-HETE-synthase results in hypertension and impaired vascular function that is 20-HETE-dependent

Specific Aims

Aim 1: To determine if smooth muscle-specific overexpression of Cyp4a12-20-HETE synthase (*Myh11-4a12*) causes hypertension and vascular dysfunction

- a) Establish transgenic mice with smooth muscle-specific overexpression of the Cyp4a12-20-HETE synthase (*Myh11-4a12*).
- b) Characterize the phenotype of the *Myh11-4a12* with respect to blood pressure and vascular function including contractility, vasodilatory response and remodeling.

Aim 2: To determine if the hypertension and vascular pathology in *Myh11-4a12* mice are 20-HETE-dependent

- a) Use a 20-HETE receptor antagonist to determine whether the hypertensive and vascular phenotype of the *Myh11-4a12* mice are 20-HETE dependent

Aim 3: To explore cellular mechanisms underlying the changes in vessel reactivity of arteries from mice with smooth muscle-specific overexpression of Cyp4a12

- a) Assess expression of known 20-HETE targets (e.g., eNOS, ACE, Rho-kinase, MLC) in vascular beds including renal microvessels and mesenteric arteries by qRT-PCR and Western blot.

- b) Examine whether activation of the Rho-kinase underlies the contractile phenotype of arteries from *Myh11-4a12* mice using pressure myography, 20-HETE receptor antagonists and a Rho-kinase inhibitor.

Materials and Methods

Animals: Mice with VSMC-specific overexpression of *Cyp4a12* were generated by crossing mice with cre-recombinase expression driven by the VSMC-specific myosin heavy chain promoter (*Myh11-Cre^{+/-}*) and *Cyp4a12*-floxed mice (*Cyp4a12-flox^{+/+}*). *Cyp4a12-flox^{+/+}* mice contain loxP sites flanking a regulatory region of the *Cyp4a12* promoter. In the presence of cre-recombinase, the regulatory region is removed and unregulated *Cyp4a12* production can occur. Pups generated were divided into wild type (WT: *Myh11-Cre^{-/-}-Cyp4a12-flox^{+/wt}*) or positive mice (*Myh11-Cre^{+/-}-Cyp4a12-flox^{+/wt}*). All mice were housed in static cages and fed standard chow. Experiments were conducted on mice between the ages of 2-4 months. A novel water-soluble 20-HETE receptor antagonist, N-disodium succinate-20-hydroxyeicosa-6(Z),15(Z)-dienoic acid (AAA), was used to assess the relevance of 20-HETE in the phenotype of these mice. Mice were divided into three groups: 1) Wild-type – vehicle; 2) *Myh11-Cre^{+/-}-Cyp4a12-flox^{+/wt}* – vehicle; and 3) *Myh11-Cre^{+/-}-Cyp4a12-flox^{+/wt}* – AAA treatment. Baseline SBP was measured before administration of AAA. Mice were administered either vehicle (tap water) or AAA at a dose of 10mg.kg⁻¹.day⁻¹ in drinking water. Systolic blood pressure was measured on days 0, 4, 8, and 12. After the last blood pressure measurement, mice were sacrificed and tissues were collected for physiological and biochemical analysis.

Blood Pressure Measurements: Systolic blood pressure (SBP) was measured using CODA non-invasive tail-cuff method (Kent Scientific, Torrington, CT). The

CODA tail-cuff system utilizes volume-pressure recording (VPR) technology to measure the expansion of the mouse's tail due to the return of blood flow after occlusion. All cuffs and bladders were checked for patency before measurements were taken. A warming plate was set to 32-35° Celsius to maintain body temperature during the measurement. The CODA software was set to have a deflation time of 20 seconds and allowed measurements of $\geq 15\mu\text{L}$. Mice underwent 30 inflation-deflation cycles. The first 5 cycles were dedicated for acclimation and was not used in blood pressure determination. The last 25 cycles were used for blood pressure measurements. All cycles were carefully examined and cycles were removed if artifacts were identified in the measurement. All mice were allowed 5-7 days to undergo the tail-cuff procedure without collecting data. Baseline measurements per mouse were obtained by taking the average SBP on three separate days. Blood pressure measurements on AAA were measured on days 0, 4, 8, and 12. The CODA system is able to measure SBP within $\pm 10\%$ of actual value.

Wired Myography: Phenylephrine-induced contraction, as well as acetylcholine and SNP induced relaxation were performed on renal interlobar arteries (RIA). Kidneys were taken out of mice and were carefully dissected in a dish containing Krebs's buffer. Isolated vessels were mounted onto wires in a chamber of a multivessel myograph. Before conducting experiments, vessels were allowed to sit in a bath containing Krebs's buffer, maintained at 37°C, and constantly being bubbled with 95/5% O₂/CO₂ for 30-60 minutes. All vessels were set to an internal

circumference that is 90% of what the circumference would be at 100mmHg. Isometric tension was measured throughout the experiment. Cumulative phenylephrine dose-response experiments were performed. Phenylephrine was administered at half-dose intervals from (10^{-9} - 10^{-4} M) directly into the tissue bath. Tension was represented as a percentage of the maximal response at 10^{-4} M phenylephrine. Percent maximal response % = [(tension at a dose Phe/(tension 10^{-4} M Phe - baseline tension))*100]. Acetylcholine or sodium nitroprusside (SNP) relaxation experiments were also performed. Before acetylcholine or SNP administration, precontraction was achieved by administering phenylephrine (10^{-6} M) to the vessel bath. Acetylcholine (10^{-8} - 10^{-4} M) or SNP (10^{-9} - 10^{-5} M) was administered in a cumulative dose-dependent fashion after phenylephrine induced precontraction. The percent relaxation was calculated by subtracting the tension after a dose of acetylcholine or SNP from the tension generated from 10^{-6} M phenylephrine, divided by the difference between the baseline tension and 10^{-6} M phenylephrine. Percent relaxation % = [(tension at a dose of Ach or SNP [M] - tension at [10^{-6} M] Phe)/ (tension at [10^{-6} M] Phe - baseline tension)*100].

Pressure Myography: Renal interlobar arteries were dissected in the same manner as for wired myography experiments. Living Systems Instrumentations (St. Albans City, VT) pressure myograph was used to induce pressures within the lumen of the vessel. The distances of the inner and outer diameters were measured using video edge detection. One end of the renal interlobar artery was mounted onto a glass canula and the other side was ligated closed. The vessel

was allowed to equilibrate for one hour at 37°C in Kreb's buffer bubbled with 95/5% O₂/CO₂. For measurements of vascular wall thickness, internal pressures of 100mmHg were induced on normotensive vessels and 140mmHg on hypertensive vessels. Measurements of outer diameter (OD) and inner diameter (ID) under passive conditions were used to calculate media thickness $[(OD - ID)/2]$, media:lumen ratio $[(OD - ID)/ID]$, and medial cross-sectional area $[CSA (\pi/4) \times (OD^2 - ID^2)]$. For measurements of myogenic response, only WT vessels were used. Each vessel underwent 5 consecutive treatments in the following order: 1) vehicle only (100% ethanol), 2) 20-HETE (10 μM), 3) 20-HETE + AAA (10 μM), 4) 20-HETE + Rho-kinase inhibitor (Y-27632, 10 μM), and 5) 20-HETE + AAA + Rho-kinase inhibitor. Passive stretch of vessels was also assessed immediately after the treatments by measuring the internal diameter of the vessel in a calcium-free Kreb's solution. Vessels were subjected to pressures of 0, 20, 40, 60, 80 and 100 mmHg and ID was measured at each pressure. The Absolute and normalized ID were determined after experiments were concluded. The normalized ID was represented as a percentage and calculated as follows:
normalized ID = (absolute ID/passive ID)*100.

Sodium Excretion Studies: On the last day of AAA treatment, mice were individually housed in metabolic cages to collect urine (Hatteras instruments). Twenty-four-hour urine collection was taken and urine samples were stored at -80°C until time to measure urinary sodium. Water consumption and urine volume

were measured to assess fluid balance. Urinary sodium measurements were performed using flame photometry.

Western blots: Mesenteric arteries were taken out and carefully dissected in ice-cold MOPS buffer to remove fat tissue. Vessels were flash-frozen in liquid nitrogen and stored at -80°C. Tissues were lysed by crushing vessels in liquid nitrogen followed by homogenization in RIPA buffer containing protease and phosphatase inhibitor. Lysates were allowed to sit on ice for 15 minutes before centrifugation. Lysates were spun at 10,000 RPM for 15 minutes at 4°C and supernatant was collected for western blot experiments. Protein estimation was performed using BCA assay. Equal amounts of protein were loaded onto a 10%-polyacrylamide gel and ran at 125V. Proteins were transferred onto a PVDF membrane using methanol-glycine-tris-base transfer buffer. After transfer, membranes were blocked in TBS buffer containing 1% bovine serum albumin for 1 hour. Cyp4a (1:1000 – Santa Cruz – cat#: sc-271983), Myh11 (1:1000 – Abcam – cat#: ab125884), ROCK1 (1:1000 – Sigma – cat#: HPA007567), Serine 1177 p-eNOS (1:100 – cell signaling technology – cat#: 9571S), total eNOS (1:100 - BD bioscience – cat#: 610297), β -Tubulin (1:2000 - Invitrogen - cat#: MA5-16308) and β -actin (1:5000 - Cell Signaling Technology – cat#: 4967) were diluted in 1% casein/TBST solution and membranes were submerged in the antibody solution overnight on a shaker at 4°C. Secondary antibodies (Li-Cor biotechnology) were diluted (1:15,000) in 1% casein/TBST solution and membranes were allowed to incubate for 2 hours at room temperature on a

shaker. Membranes were visualized on the Li-Cor Odyssey Clx membrane scanner and quantified using ImageStudio software version 5.2.5. All western blots were represented as a fold change compared to wild type. To calculate this, first the ratio between the protein of interest and the loading control (β -actin or β -tubulin) was determined. The ratio for the WT was then average. Lastly, WT and experimental samples were all divided by the average WT ratio to determine the fold change.

For phospho-myosin light chain western blotting, vessels were dissected then placed in 5% trichloroacetic acid/acetone solution and immediately placed in a -80°C freezer until time to homogenize tissue. On the day of tissue homogenization, vessels were taken out of the freezer and allowed to thaw at room temperature for 30 minutes. After 30 minutes, vessels were moved into a 100% acetone solution and sat at room temperature for 30 minutes. Vessels were taken out and weighed so that an approximately equal mass of vessel could be used. Vessels were homogenized in 50 μ L of solution containing: 8M urea, 20mM tris-base, 22mM glycine, 10mM DTT, 5mM EGTA, 5mM Na₂EDTA. Samples were spun at 10,000 RPM for 15 minutes at room temperature. The supernatant was collected and an equal volume was mixed with Lamelli sample buffer and loaded onto a 12% PAGE gel. The gel ran at 125V for two hours. The gel was transferred overnight onto a PVDF membrane in buffer containing: 25mM Tris-base, 192mM glycine, and 20% methanol. The next day, membranes were taken out and blocked in 1% BSA in TBS. Phospho-myosin light chain (cell signaling technology - cat#: 3674S) was diluted in 1% casein/TBST solution

(1:250) and incubated overnight at 4°C. The next day, membranes were incubated in Li-Cor secondary antibody (1:15,000) in 1% casein/TBST buffer for 2 hours. Membranes were visualized on the Li-Cor Odyssey Clx membrane scanner and quantified using ImageStudio software version 5.2.5. Immediately after membrane visualization, membranes were stripped using Li-Cor NewBlot IR stripping buffer according to manufacturer's protocol. Membranes were blocked with 1% BSA/TBS blocking buffer for 1 hour followed by incubation with myosin light chain antibody (1:250 - cell signaling technology - cat#: 3672S) in 1% casein/TBST solution. Secondary antibody incubation and quantification was performed the same as for phospho-myosin light chain. The values were represented as a fold change using the same calculations as described above.

Reverse Transcription Polymerase Chain Reaction: Mesenteric arteries and RIA were dissected and flash frozen in liquid nitrogen and stored at -80°C. Messenger RNA was obtained using the miRNeasy micro kit (Qiagen – cat: 217084). Equal amounts of RNA were used to generate cDNA using the Quantitech cDNA synthesis kit (Qiagen). Taqman primer/probes for *Cyp4a12* (Mm00514494_m1), *Myh11* (Mm00443013_m1), *Tagln* (Mm00441661_g1), *Acta2* (Mm00725412_s1); *Col4a4* (Mm00801574_m1); *Col1a1* (Mm00801666_g1), *Ace* (Mm00802048_m1), and *Tuba1a* (Mm00846967_g1) were purchased from ThermoFisher. For all reactions, 2 µl cDNA was mixed in 18 µl of master mix containing: 1 µl of 20X primer/probe, 10 µl 2X Taqman advance fast master mix and 7 µl nuclease free water. The thermal profile for

qPCR reaction was: 50°C for 2 minutes, 95°C for 20 seconds and 40 cycles of 95°C for 3 seconds and 60°C for 30 seconds. Relative expression was calculated using the $2^{(-\Delta\Delta Ct)}$ method. Ct values were determined using the QuantStudio 3 RT-PCR machine for all genes of interest. The change in Ct (ΔCt) values were determined by taking the difference between the experimental gene from the housekeeper gene (*Tuba1a*). After the determination of the ΔCt , the $\Delta\Delta Ct$ value was calculated. To do this, the WT ΔCt was averaged. The difference between the ΔCt values for each mouse and the average ΔCt values was determined. Lastly, 2 was raised to the $(-\Delta\Delta Ct)$ to determine the relative expression of the gene of interest.

20-HETE Measurements: 20-HETE was quantified by LC-MS/MS-based lipidomics. Blood was withdrawn at the end of the experiment by aspiration from the inferior vena cava. Briefly, animals were anesthetized with isoflurane, and their abdomens were swabbed with 70% alcohol and opened by a midline longitudinal incision. Next, the caudal (inferior) vena cava was identified and punctured, and blood was drawn into a heparinized syringe. Blood was centrifuged at 2,000 rpm for 15 min to separate the plasma. Plasma samples were subjected to chloroform-methanol extraction and alkali hydrolysis for assessment of free and esterified 20-HETE. Renal preglomerular arteries and mesenteric arteries were microdissected and incubated in Krebs's bicarbonate buffer, pH 7, 1 mM NADPH at 37°C for 1 h. Tissue incubations were terminated with 2 volumes of cold methanol, internal standards were added, and samples

were kept at -80°C. Urine was mixed with two parts of methanol before LC-MS/MS. Eicosanoids were extracted with solid-phase Strata-X Polymeric Reversed Phase 60-mg cartridges (Phenomenex, Torrance, CA). Identification and quantification of 20-HETE were performed on a Shimadzu Triple Quadrupole Mass Spectrometer LCMS-8050 equipped with a Nexera UHPLC using multiple reaction monitoring mode. MS conditions were ionization mode: negative heated electrospray (HESI); applied voltage: -4.5 to approximately -3 kV; nebulizer gas: 3.0 L/min N₂; drying gas: 5.0 L/min N₂; heating gas: 12.0 L/min air; interface temperature: 400°C; desolvation line temperature: 100°C; heat block temperature: 500°C; and internal standard: d₆ 20-HETE. UHPLC conditions were as follows: analytical column measures were Zorbax Eclipse Plus C18 RRHD (50-mm length x 2.1-mm inner diameter, 1.8 μm); mobile phase A: 95% water-5% acetonitrile 0.05% acetic acid; mobile phase B: acetonitrile 0.05%; time program 40% B (0 min) → 75% B (3 min) → 85% B (7.5 min); flow rate: 0.4 mL/min; injection volume: 5 μL; column oven temperature: 40°C. Synthetic standards were used to obtain standard curves (0.5–500 pg) for each compound. These standard curves were used to calculate final concentrations of 20-HETE. All solvents were HPLC grade or higher.

Statistics: All values are represented as mean ± SEM. Statistical analysis was performed on GraphPad Prism 8 (version 8.4.3). Two-tailed student t-test was used to determine significance between two groups. One-way ANOVA with Tukey post-hoc test was used to compare differences between three or more

means. 2-way ANOVA repeated measures with Sidak's post hoc test was used for phenylephrine, acetylcholine and sodium nitroprusside dose-response analysis. For wire and pressure myography experiments, both number of mice (N) and number of vessels (n) were reported. Experiments that compared vessel reactivity between two genotypes (WT and *Myh11-4a12* mice) use N for statistical calculations. Experiments that assessed the effectiveness of AAA on acetylcholine induced relaxation within one genotype used n for statistical calculations. EC₅₀ values from phenylephrine cumulative dose response curves were calculated and were compared using one-way ANOVA with Tukey post-hoc test. R_{max} values from acetylcholine or SNP induced relaxation were compared using one-way ANOVA with Tukey post-hoc test. p-values <0.05 were considered to be statistically significant.

Results:

Aim 1: To determine if smooth muscle-specific overexpression of Cyp4a12-20-HETE synthase causes hypertension and vascular dysfunction.

***Myh11-Cre^(+/+)-Cyp4a12-Flox^(+/wt) (Myh11-4a12)* had significantly elevated Cyp4a12 levels in vessels that resulted in elevated 20-HETE**

Myh11-4a12 mice had a significant increase of *Cyp4a12* mRNA expression in resistant vessels (mesenteric arteries: 8.62 ± 1.26 vs 1.44 ± 0.30 ; RIA: 5.95 vs 1.12, relative expression to *Tuba1a*, $p < 0.0001$) compared to WT (**Figure 1A and 1B**). The increase in expression was not observed in liver (**Figure 1C**: 1.56 ± 0.54 vs 1.91 ± 0.37 relative expression to *Tuba1a*). The overexpression of mRNA translated to increased Cyp4a protein levels when comparing mesenteric arteries of *Myh11-4a12* mice to WT (**Figure 2A**: 1.95 ± 0.21 vs 1.00 ± 0.21 Cyp4a/ β -actin fold expression, $p < 0.05$). Increases in Cyp4a protein expression were not observed in livers (**Figure 2B**: 1.00 ± 0.15 vs 1.00 ± 0.15 , Cyp4A/ β -actin fold change). Furthermore, elevated *Cyp4a12* was associated with increased 20-HETE levels in mesenteric arteries (3334 ± 891 pg/mg protein vs 545 ± 197 pg/mg protein, $p < 0.05$), RIA (1895 ± 376 pg/mg protein vs 242 ± 63 pg/mg protein, $p < 0.05$), and plasma (391 ± 52 pg/mL vs 242 ± 18 pg/mL, $p = 0.05$) without any changes in urinary levels (117 ± 29 pg/mL vs 146 ± 27 pg/mL, $p = 0.48$) (**Figure 3A-D**).

***Myh11-4a12* mice are hypertensive and have impaired vascular function.**

Systolic blood pressure (SBP) measured at 8-10-weeks of age was significantly higher in *Myh11-Cyp4a12* mice compared to WT mice (**Figure 5A**: 144 ± 2 vs 130 ± 1 mmHg, $p < 0.0001$). Isolated RIA from *Myh11-4a12* mice displayed impaired acetylcholine-induced relaxation after precontraction with phenylephrine compared to RIA from WT mice (**Figure 5B**: Maximal relaxation: $47\% \pm 6.9$ vs. $80\% \pm 4.3$ $p < 0.001$). Renal interlobar arteries from *Myh11-4a12* mice given a NO donor (SNP) were able to relax to a degree similar to WT (**Figure 5C**: Maximal relaxation: $85\% \pm 4.0$ vs $80\% \pm 9.0$) Measurements of vessel wall thickness were taken to assess 20-HETE's effects on vascular remodeling. *Myh11-4a12* mice had an increase media:lumen ratio compared to WT (**Figure 6A**: 0.332 ± 0.027 vs 0.164 ± 0.010 , $p < 0.0001$, student t-test). Media thickness (**Figure 6B**: 25.70 ± 1.22 μm vs 15.00 ± 0.71 μm , $*p < 0.05$) and media cross-sectional area (**Figure 6C**: 15718 ± 1496 μm^2 vs 10407 ± 660 μm^2 , $*p < 0.05$) were also elevated in *Myh11-4a12* mice compared to WT mice.

Markers of smooth muscle cell contraction and NO signaling were altered in *Myh11-4a12* mice.

20-HETE has been documented to have multiple actions on vessels to increased contractility and impaired relaxation. Phosphorylation of myosin light chain at serine 19 was used as a marker for increased cellular signaling for VSMC contraction. Mesenteric arteries from *Myh11-4a12* mice had a 40% increase in phosphorylation of myosin light chain compared to WT mice (**Figure 7**: 1.40 ± 0.13 vs 1.00 ± 0.08 Ser19 p-MLC/total-MLC fold change, $p < 0.05$).

Phosphorylation of eNOS was used as a marker for EC cell function and enhanced relaxation. In aortas of *Myh11-4a12* mice, there were reductions in both phosphorylated and total eNOS expression that was significantly lower than WT mice (**Figure 8**: 0.43 ± 0.19 vs 1.23 ± 0.26 Serine 1177/ β -tubulin fold change, * $p < 0.05$ and 0.57 ± 0.14 vs 1.00 ± 0.08 total eNOS/ β -tubulin fold change).

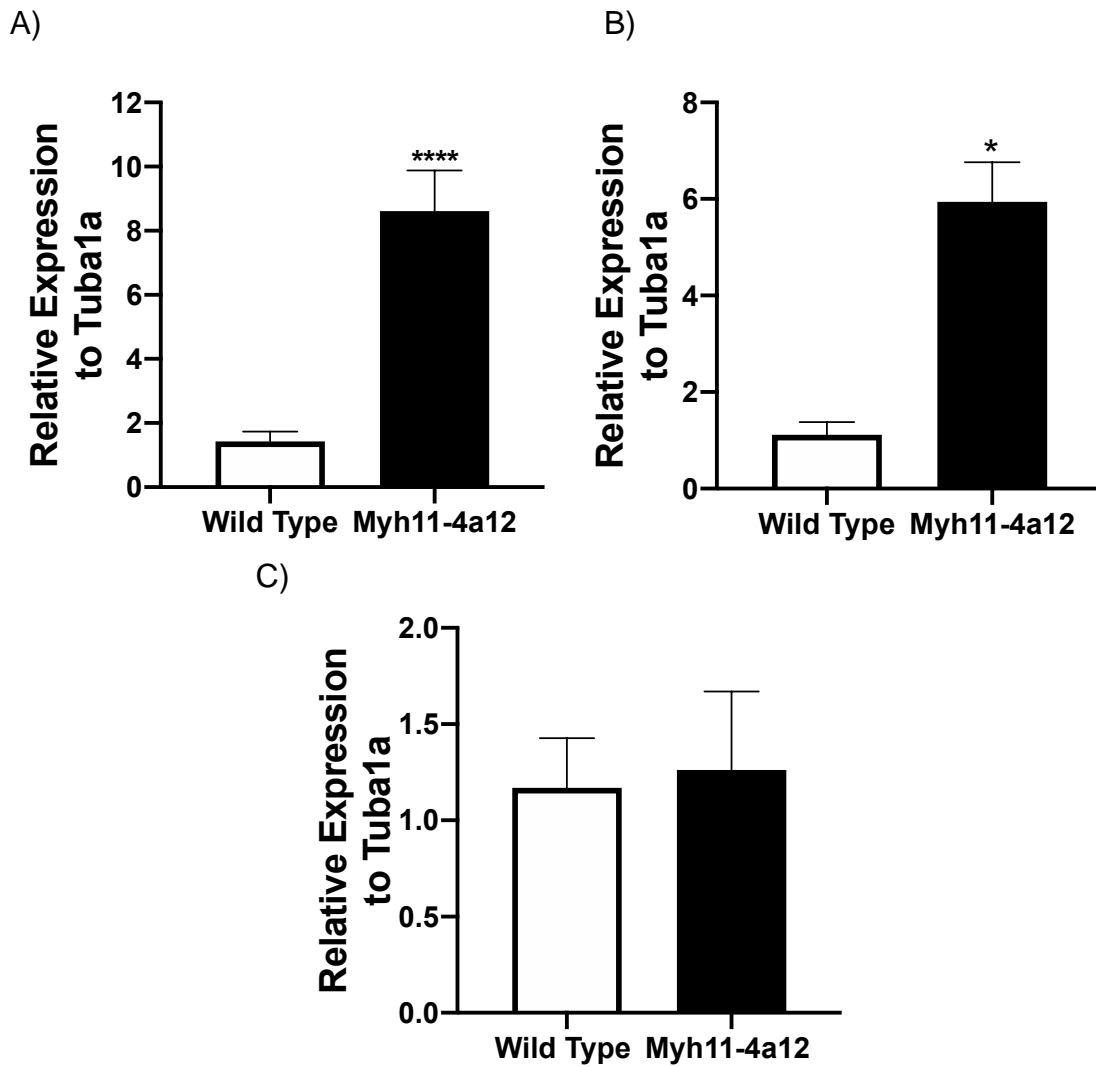


Figure 1: *Myh11-4a12* mice display overexpression of *Cyp4a12* in vessels.

RT-PCR result: A) mesenteric artery (N=14/group; ***<0.001 student t-test), B) RIA (N=6/group, *<0.05 t-test) and C) Liver (N=6 wild type, n=7 *Myh11-4a12*)

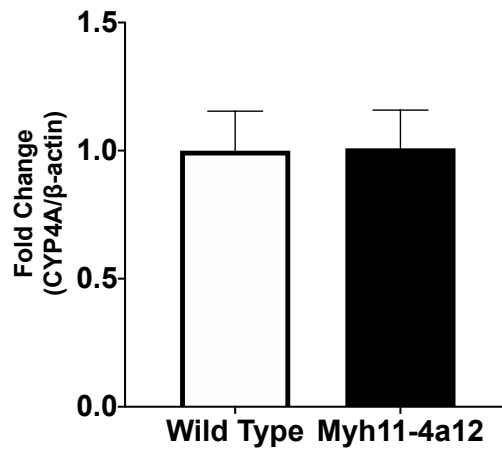
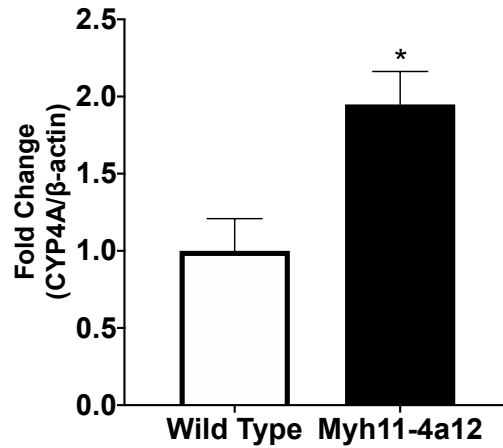
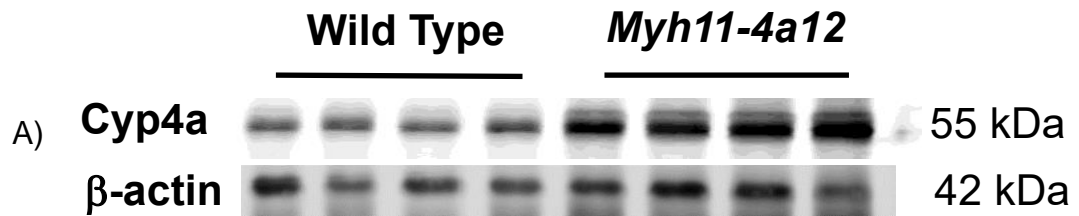


Figure 2: *Myh11-4a12* mice have elevated Cyp4a protein in vessels.

A) Mesenteric artery (N=4/group, * $p < 0.05$ compared to wild type, student t-test) but no difference was observed in B) liver (N=8/group, student t-test).

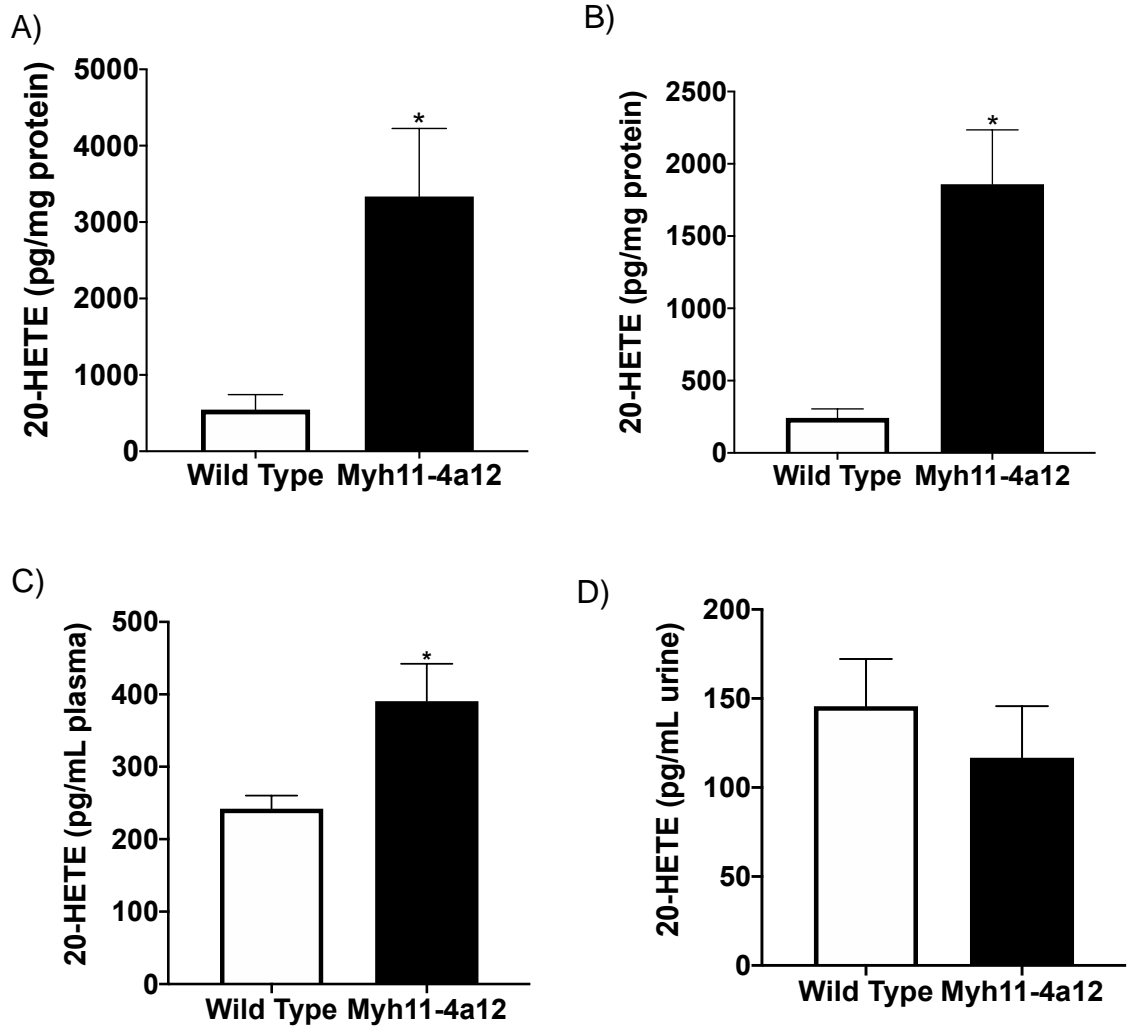


Figure 3: *Myh11-4a12* mice display elevated 20-HETE.

A) Mesenteric arteries (N=5 WT, n=6 Myh11-4a12), B) RIA (N=3/group), C) Plasma (N=4 WT, N=6 Myh11-4a12) but not in D) Urine (N=5/group). Mean \pm SEM student t-test *p<0.05.

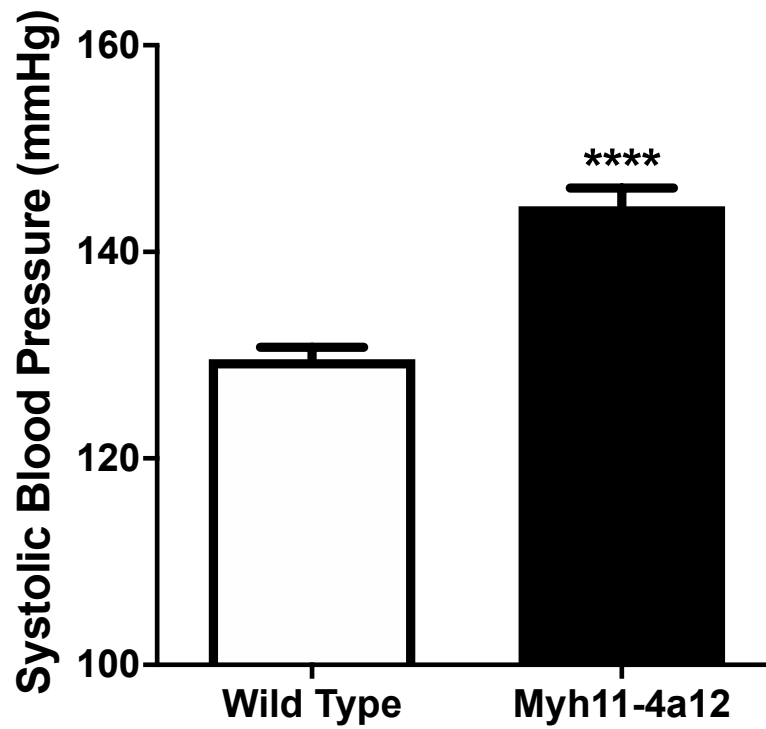
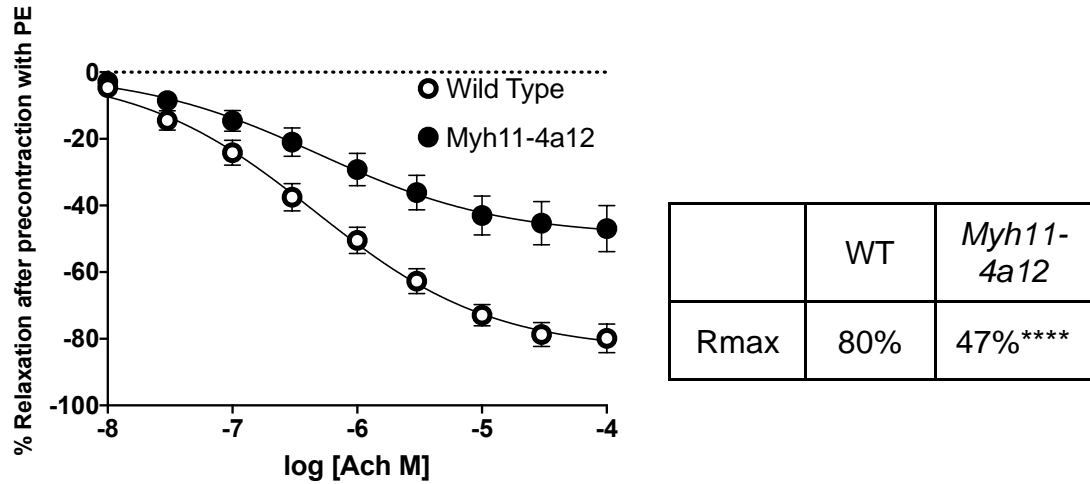


Figure 4: Mice with smooth muscle-specific overexpression of *Cyp4a12* are hypertensive.

Baseline systolic blood pressure measurement. N=22 Wild type; N=27 *Myh11-4a12*. ****p<0.0001, student t-test.

A)



B)

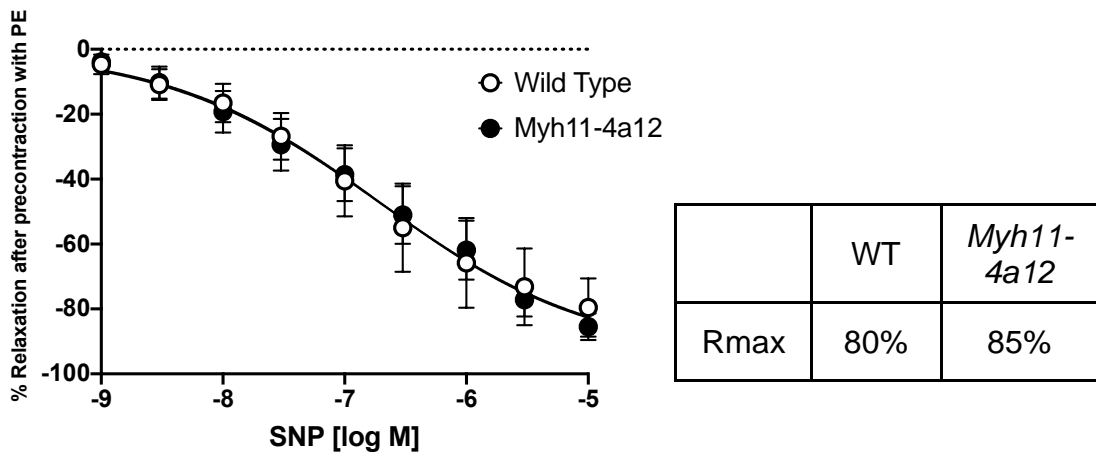


Figure 5: Mice with smooth muscle-specific overexpression of *Cyp4a12* have impaired relaxation.

A) Acetylcholine-induced relaxation after phenylephrine precontraction. Wild type N=13 mice, n=26 vessels and *Myh11-4a12* N=15 mice, n=28 vessels.

*** $p < 0.001$, t-test. B) Administration of SNP improved relaxation of vessels with overproduction of 20-HETE. Wild Type: n=3 mice; *Myh11-4a12*: n=4 mice. t-test. Means \pm SEM,

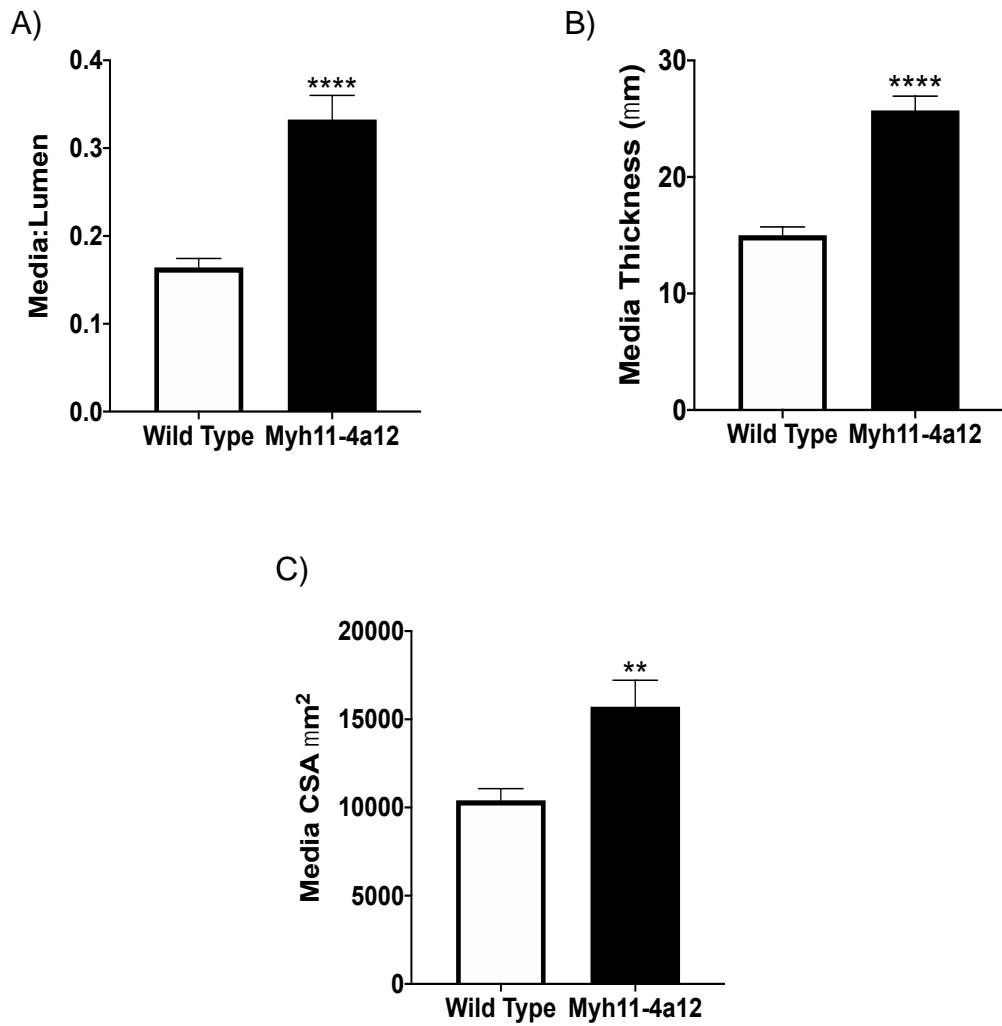


Figure 6: Renal interlobar artery measurements of vascular remodeling are elevated in *Myh11-4a12* mice.

A) Media:lumen ratio, B) Media thickness, and C) Media cross-sectional area. Wild type N=12 mice, n=24 vessels, *Myh11-4a12* N=14 mice, n=28 vessels; **p<0.01, ****p<0.0001, student t-test.

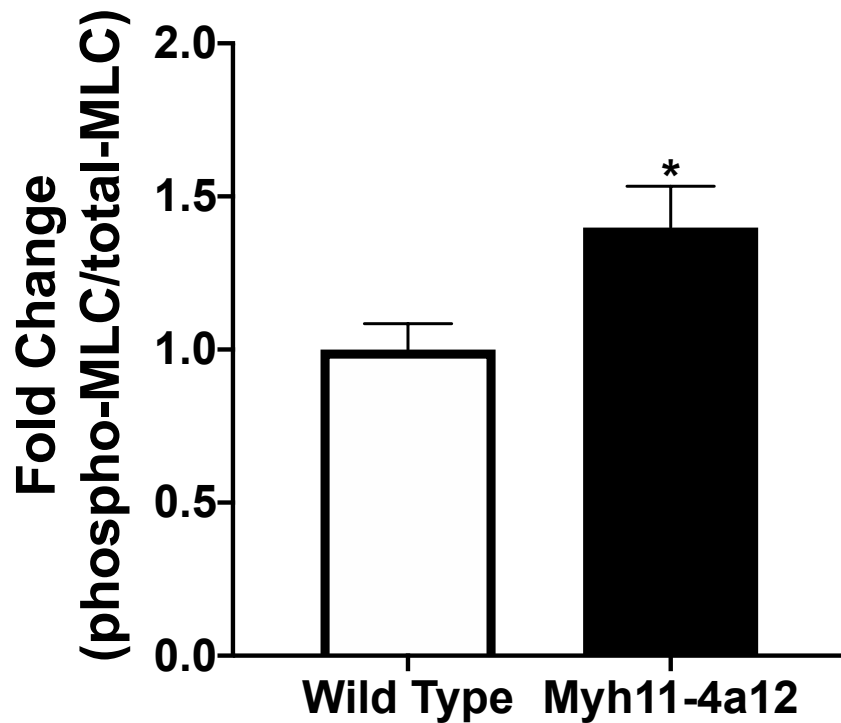
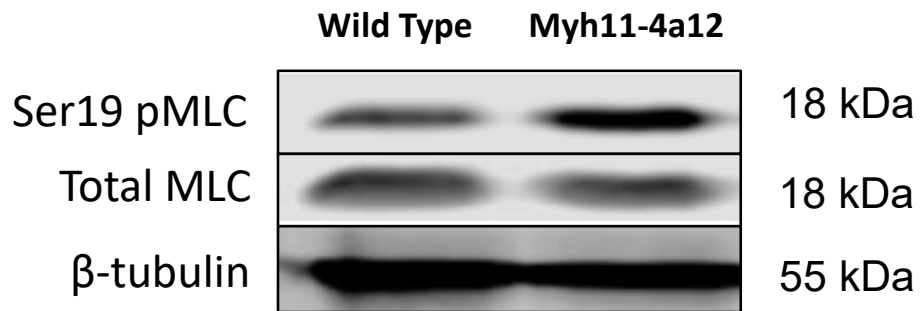


Figure 7: Baseline expression of myosin light chain phosphorylation at serine 19 in mesenteric arteries were elevated in *Myh11-4a12* mice.

N=12 wild type; N=10 *Myh11-4a12*. *p<0.05 student t-test.

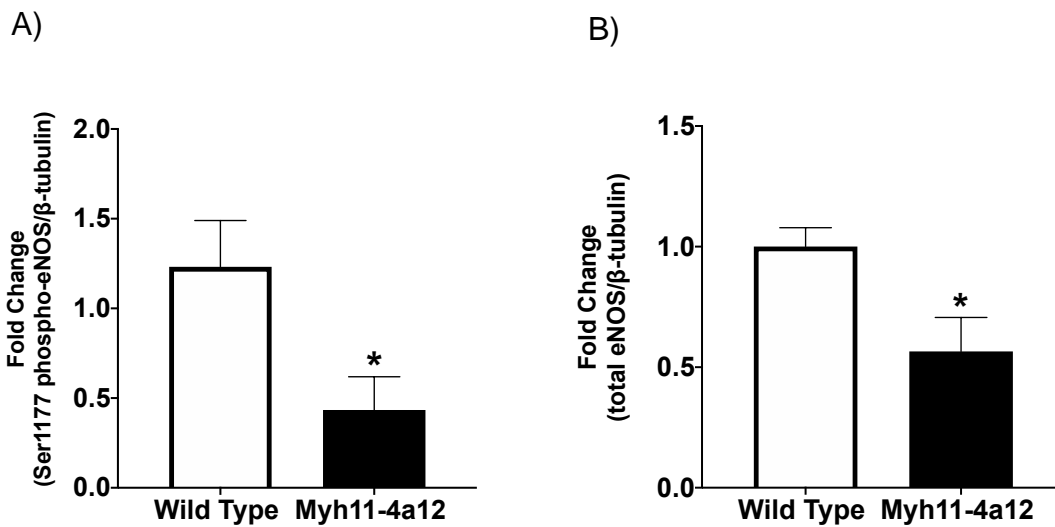
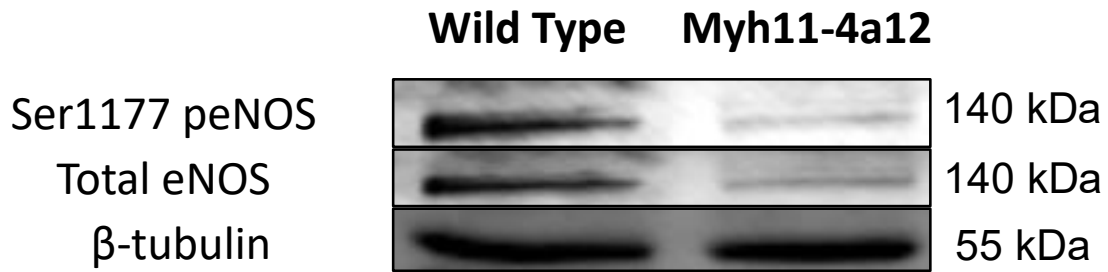


Figure 8: Baseline expression of phosphorylated and total eNOS was reduced in aortas of *Myh11-4a12* mice.

A) Serine 1177 phosphorylated eNOS to β -tubulin ration and B) total eNOS to β -tubulin. N=6/group, *p<0.05, student t-test

Aim 2: To determine if the vascular pathology in *Myh11-4a12* mice is 20-HETE-dependent.

Administration of AAA decreased systolic blood pressure and improved vascular function in mice with smooth muscle-specific *Cyp4a12* overexpression.

Myh11-4a12 mice were hypertensive compared to WT on day 0 (**Figure 9: *Myh11-4a12* ((combine): 146 ± 3 mmHg vs WT – vehicle: 132 ± 3 mmHg, p<0.001, student t-test).** Twelve days of AAA treatment normalized SBP to WT levels with values starting to decrease at day 4 (Day 12: *Myh11-4a12* – AAA 126 ± 1 vs 129 ± 1 mmHg). Wild type mice on AAA had no changes in SBP compared to WT mice on vehicle (data not shown). Administration of AAA appeared to have no effect on 20-HETE levels in the plasma. *Myh11-4a12* mice had elevated 20-HETE levels compared to WT (**Figure 10: 298 ± 35 vs 157 ± 23 pg/mL plasma, p<0.05)** however, *Myh11-4a12* mice on AAA (298 ± 58 pg/mL plasma) had a similar value compared to *Myh11-4a12* mice on vehicle.

Fluid balance and urinary sodium excretion was also assessed to determine if the blood pressure lowering effect of AAA was also due to changes in the renal handling of salt and fluid. Mean values for water consumption appeared similar between the three groups (**Figure 11A: Wild type – vehicle: 0.38 vs *Myh11-4a12* – vehicle: 0.38 vs *Myh11-4a12* – AAA 0.37 mL/gram body weight/24 hours).** Urine volume was similar between WT and *Myh11-4a12* mice on vehicle (**Figure 11B: 52.0 vs 55.6 μL/gram body weight/24 hours).** Urine

excretion appeared to increase in *Myh11-4a12* mice on AAA (75.6 $\mu\text{L}/\text{gram body weight}/24 \text{ hours}$), however, no conclusion was made due to the small sample size. Similar trends were observed when measuring urinary sodium excretion. Average values for urinary sodium excretion were similar between *Myh11-4a12* and WT mice on vehicle (6.91 $\mu\text{mole}/\text{gram body weight}$ vs 7.71 $\mu\text{mole}/\text{gram body weight}/24 \text{ hours}$). While there was an upward trend in sodium excretion in *Myh11-4a12* mice on AAA, no conclusions could be determined due to the small sample size (11.35 $\mu\text{mole}/\text{gram body weight}/24 \text{ hours}$).

After day 12, mice were sacrificed and RIA were isolated for wire myography. RIA from *Myh11-4a12* mice displayed impaired acetylcholine-induced relaxation compared to WT mice (R_{max} : 67% \pm 5 vs 90% \pm 2, $P < 0.0001$). *Myh11-4a12* mice on AAA had improved acetylcholine relaxation with values similar to WT (R_{max} : 96% \pm 1) (**Figure 12A**). Changes in phenylephrine-induced contractions were also observed. RIA from *Myh11-4a12* mice were more sensitive to phenylephrine-induced contraction compared to WT (EC_{50} : 1.63 $\times 10^{-7}$ μM vs. 5.00 $\times 10^{-7}$ μM , $p < 0.0001$). The sensitivity of phenylephrine for *Myh11-4a12* mice on AAA (EC_{50} : 4.22 $\times 10^{-7}$ μM) was not different compared to WT (**Figure 12B**).

Ex vivo experiments were performed to assess the direct actions of AAA in RIA to promote relaxation. Both WT and *Myh11-4a12* vessels were treated with vehicle first followed by 10 μM AAA. Wild type vessels had no apparent difference in the ability to relax after acetylcholine-induced relaxation (**Figure 13A**). On the other hand, *Myh11-4a12* mice displayed improved relaxation

response after acetylcholine administration. *Myh11-4a12* vessels had a maximal % relaxation of $40 \pm 6\%$ after vehicle treatment. AAA pretreatment resulted in improved relaxation ($63 \pm 7\%$, $p < 0.05$) (**Figure 13B**). Comparisons were made between the four groups at the highest doses of acetylcholine administration. *Myh11-4a12* vessels on vehicle had significantly impaired relaxation response compared to WT either on vehicle or AAA (**Figure 13B**: $40 \pm 6\%$ vs. $67 \pm 6\%$ WT – vehicle and $64 \pm 6\%$ WT – AAA, $p < 0.05$). AAA was able to significantly improve the ability of the vessels to relax in *Myh11-4a12* mice. *Myh11-4a12* vessels after AAA had similar relaxation values compared to WT on vehicle or AAA (**Figure 13C**: $63 \pm 4\%$)

AAA administration improved media:lumen ratio but did not affect media thickness or cross-sectional area of RIA

Renal interlobar arteries from *Myh11-4a12* mice had a media:lumen ratio that was significantly higher than WT (**Figure 14A**: 0.277 ± 0.025 vs 0.163 ± 0.006 , $P < 0.0001$). RIA from AAA-treated *Myh11-4a12* mice showed a reduction in media:lumen ratio (0.129 ± 0.013 , $p < 0.05$) when compared to *Myh11-4a12* on vehicle (**Figure 14A**). Analysis of media wall thickness and media cross-sectional area show that AAA did not have an effect on vessel wall thickness. Both *Myh11-4a12* mice either on vehicle or AAA had a thicker media (**Figure 14B**: $23.85 \pm 2.25 \mu\text{m}$ and $20.72 \pm 1.37 \mu\text{m}$ vs $15.86 \pm 0.83 \mu\text{m}$, $p < 0.0001$ WT - vehicle vs *Myh11-4a12* - vehicle and $p < 0.05$ WT - vehicle vs *Myh11-4a12* – AAA) and cross-sectional area (**Figure 14C**: $15114 \pm 1871 \mu\text{m}^2$ and $14268 \pm 1259 \mu\text{m}^2$ vs

10560 ± 641 μm², p<0.05 WT - vehicle vs *Myh11-4a12* - vehicle and p=0.08 WT - vehicle vs *Myh11-4a12* – AAA) compared to WT. Western blot analysis for myosin heavy chain 11, a marker of vascular smooth muscle cell differentiation, is in line with these results. *Myh11-4a12* mice either on vehicle or AAA appeared to have higher myosin heavy chain expression compared to WT on vehicle (**Figure 14D**: 3.10 ± 0.98 Myh11/β-tubulin fold change and 3.25 ± 0.72 Myh11/β-tubulin fold change vs 1.00 ± 0.10 Myh11/β-tubulin fold change).

Markers of VSMC differentiation were elevated in *Myh11-4a12* mice.

At baseline, the vessel wall was thicker in *Myh11-4a12* mice compared to WT mice. This may be due to 20-HETE's ability to cause VSMC proliferation which increases the number of mature cells within the vessel wall. To determine this, markers of VSMC differentiation [*Myh11*, *Sm22a*, *Acta2*] were measured in renal interlobar arteries (**Figure 15**). *Myh11* (RIA: 1.67 ± 0.22 vs 1.18 ± 0.22, relative expression to *tuba1a*), *Tagln* (2.13 ± 0.25 vs 1.17 ± 0.26 relative expression to *tuba1a*, p<0.05 t-test), and *Acta2* (RIA: 1.94 ± 0.23 vs 1.14 ± 0.20, relative expression *tuba1a*, p<0.05 t-test) mRNA expression were all elevated compared to WT mice.

No differences in collagen expression were observed between *Myh11-4a12* and wild type mice.

20-HETE has been documented to promote increases in collagen synthesis in rats (Soler *et al.*, 2018). Messenger RNA of Collagen I and Collagen IV were assessed to determine if increase in collagen synthesis was occurring which may contribute to the stiffening of the vessels and increase in blood pressure. Collagen I (0.76 ± 0.28 vs 1.25 ± 0.25 , relative expression to *Tuba1a*) and collagen IV (1.12 ± 0.29 vs 1.25 ± 0.30 , relative expression to *Tuba1a*) were not different between *Myh11-4a12* and WT mice in mesenteric arteries (**Figure 16**).

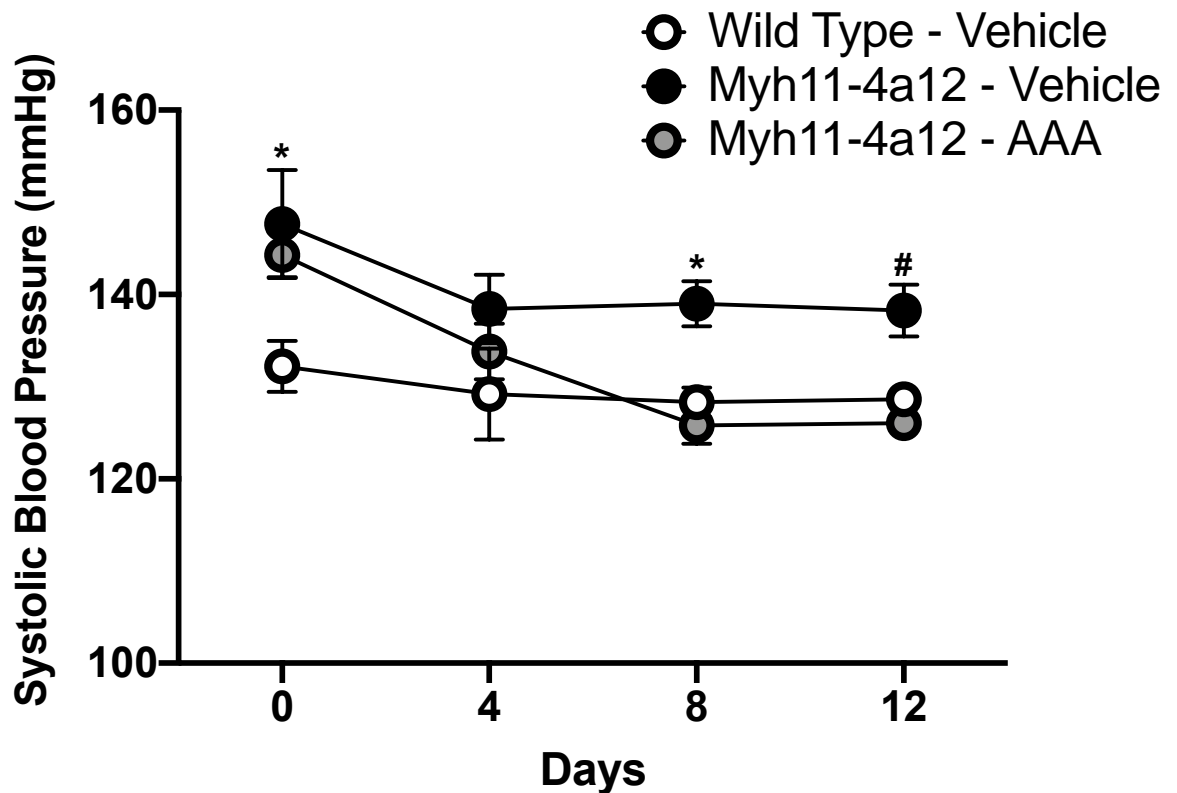


Figure 9: Administration of a 20-HETE receptor antagonist (AAA) was able to lower blood pressure after 12 days.

A) Wild Type or *Myh11-4a12* mice underwent either vehicle treatment or AAA (10mg/kg/day) treatment for 12 days. N=12 Wild type – vehicle; N=11 *Myh11-4a12* – vehicle; N=14 *Myh11-4a12* – AAA. * $p < 0.05$ of *Myh11-4a12* compared to wild type. # $p < 0.05$ *Myh11-4a12* – vehicle to *Myh11-4a12* – AAA. 2-way ANOVA with Tukey post-hoc test.

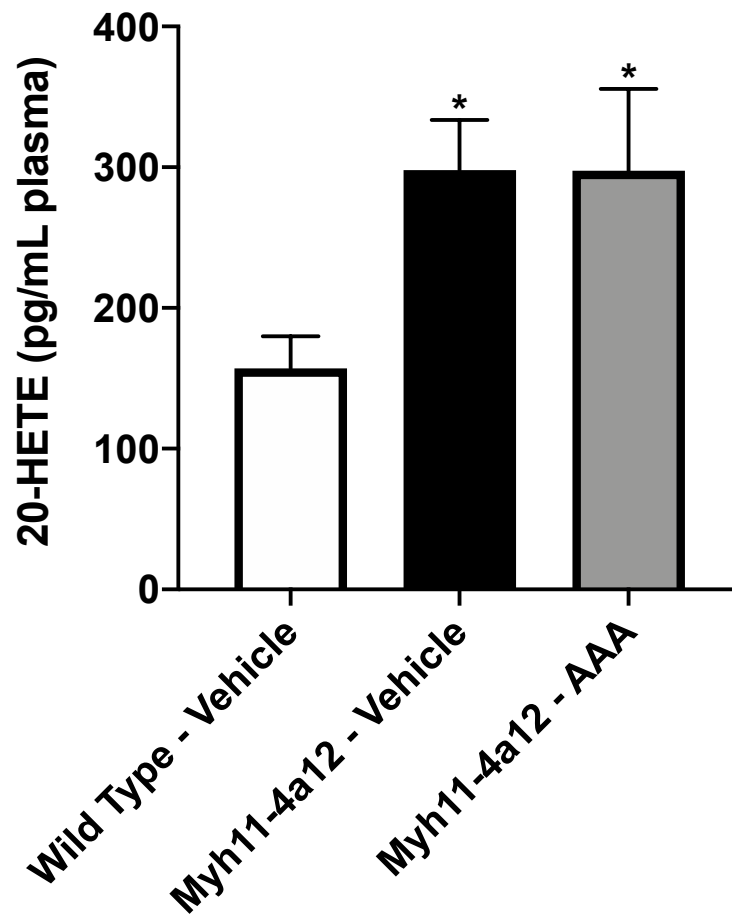


Figure 10: Plasma 20-HETE levels were unchanged after 12-day AAA treatment.

Wild type - Vehicle N=13, *Myh11-4a12* - Vehicle N=15, *Myh11-4a12* - AAA N=10. * $p < 0.05$ one-way ANOVA vs wild type - vehicle.

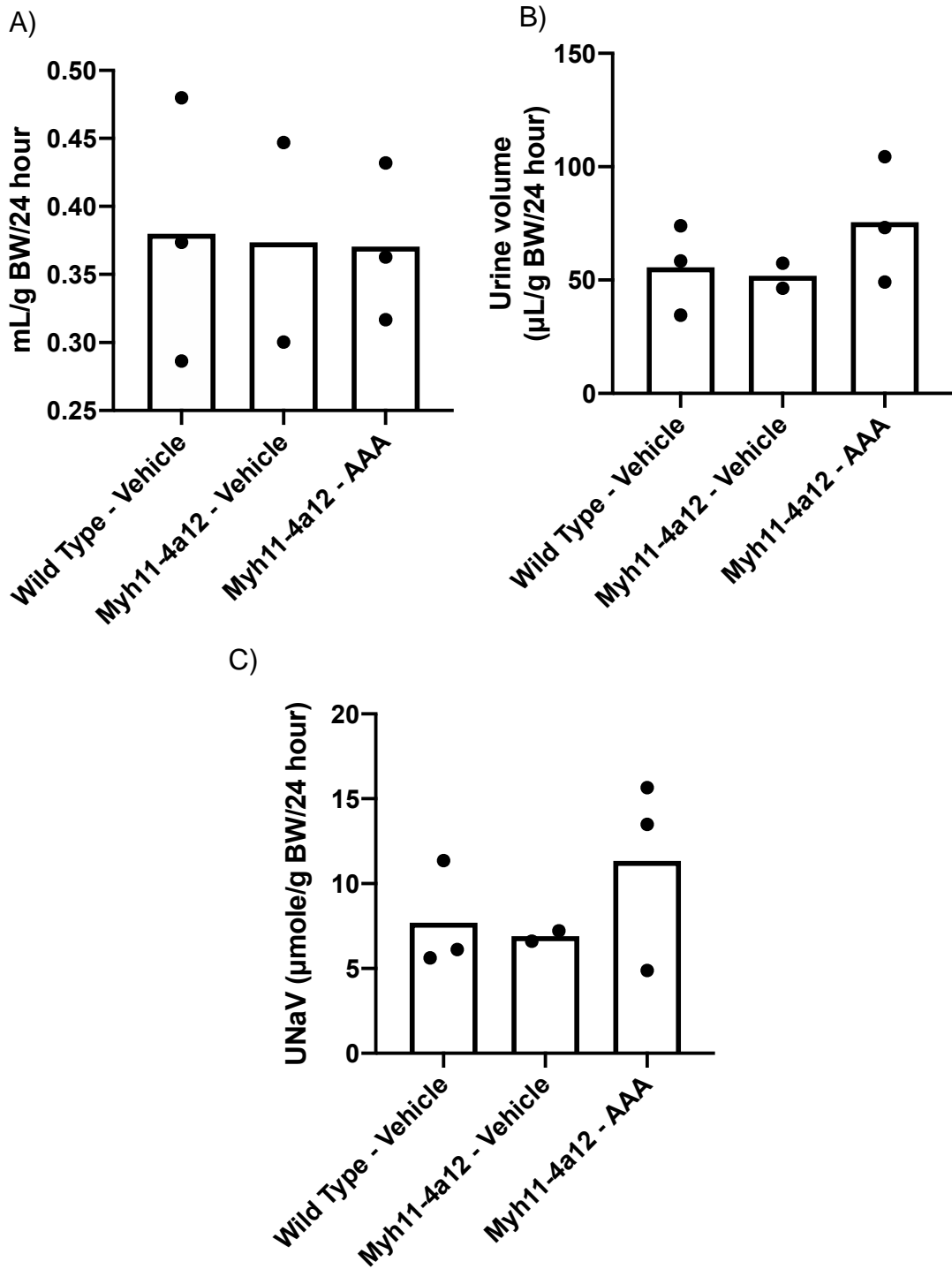


Figure 11: Urine volume and sodium excretion in WT and *Myh11-4a12* mice treated with and without AAA.

A) water consumption, B) urine volume, C) urinary sodium. Wild type – vehicle N=3, *Myh11-4a12* - vehicle N=2, *Myh11-4a12* – AAA N=3.

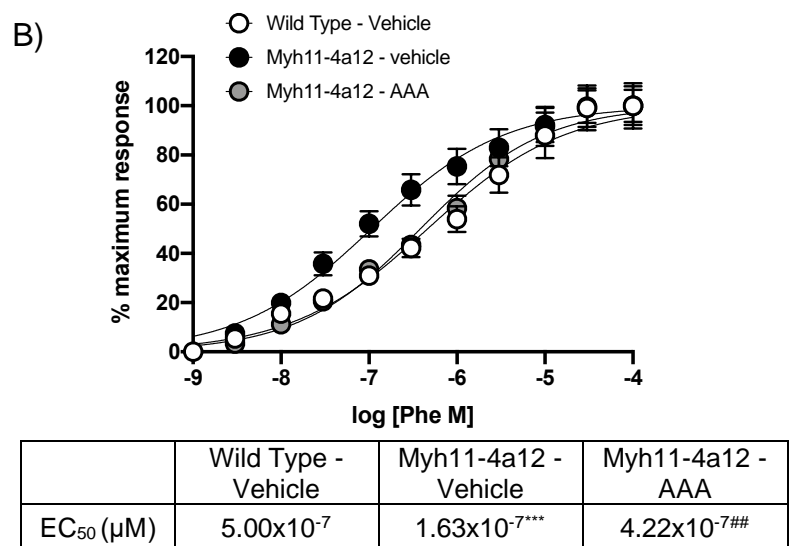
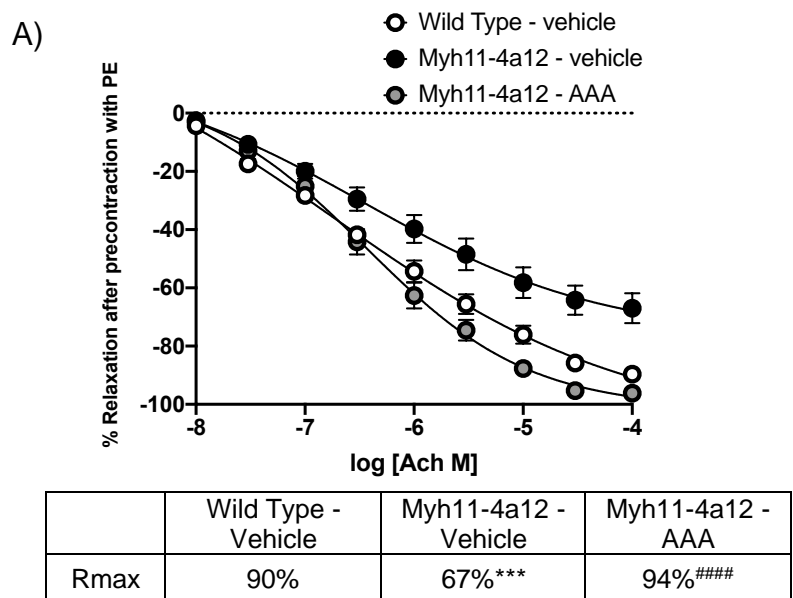


Figure 12: Vascular activity was improved after 12 days of AAA treatment.

A) Dose response acetylcholine induced relaxation on RIA after 12 days of AAA treatment. Wild Type – vehicle N=7 mice, n=14 vessels; *Myh11-4a12* – vehicle N=7 mice, n=14 vessels; *Myh11-4a12* – AAA N=7 mice, n=14 vessels.

***p<0.001 Wild Type - vehicle vs *Myh11-4a12* -vehicle; ####p<0.0001 *Myh11-4a12* - vehicle vs *Myh11-4a12* – AAA. One-way ANOVA. B) Dose response phenylephrine induced contraction on RIA after 12 days of treatment. Wild Type – Vehicle N=7 mice, n=14 vessels; *Myh11-4a12* – vehicle N=9 mice, n=18 vessels; *Myh11-4a12* – AAA N=6 mice, n=12 vessels. ***p<0.001, ##p<0.01 One-way ANOVA

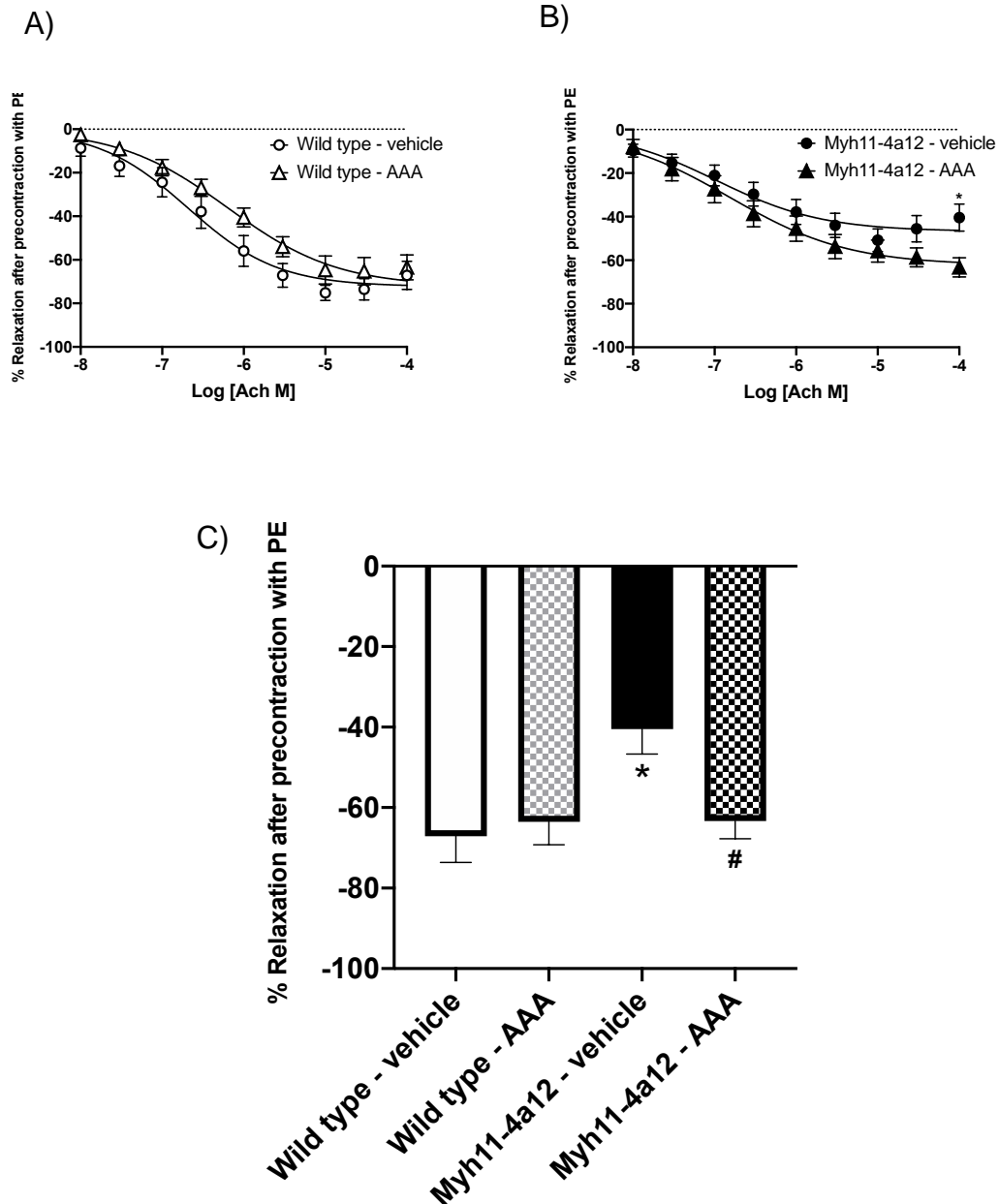


Figure 13: *Myh11-4a12* mice had improved relaxation with AAA treatment *ex vivo*.

A) Wild type N=3 mice, n=9 vessels. B) *Myh11-4a12* N=6 mice, n=17 vessels vehicle and n=16 vessels AAA treatment. *p<0.05 2-way ANOVA. C) comparisons of all treatments at 10⁻⁴M acetylcholine. P<0.05 one-way ANOVA.

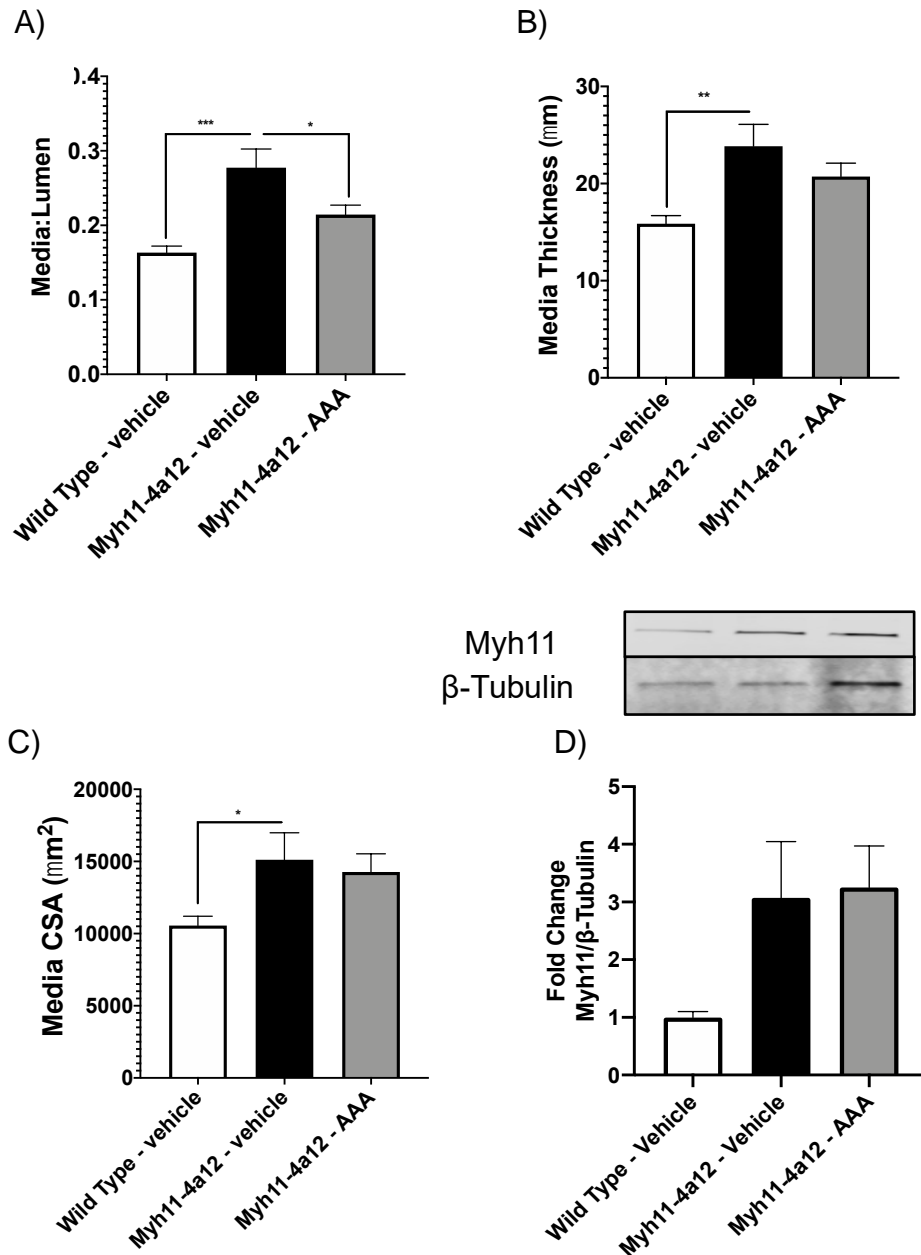


Figure 14: *Myh11-4a12* mice have an elevated media:lumen ratio that was reduced with AAA treatment, however, AAA did not reduce the thickness of the vessel.

Renal interlobar arteries underwent pressurized myography and the inner and outer diameters were measured. A) media:lumen ratio; B) media thickness; C) media cross-sectional area (CSA). Wild type – vehicle N=9 mice, n=18 vessels *Myh11-4a12* – vehicle N=7 mice, n=14 vessels, *Myh11-4a12* – AAA N=8 mice, n=16 vessels. Mean \pm SEM one-way ANOVA *p<0.05, **p<0.01, ***p<0.001. D) Western blot analysis for smooth muscle-specific myosin heavy in mesenteric arteries. N=5 wild type - vehicle, N=4 *Myh11-4a12* – vehicle, N=5 *Myh11-4a12* – AAA. Mean \pm SEM, one-way ANOVA.

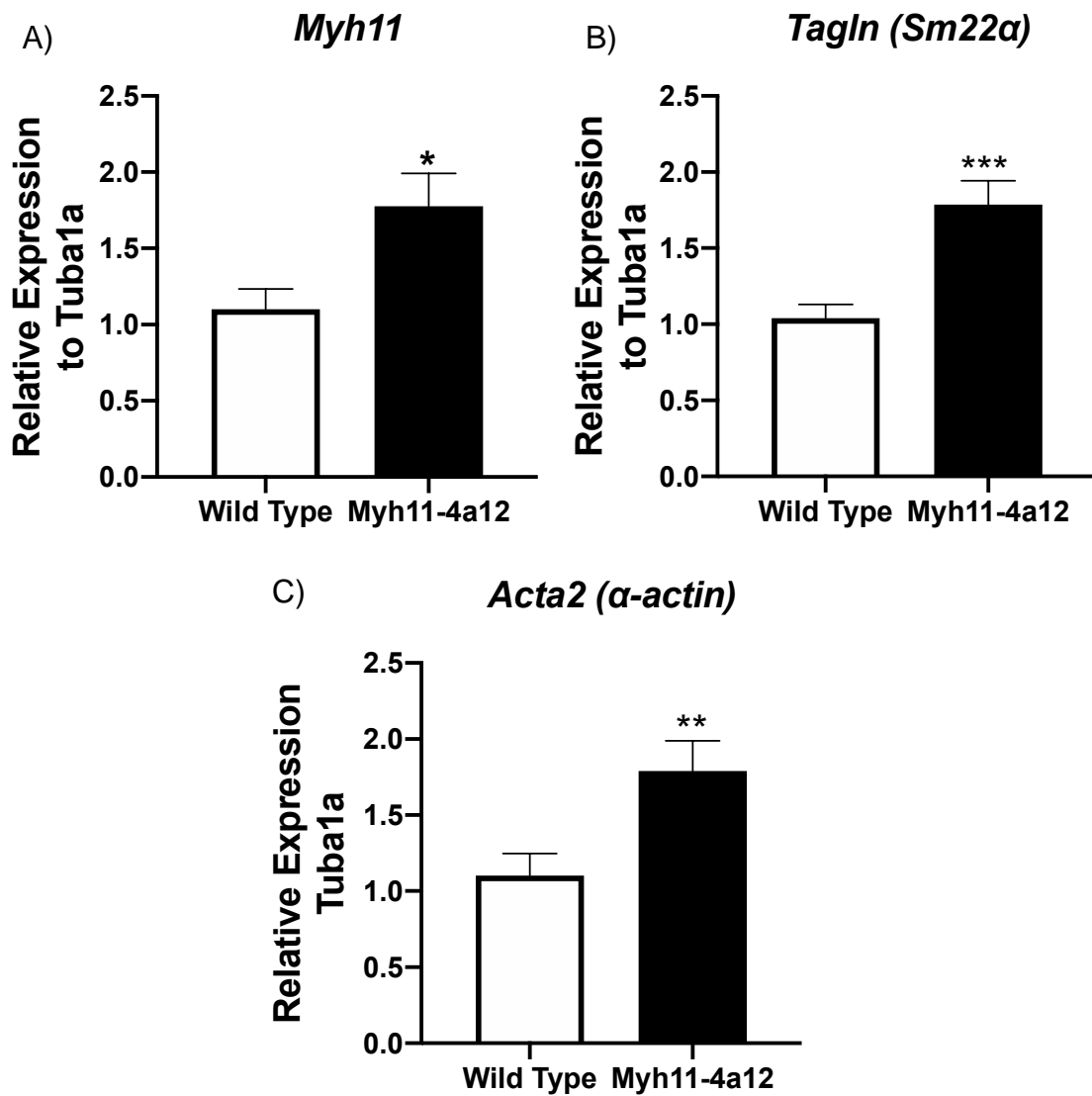


Figure 15: Increases in markers of VSMC differentiation were observed in RIA of *Myh11-4a12* mice.

A) *Myh11* (N=6/group) B) *Tagln* (wild type: N=7; *Myh11-4a12*: N=6); C) *Acta2* (N=6/group) Means \pm SEM, * $p < 0.05$, ** $p < 0.01$, *** $p < 0.001$ student t-test.

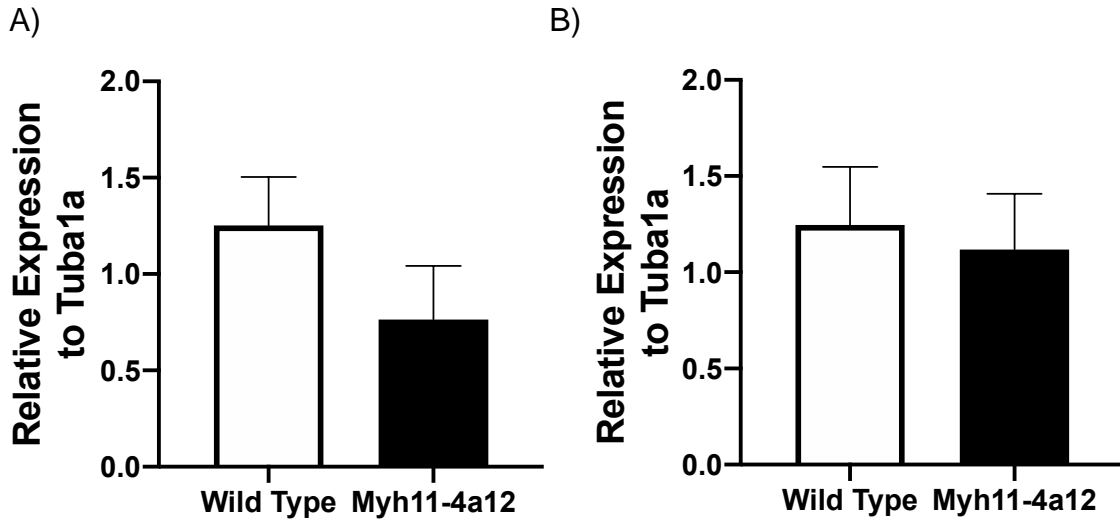


Figure 16: No differences in collagen expression were observed between *Myh11-4a12* and wild type mice.

A) Collagen I and B) Collagen IV. Wild Type: N=11; *Myh11-4a12*: N=8. Means ± SEM, student t-test.

Aim 3: To explore cellular mechanisms underlying the increased contractility of arteries from mice with smooth muscle-specific overexpression of *Cyp4a12*.

No changes were observed in *ACE* mRNA expression between wild type and *Myh11-4a12* mice.

ACE expression has been shown to increase with elevated 20-HETE. Increases in ACE result in increases in angiotensin II which may have a direct action on vessels to cause contraction. ACE is primarily expressed in the endothelium, however, there is also ACE expression in the VSMC (Fishel *et al.*, 1995). After measuring *Ace* mRNA in mesenteric arteries, there was no difference between *Myh11-4a12* and WT mice (**Figure 17:** 1.36 ± 0.26 vs 1.03 ± 0.126 , relative expression to *tuba1a*)

***Myh11-4a12* mice appeared to have reductions in eNOS activation which was increased with AAA treatment.**

Myh11-4a12 mice with elevated 20-HETE have impaired relaxation to acetylcholine, and administration of a 20-HETE receptor antagonist improves the relaxation of the vessel to a level similar to wild type. Furthermore, administration of a NO donor allowed the vessel from *Myh11-4a12* mice to relax to a degree similar to WT. This suggests that vessels from *Myh11-4a12* mice have an impairment in NO bioavailability. The inhibition of eNOS activation is one possible reason for this impairment. Activation of eNOS was measured by

phosphorylation of eNOS at Serine 1177 via western blotting. *Myh11-4a12* mice appeared to have reductions in Serine 1177 phosphorylation compared to wild type in aorta (**Figure 18A**: 0.43 ± 0.19 vs 1.23 ± 0.26 , Ser1177 p-eNOS/ β -tubulin fold change). *Myh11-4a12* mice also appeared to have lower total eNOS expression compared to WT (**Figure 18B**: 0.57 ± 0.14 vs 1.00 ± 0.08 total eNOS/ β -tubulin fold change). AAA treatment appeared to increase phosphorylation (1.42 ± 0.58 , Ser1177 p-eNOS/ β -tubulin fold change) and total eNOS (1.20 ± 0.58 , total eNOS/ β -tubulin fold change) levels of *Myh11-4a12* mice to a value greater than WT. Vasodilator-stimulated phosphoprotein (VASP) phosphorylation at Serine 239 was also measured because it is an indicator that NO from the EC is able to reach the VSMC. *Myh11-4a12* mice had reductions in VASP phosphorylation compared to WT (0.61 ± 0.09 vs 1.00 ± 0.04 , Ser239 p-VASP/total VASP fold change, $p < 0.01$) which was unchanged when *Myh11-4a12* mice were given AAA (**Figure 18C**: 0.63 ± 0.07 , Ser239 p-VASP/total VASP fold change). In mesenteric arteries, changes in phosphorylation of eNOS were also observed. *Myh11-4a12* mice appeared to have reduced eNOS phosphorylation (**Figure 19**: 0.57 ± 0.06 vs 1.00 ± 0.23 Ser1177 p-eNOS/total eNOS, $p = 0.15$) and *Myh11-4a12* mice that were given AAA had increase phosphorylated eNOS levels (1.07 ± 0.08 p-eNOS/total eNOS, $p = 0.20$). Unlike aortas, there were no differences in total eNOS protein expression between the three groups.

Administration of the 20-HETE receptor antagonist was able to reduce phosphorylation of myosin light chain.

20-HETE's ability to change the sensitivity of RIA to phenylephrine suggests that 20-HETE can mediate actions to cause changes in phosphorylation state of myosin light chain. When probing for the phosphorylation of Serine 19 on the regulatory subunit of myosin light chain, there was approximately a 60% increase in the *Myh11-4a12* group compared to wild type (1.60 ± 0.23 vs 1.00 ± 0.06 Ser19 p-MLC/total MLC fold change, $p < 0.05$ one-way ANOVA). *Myh11-4a12* mice treated with AAA had reduced phospho-myosin light chain levels (0.94 ± 0.11 , Ser19 p-MLC/total MLC fold change, $p < 0.05$ vs *Myh11-4a12* – vehicle, one-way ANOVA) that were similar to wild type (**Figure 20**).

20-HETE was able to increase Rho-kinase activity which was attenuated with AAA.

Upstream of myosin light chain is Rho-kinase (ROCK). RhoA-GTP activates ROCK which causes the phosphorylation and inhibition of myosin light chain phosphatase. Inhibition of myosin light chain phosphatase allows for the phosphate group on myosin light chain to stay on so it remains in a contractile state. ROCK1 protein was measured in RIA and there was a 60% increase in *Myh11-4a12* mice compared to wild type (**Figure 21**: 1.60 ± 0.21 vs 1.00 ± 0.18 , $p < 0.05$). AAA treatment did not affect the protein expression of ROCK1 (data not shown). Although AAA was not able to decrease ROCK1 expression, it is

possible that AAA can change activity of ROCK. To assess this, WT RIAs were used and pressure myography was performed to assess AAA and ROCK inhibitor, Y-27632, on 20-HETE-induced changes in myogenic response. Treating RIA with 20-HETE produced a downward shift in the absolute ID and the normalized ID curves (**Figure 22 A&B**). Co-treatment with 20-HETE plus AAA or ROCK inhibitor (Y-27632) shifted the curve upward overlapping the vehicle treated vessels. Lastly, combined treatment of 20-HETE with AAA and ROCK inhibitor did not result in any further upward shifts in either the absolute ID or normalized ID curves. The most significant changes happened at pressure of 80 mmHg and 100 mmHg (**Figure 23**). At 80 mmHg, 20-HETE reduced the absolute ID ($106 \pm 2.5 \mu\text{m}$ vs $124 \pm 2.6 \mu\text{m}$, $p < 0.01$) and the normalized ID ($42 \pm 0.86\%$ vs $48 \pm 0.79\%$, $p < 0.001$) significantly compared to WT. Co-treatment with 20-HETE plus AAA (absolute ID: $124 \pm 2 \mu\text{m}$, $p < 0.001$; normalized ID: $48.8 \pm 0.89\%$, $p < 0.0001$) or Y-27632 (absolute ID: $126 \pm 3 \mu\text{m}$, $p < 0.001$; normalized ID: $49 \pm 1.2\%$, $p < 0.0001$) increase the absolute ID and the normalized ID significantly compared to 20-HETE only. Treatment of RIA with 20-HETE plus AAA and Y-27632 did not produce any further increase in absolute ID ($113 \pm 4.6 \mu\text{m}$, $p < 0.001$ vs 20-HETE treatment) or normalized ID ($49 \pm 1.4\%$, $p < 0.0001$ vs 20-HETE treatment). Similar results were observed at 100 mmHg. Administration of 20-HETE in the bath reduced the absolute ID (90 ± 3.3 vs $106 \pm 3.2 \mu\text{m}$, $p < 0.05$) and the normalized ID (33 ± 1.1 vs $39 \pm 0.94\%$, $p < 0.01$) compared to vehicle treated. Adding either AAA (Absolute ID: $109 \pm 3.4 \mu\text{m}$, $p < 0.01$; normalized ID: $41 \pm 0.97\%$, $p < 0.001$) or Y-27632 (Absolute ID: 108 ± 3.7 , $p < 0.01$; normalized ID: $40 \pm$

1.1%, $p < 0.001$) blunted the increased myogenic response due to 20-HETE.

Treatment with 20-HETE, AAA and Y-27632 did not further increase the absolute ID ($113 \pm 4.6 \mu\text{m}$, $p < 0.001$) and normalized ID ($41 \pm 1.5\%$, $p < 0.001$).

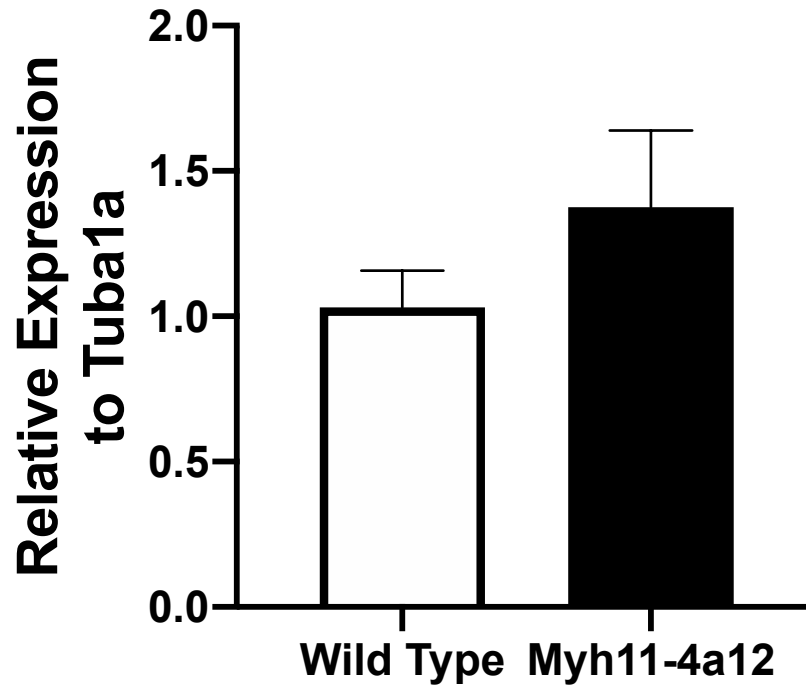


Figure 17: No differences in *ACE* mRNA expression were observed between *Myh11-4a12* and wild type mice in mesenteric arteries.

Wild Type: N=5; *Myh11-4a12*: N=8. Means \pm SEM, student t-test.

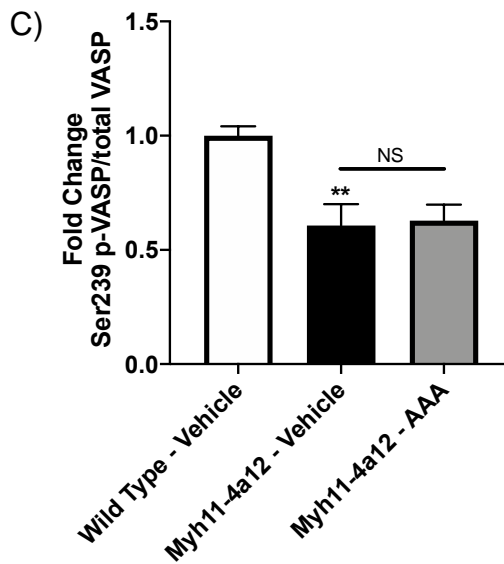
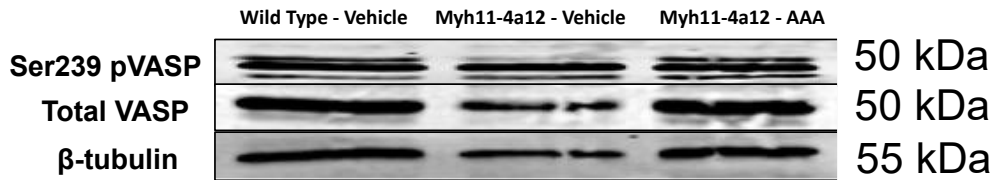
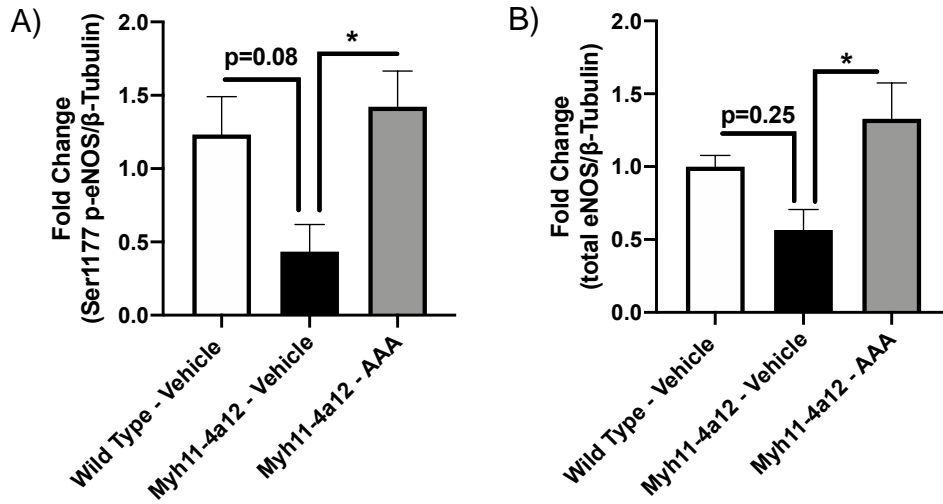
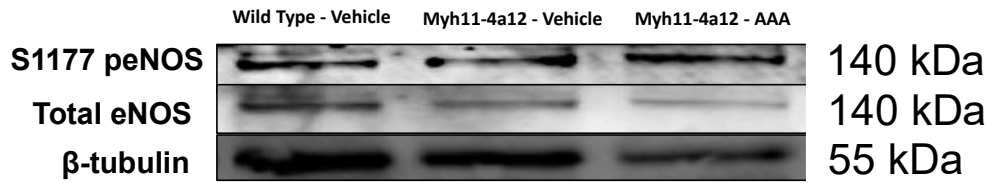


Figure 18: Western blot analysis of eNOS and VASP phosphorylation in aorta.

A) Serine 1177 phospho-eNOS/β-tubulin and B) total eNOS/ β-tubulin. N=6 wild type – vehicle and *Myh11-4a12* – vehicle; N=7 *Myh11-4a12* – AAA, *p<0.05 one-way ANOVA. C) Serine 239 phospho-VASP/total VASP. N=5 wild type – vehicle N=4 *Myh11-4a12* – vehicle and *Myh11-4a12* – AAA, **p<0.01, One-way ANOVA.

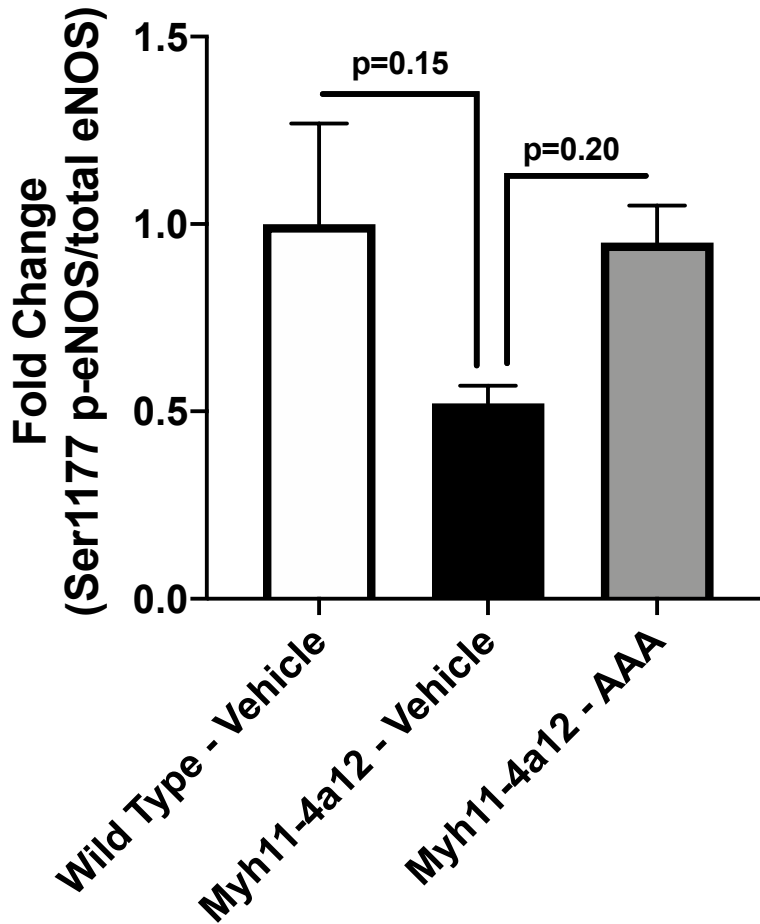
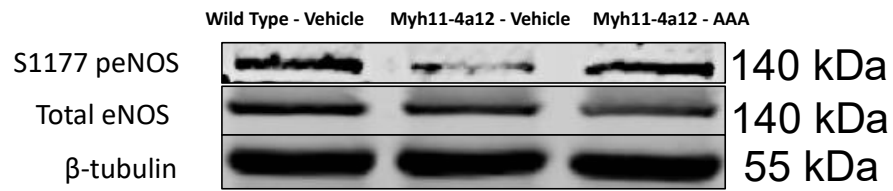


Figure 19: Phosphorylation of eNOS at serine 1177 after 12 days of AAA treatment in mesenteric arteries of Myh11-4a12 mice.

Wild type – vehicle: N=5, *Myh11-4a12* – vehicle: N=5, *Myh11-4a12* – AAA: N=5.

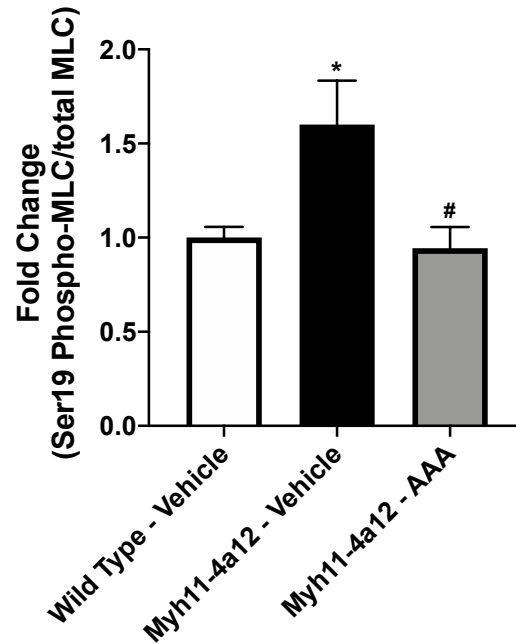
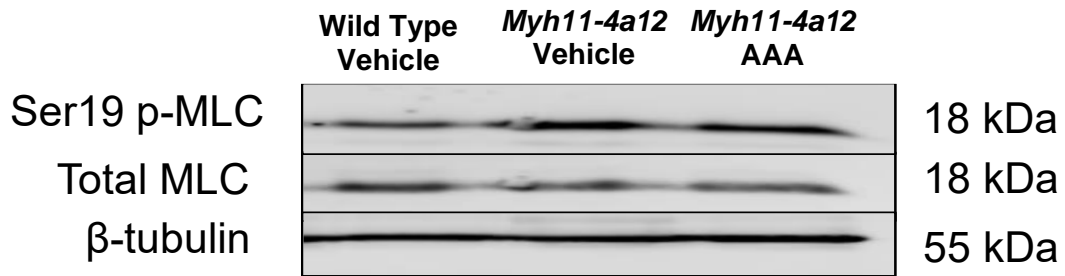


Figure 20: *Myh11-4a12* mice have elevated phosphorylation of myosin light chain that was reduced with 12 day AAA treatment.

A) Western blot analysis of Serine 19 phospho-myosin light chain expression in mesenteric arteries after 12-day AAA treatment (N=7 Wild Type – Vehicle and *Myh11-4a12*-vehicle; N=6 *Myh11-4a12* - AAA, one-way ANOVA).

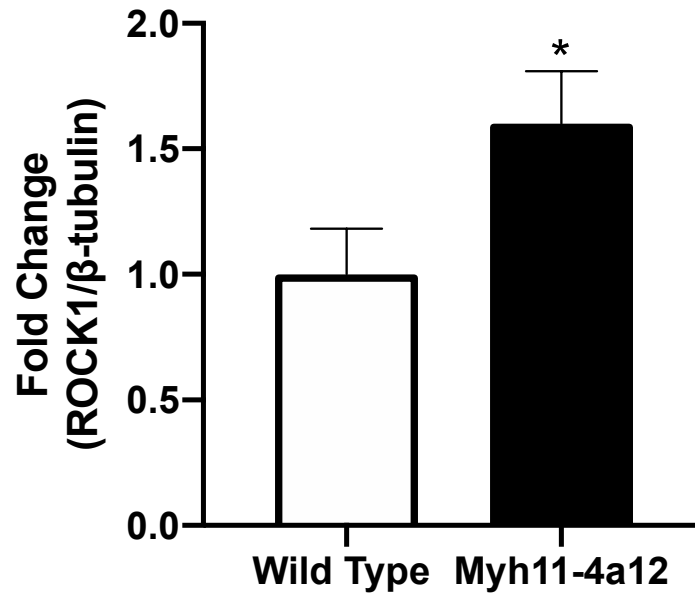
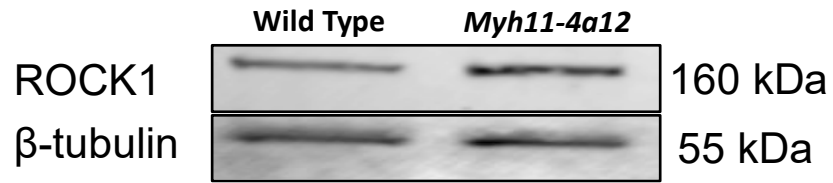


Figure 21: ROCK1 protein expression was elevated in *Myh11-4a12* mice.

Wild type: N=5; *Myh11-4a12*: N=6, * $p < 0.05$, student t-test.

○ Vehicle ● 20-HETE □ 20-HETE + AAA
 ■ 20-HETE + Y-27632 ▲ 20-HETE + AAA + Y-27632

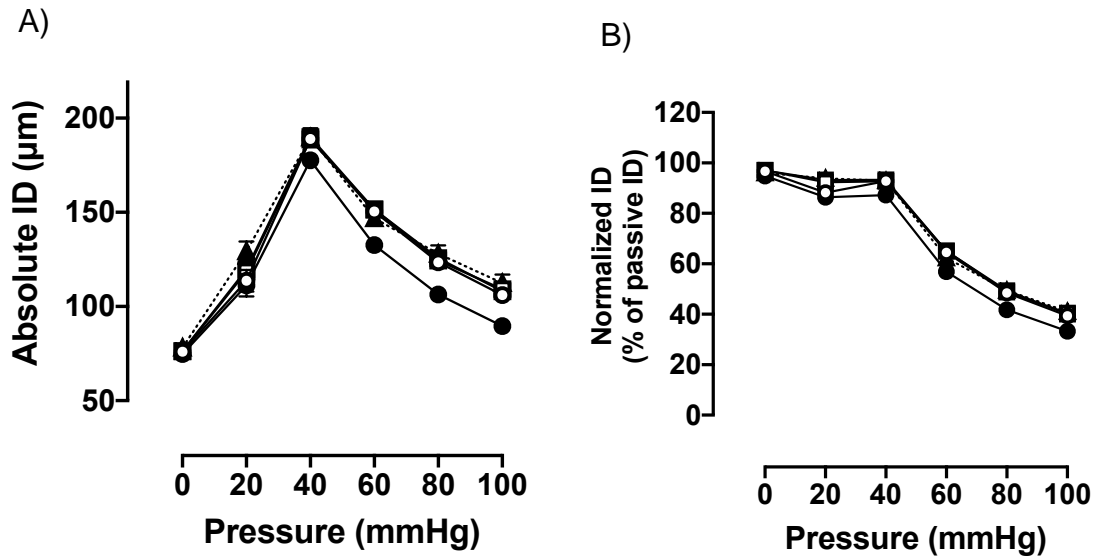


Figure 22: Addition of AAA or Y-27632 prevented 20-HETE-mediated increase in myogenic tone of RIA from WT mice.

A) absolute internal diameter (ID) and B) percent myogenic tone. Vehicle, 20-HETE only, 20-HETE + AAA, 20-HETE + Y-27632 – N= 6 mice, n=12 vessels; 20-HETE + AAA + Y-27632 – N = 4 mice, n=8 vessels.

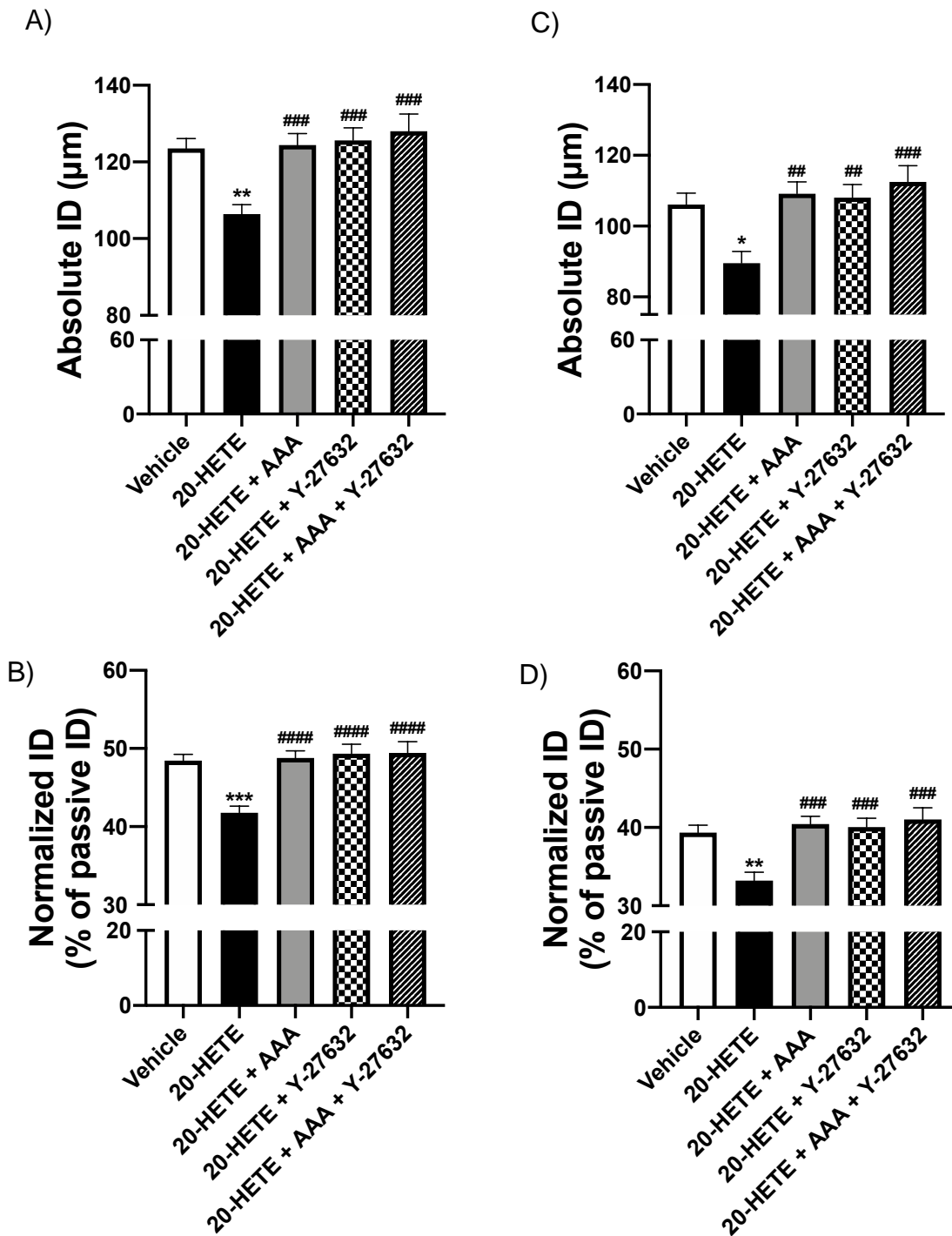


Figure 23: Absolute internal diameter (ID) and percent myogenic tone values of WT RIA at 80mmHg and 100mmHg.

A) absolute and B) normalized ID at 80 mmHg and C) absolute and D) normalized ID at 100 mmHg. Vehicle, 20-HETE only, 20-HETE + AAA, 20-HETE + Y-27632 – N = 6 mice, n=12 vessels; 20-HETE + AAA + Y-27632 – N = 4 mice, n=8 vessels. *p<0.05, **p<0.01, ***p<0.001 vs vehicle treated. ##p<0.01, ###p<0.001 vs 20-HETE treated one-way ANOVA.

Discussion

The present study provides evidence to show the actions of 20-HETE within the vascular smooth muscle cell to promote hypertension and vascular dysfunction. The main findings of this study include: 1) vascular smooth muscle-specific overexpression of *Cyp4a12* and increased vascular production of 20-HETE was sufficient to promote increases in blood pressure and impairment in vascular function; 2) treatment with a novel, water-soluble 20-HETE receptor antagonist (AAA) reversed the pathology associated with 20-HETE overproduction; 3) elevated 20-HETE changes signaling within the VSMC and EC which was reversed with AAA treatment. The signaling mechanisms that were assessed were Rho-kinase-mediated myosin light chain phosphorylation and NO signaling.

The actions of 20-HETE within the vasculature have been extensively shown in animal models with global overproduction of 20-HETE. These models have consistently shown that increased 20-HETE within the vasculature promotes hypertension and vascular dysfunction. The limitation of using global models of 20-HETE production is the difficulty to dissect how 20-HETE within specific cell types contributes to changes in vascular function. The utilization of animal models with site-specific expression of 20-HETE can better show the mechanism in which 20-HETE produces changes in vascular function with a certain cell type.

In this study, the cre/flox system was utilized to target *Cyp4a12* overexpression to the smooth muscle cell. The reason for this approach of

Cyp4a12 overexpression was to overproduce 20-HETE in the primary site of synthesis (Harder *et al.*, 1994; Gebremedhin *et al.*, 1998). 20-HETE has been shown to produce effects within the VSMC to change blood pressure and vascular function *in vitro* and in models of global overproduction of 20-HETE. This is the first time that *Cyp4a12* was endogenously overexpressed in the VSMC to produce 20-HETE in a mouse.

The mouse model that was used in the present study was appropriate to assess the consequence of 20-HETE overproduction generated by the VSMC. The cre/lox system was used to target *Cyp4a12* production, specifically in the VSMC. The *Cyp4a12-flox* gene was constructed to have the regulatory unit of the gene flanked with the LoxP site. In the presence of cre-recombinase, the regulatory unit of the gene was removed to allow for unregulated production of *Cyp4a12* (Gilani *et al.*, 2020). *Cyp4a12-flox* expression was targeted to the VSMC by site-specific cre-recombinase production under the control of the smooth muscle-specific myosin heavy chain promoter (*Myh11-Cre*) (Xin *et al.*, 2002). This was evident when probing for *Cyp4a12* expression at the mRNA and protein level. In mesenteric and RIAs, there was significant increase in *Cyp4a12* mRNA expression compared to WT mice. There was also a significant increase in *Cyp4a* protein levels in the mesenteric artery compared to WT mice. These changes were not observed in the liver.

The result of the VSMC-specific overexpression of *Cyp4a12* was elevated 20-HETE levels. Elevated 20-HETE levels were observed in mesenteric arteries, RIA, and plasma; however, no change in 20-HETE was observed in urine. This

gives evidence that 20-HETE production is directed to the vessels, but the 20-HETE produced in the vessels can be found in circulating stores. Mice with elevated 20-HETE also had elevated systolic blood pressure and impairments in acetylcholine-induced relaxation. When performing western blots to reinforce the results from the *ex vivo* experiments in vessels, changes in eNOS expression in the aorta and serine 19 phospho-myosin light chain expression were also observed. Altogether, the results demonstrate that VSMC-specific *Cyp4a12* expression results in elevated 20-HETE and impairments in vascular activity, which contribute to changes in systolic blood pressure.

Global overexpression models of 20-HETE are shown to cause increases in blood pressure and impairment in vascular reactivity. One model of global overproduction of 20-HETE is the *Cyp4a14^{-/-}*-mouse. The *Cyp4a14^{-/-}*-mouse has global overexpression of *Cyp4a12*, the main 20-HETE-producing enzyme in mice, and its expression is driven by the androgen promoter. This mouse model resulted in elevated 20-HETE levels in male mice but not in female (Holla *et al.*, 2001). Increase in blood pressure and impairment in vascular reactivity are associated with elevated 20-HETE in these mice. In a report by Pandey *et al.* (2017), they showed that *Cyp4a14^{-/-}*-mice had increases in blood pressure and changes in phenylephrine-induced contraction that were reversed with a 20-HETE antagonist (Pandey *et al.*, 2017).

Another model of constitutive 20-HETE overproduction was the Tie2-CYP4F2-Tr mouse model. CYP4F2 is a major 20-HETE-producing enzyme in humans with CYP4F2 activity associated with hypertension (Ward *et al.*, 2008).

The investigators were interested in CYP4F2 expression within the vessels which may contribute to 20-HETE-dependent vascular pathology. In their report, they generated a mouse model that had *CYP4F2* expression controlled by the EC-specific Tie-2 promoter (Cheng *et al.*, 2014). These mice exhibit elevated CYP4F2 expression with corresponding 20-HETE elevation, specifically in the EC. There were no differences in blood pressure and acetylcholine-induced relaxation but there were differences in phenylephrine-induced contraction. Furthermore, the investigators showed a pro-angiogenic phenotype in the Tie2-CYP4F2-Tr mouse. This suggests that EC-specific CYP4F2 expression primarily drives changes in angiogenesis and changes in vascular function may be secondary to the actions of 20-HETE in the EC.

Each mouse model has its utilities when studying the mechanism of vascular impairment dependent on 20-HETE. The *Cyp4a14*^{-/-} mouse model is a good model for reliable, global 20-HETE overproduction (CC Wu *et al.*, 2013; Ding *et al.*, 2013; Pandey *et al.*, 2017). It has been used to identify the ability of 20-HETE to impair vascular function (Ding *et al.*, 2013; Pandey *et al.*, 2017). However, the limitation of using the *Cyp4a14*^{-/-} mouse is its inability to identify 20-HETE's action within specific tissue types to promote vascular impairments. The Tie2-CYP4F2-Tr is one model of 20-HETE overproduction within the EC. It has been documented that this mouse line was not able to produce any changes in blood pressure, but was able to promote a pro-angiogenic phenotype (Cheng *et al.*, 2014). Thus, there are limitations of using the Tie2-CYP4F2-Tr mouse when it comes to assessing mechanisms of blood pressure. In the present study, the

Myh11-4a12 mouse showed elevated 20-HETE levels in vessels which were associated with increases in blood pressure and impairments in vascular function. Thus, the different phenotypes observed with different mouse models of 20-HETE overproduction are influenced by the site of 20-HETE overproduction.

AAA was used to assess the dependence of 20-HETE on blood pressure, vascular reactivity and remodeling. In the present study, 12 days of AAA treatment was sufficient to lower blood pressure to a value similar to the wild type controls. Phenylephrine-induced contraction and acetylcholine-induced relaxation both were improved after 12 days of AAA treatment. *Ex vivo* experiments to assess AAA direct action on RIA showed that mice with *Cyp4a12* overexpression had improved relaxation compared to untreated mice, and no changes were observed in WT mice. Interestingly, when assessing vascular remodeling, only the media:lumen ratio was affected by AAA. Media thickness or cross-sectional area was unchanged after AAA treatment.

AAA has been documented as a 20-HETE receptor antagonist capable of lowering blood pressure in models of 20-HETE-dependent hypertension (Sedláková *et al.*, 2018). In a report by Sedláková *et al.* (2018), they used the Cyp1a1-Ren-2 rat model that has overproduction of 20-HETE and angiotensin II (Sedláková *et al.*, 2018). The investigators administered AAA for 12 days in the drinking water and they showed a significant reduction in systolic blood pressure compared to untreated hypertensive rats. The reduction in systolic blood pressure was accompanied by improved renal function. The spontaneous hypertensive rat is another model of hypertension that is 20-HETE-dependent.

Two reports showed that AAA treatment in the spontaneous hypertensive rat lowers blood pressure and improves renal function. In one report, AAA was administered IV and reductions in mean arterial blood pressure were observed (Walkowska *et al.*, 2021). The changes in mean arterial blood pressure were accompanied by improvements in renal blood flow. Another report using the spontaneous hypertensive rat administered AAA in the drinking water rather than IV. The authors reported reductions in systolic blood pressure after 36 days of AAA treatment, although the reduction was not significant compared to the hypertensive controls (Gawrys *et al.*, 2020). The reduction in systolic blood pressure was accompanied by improvements in renal function as assessed by reductions in albuminuria.

Fluid balance and sodium excretion was measured to determine if the blood pressure lowering effect of AAA had a renal component. Previous reports suggest that AAA was able to improve renal parameters which contributed to the lowering of blood pressure (Sedláková *et al.*, 2018; Gawrys *et al.*, 2020; Walkowska *et al.*, 2021). The goal of this experiment was to examine if AAA can affect sodium excretion and fluid balance in *Myh11-4a12* mice. The *Myh11-4a12* mice displayed no differences in 20-HETE levels in the urine compared to WT mice. Urine volume and sodium excretion were similar between WT and *Myh11-4a12* mice. AAA appeared to increase urine volume and sodium excretion in *Myh11-4a12* mice compared to *Myh11-4a12* mice on vehicle. Due to the similar values between WT and *Myh11-4a12* mice and the small sample size, no conclusions were made surrounding AAA and its effects across the kidney.

20-HETE within the kidney display effects to promote changes in blood pressure through regulation of salt and fluid handling. *In vivo* experiments have demonstrated 20-HETE's pro- and anti-hypertensive role in the kidney. In experiments that manipulate 20-HETE levels acutely, 20-HETE was shown to be antihypertensive. Elevated 20-HETE within the kidney inhibits Na⁺/K⁺-ATPase (Schwartzman *et al.*, 1985; Nowicki *et al.*, 1997), and NKCC2 (Amlal *et al.*, 1998; Ito and Roman, 1999). These actions facilitate the reduction of blood pressure through increased salt and fluid excretion. On the other hand, 20-HETE has been shown to elevate blood pressure through changes in renal blood flow and sodium reabsorption in animal models with 20-HETE-dependent hypertension. Animal models of 20-HETE-dependent hypertension include: 1) *Cyp4a14*^{-/-} (Quigley *et al.*, 2009; Pandey *et al.*, 2017), 2) *Cyp4a11* transgenic mouse (Savas *et al.*, 2016), 3) proximal tubule targeted *Cyp4a12* (*PT-4a12*) mouse (Gilani *et al.*, 2020). The *Cyp4a14*^{-/-} mouse display reductions in renal blood flow (Pandey *et al.*, 2017) and increase in activity of the sodium hydrogen exchanger (NHE₃) (Quigley *et al.*, 2009), both which promote sodium and fluid retention. In both the *Cyp4a11* transgenic and *PT-4a12* mouse, 20-HETE has been shown to increase expression of serum- and glucocorticoid-inducible kinase-1 (SGK-1) and increase activity of the sodium chloride exchanger (NCC) to increase sodium and fluid reabsorption (Savas *et al.*, 2016; Gilani *et al.*, 2020).

The differences in the actions of 20-HETE on renal function may be due to the acute vs chronic manipulations of 20-HETE levels. In the experimental models to address the anti-hypertensive actions of 20-HETE, experiments were

done on wild type animals (Schwartzman *et al.*, 1985; Nowicki *et al.*, 1997; Amlal *et al.*, 1998) or the Dahl salt-sensitive hypertensive rat (Ito and Roman, 1999). The changes in blood pressure have been induced either by exogenous administration of 20-HETE or pharmacological manipulations to endogenously increase 20-HETE. In mouse models with 20-HETE-dependent hypertension, 20-HETE is elevated in renal microvessels (CC Wu *et al.*, 2013) or urine (Gilani *et al.*, 2020). 20-HETE in these animal models are constitutively elevated and the prolonged 20-HETE exposure is associated with compensatory changes in renal blood flow and salt reabsorption resulting in hypertension.

The mechanism by which 20-HETE promotes smooth muscle cell contraction has been studied extensively. 20-HETE is able to inhibit the BK_{Ca}²⁺-channel to increase levels of intracellular calcium (Lauterbach *et al.*, 2002; Garcia *et al.*, 2017). This action has been shown to be dependent on 20-HETE binding to its receptor (GPR75) (Garcia *et al.*, 2017). 20-HETE can increase activity of Rho-kinase promoting the sensitization of smooth muscle cells to contraction (Randriamboavonjy *et al.*, 2003). However, there are no current reports to suggest that this action is mediated by the 20-HETE receptor.

Vascular smooth muscle cells have a unique property in which they can display one of two phenotypes. On one hand, they can exhibit a synthetic phenotype in which VSMC are capable of synthesizing proteins to induce migration and proliferation (D Stec *et al.*, 2007; Orozco *et al.*, 2013). On the other hand, VSMC can exhibit a contractile phenotype. The phenotype in which the VSMC is exhibiting can be shown through measurements of VSMC differentiation

markers. The markers used for the determination of the VSMC phenotype are: *Myh11*, *Tagln*, and *Acta2* (Frismantiene *et al.*, 2018). If the VSMC is exhibiting a synthetic phenotype, the expression of VSMC markers should be lower compared to controls. If the VSMC is exhibiting a contractile phenotype, the markers should be elevated compared to controls. The present study suggests that the *Myh11-4a12* mice vessels are in a contractile phenotype (Frismantiene *et al.*, 2018). Markers of VSMC differentiation were measured and mRNA levels of *Myh11*, *Tagln*, and *Acta2* were all elevated compared to wild type mice. The elevated markers of VSMC differentiation suggest that there are more cells that are capable of contraction.

To assess the cellular signaling involved in VSMC contraction, phosphorylation of myosin light chain (MLC) at serine 19 was performed. Phosphorylation of MLC is the downstream signaling event that needs to occur before excitation contraction coupling can occur in the VSMC (Driska *et al.*, 1981). Two reasons why MLC can remain phosphorylated include: 1) increase intracellular calcium promoting increase MLCK activity (Raina *et al.*, 2009) and/or 2) activation of ROCK signaling which inhibits myosin phosphatase and prevents the dephosphorylation of MLC (Noma *et al.*, 2012). In the current study, ROCK expression and activity were assessed because it has not been determined if 20-HETE-mediated changes in ROCK activity is receptor mediated.

Myh11-4a12 mice had elevated phosphorylation levels compared to wild type and AAA treatment was able to reduce it. This suggests that myosin light chain phosphorylation is dependent on the 20-HETE receptor. ROCK1 protein

levels were measured and *Myh11-4a12* mice treated with either vehicle or AAA had elevated levels compared to wild type animals. This indicates that ROCK1 expression is not dependent on the 20-HETE receptor. If the 20-HETE receptor is not affecting ROCK expression, it may affect ROCK activity. *Ex vivo* experiments were performed in wild type mice to assess the mechanism in which 20-HETE increases myogenic tone. The current report shows that 20-HETE shifts the internal diameter curve downward, suggesting an increase in myogenic tone. Co-administration of 20-HETE plus AAA or Rho-kinase inhibitor (Y-27632) shift the internal diameter curve upward similar to control values. Finally, co-treatment of 20-HETE with AAA and Y-27632 had no further changes in myogenic tone. This suggests that Rho-kinase activity is acting downstream of the 20-HETE receptor to promote changes in the myogenic response.

The finding above is similar to that in the report by Randriamboavonjy *et al.* (2003). They determined that 20-HETE was capable of inducing contraction in small coronary arteries. Furthermore, they showed that small coronary arteries treated with 20-HETE had increased phosphorylation of MLC (Randriamboavonjy *et al.*, 2003). The 20-HETE-induced phosphorylation of MLC was prevented with Y-27632 treatment. The findings from Randriamboavonjy study and the results from the present study suggests 20-HETE, through its receptor, is capable of promoting Rho-kinase activity, and allows for MLC phosphorylation, promoting VSMC contraction.

Treatment of *Myh11-4a12* mice with AAA was unable to reverse the remodeling phenotype in these mice. Media thickness and cross-sectional area

remained elevated after 12 days of AAA therapy. In addition, Myh11 protein expression was also unaffected with AAA treatment. In this model of 20-HETE overexpression, VSMCs are in the contractile phenotype rather than the synthetic. This was shown when comparing expression to smooth muscle-specific differentiation markers. *Myh11-4a12* had elevated *Myh11*, *Tagln* and *Acta2* mRNA expression compared to wild types. If the VSMC were in a synthetic state, there should have been a reduction in the VSMC differentiation markers compared to WT mice (Frismantiene *et al.*, 2018). The mouse model used in this experiment was a constitutive overexpression of *Cyp4a12*. It is possible that the proliferative phenotype occurred early in development and then switched to a contractile phenotype once the mouse reached adulthood.

In other models of 20-HETE overexpression, the use of 20-HETE antagonists was able to prevent the remodeling phenotype (Ding *et al.*, 2013; Garcia, *et al.*, (2015b)). In these experimental models, 20-HETE was induced by DHT and was treated with a 20-HETE antagonist at the same time. Pharmacological antagonism of 20-HETE can prevent vascular remodeling in 20-HETE-dependent models; however, 20-HETE antagonism may not be able to reverse remodeling after it has been established. Further studies will have to be performed to understand the mechanisms in which 20-HETE induces VSMC proliferation.

Another finding in the present study was that *Myh11-4a12* mice had impairment in NO signaling. When assessing phosphorylation of eNOS at Serine 1177 in the aorta, *Myh11-4a12* mice had lower phosphorylated eNOS levels

compared to wild type. The change in phosphorylated eNOS levels was attributed to a reduction in total eNOS expression in aorta. This observation was also shown in a rat model with endothelial specific *Cyp4a2* overexpression (Inoue *et al.*, 2009). The changes in phosphorylated eNOS expression in mesenteric arteries were attributed to changes in eNOS activity. Regardless, the reduction in eNOS phosphorylation will result in decreased NO bioavailability. The differences in changes in eNOS phosphorylation may be due to differences that can be observed in different vascular beds (Aird, 2007). *Myh11-4a12* mice treated with AAA had elevated phosphorylated eNOS expression in both aorta and mesenteric arteries. Thus, changes in eNOS activation are due to 20-HETE acting through its receptor.

The changes in eNOS phosphorylation were also accompanied by changes in VASP phosphorylation. VASP is a protein within the smooth muscle that is activated by PKG. Activation of PKG requires NO from the EC to diffuse to the VSMC to activate soluble guanylyl cyclase and increase cGMP. Thus, it can be used as a marker for NO signaling occurring within the VSMC (Oelze *et al.*, 2000). In aortas of *Myh11-4a12* mice, there was a significant reduction of phosphorylated VASP compared to wild type. However, 12-day AAA therapy was not able to increase phosphorylated VASP in *Myh11-4a12* mice. This result implies that other mechanisms may be present to reduce NO bioavailability that are unaffected by AAA treatment.

At baseline values, *Myh11-4a12* had impaired acetylcholine-induced relaxation that was restored when vessels were treated with sodium nitroprusside

(NO donor). This gives evidence that *Myh11-4a12* mice have impairments in NO mediated vasodilation. One explanation that was shown in the present study was that eNOS activation was reduced. Another action that may have occurred is the increased production ROS. 20-HETE has been shown to increase ROS in both endothelium and VSMCs (Guo *et al.*, 2007; Lakhkar *et al.*, 2016). The generation of ROS can sequester NO away from the VSMC and prevent the activation of PKG.

Within the EC and VSMC, 20-HETE has been documented to display different mechanisms in ROS generation. 20-HETE was shown to increase NADPH oxidase activity in pulmonary EC (Medhora *et al.*, 2008); however, 20-HETE in human umbilical vein EC and human microvascular EC display NADPH oxidase-independent ROS generation (Guo *et al.*, 2007). 20-HETE was also shown to generate ROS in VSMC by promoting increased superoxide production by the mitochondria (Lakhkar *et al.*, 2016). The differences in cell-specific mechanism of ROS generation may explain why increases in eNOS phosphorylation after AAA was not accompanied by increased VASP phosphorylation. It is possible that AAA was not able to ameliorate all the ROS-generating effects of 20-HETE. Future studies will have to be performed in order to assess the mechanism of ROS generation in *Myh11-4a12* mice and whether AAA is capable of changing ROS amounts.

This study provides evidence that 20-HETE, through its receptor, is capable of increasing blood pressure and promoting changes in small artery vascular activity. One limitation of this study is that it cannot conclude that 20-

HETE is acting through GPR75 to promote smooth muscle contraction. There are no current reports showing direct binding of AAA to GPR75; however, work is being done to show that AAA binds to GPR75 (unpublished data). The relevance of GPR75 can be assessed by using siRNA capable of downregulating GPR75 expression. In the report by Garcia and colleagues (2017), they used siRNA to downregulate GPR75 expression in the vessels which promoted reductions in blood pressure and improvement in vascular reactivity. Furthermore, they showed that knock down of GPR75 reduced phosphorylation of the BK_{Ca}²⁺-channel which inhibits the activity of the transporter (Garcia *et al.*, 2017). Similar approaches can be used to assess the relevance of GPR75 on Rho-kinase activity. Furthermore, there are GPR75 global knockout and GPR75-flox mice that are available to further dissect the mechanisms in which GPR75 is involved.

A second limitation of this study was that the mouse model used was a constitutive overexpression of *Cyp4a12*. Due to this, it cannot be determined whether 20-HETE is causing increases in blood pressure that promotes vascular remodeling or if 20-HETE is causing remodeling followed by increases in blood pressure. In one report, the investigators suggest that remodeling in vessels is independent in changes of blood pressure. 20-HETE overproduction was induced by DHT treatment and, in order to mitigate the increase in blood pressure, reserpine was administered (Ding *et al.*, 2013). Mice treated with both DHT and reserpine experienced vascular remodeling without increases in blood pressure. The utilization of an inducible model of *Cyp4a12* expression in the VSMC may be able to show 20-HETE's contribution on blood pressure and

vascular remodeling. There is a mouse line with cre-recombinase expression targeted in the VSMC that is inducible with tamoxifen treatment (Wirth *et al.*, 2008). Similar experiments can be performed in which mice can be co-administered tamoxifen and AAA to determine if 20-HETE receptor antagonism can prevent remodeling in resistant vessels with *Cyp4a12* overexpression. Furthermore, AAA can be administered after tamoxifen-induced *Cyp4a12* expression to determine if 20-HETE receptor antagonism can reverse the remodeling phenotype (Gilani *et al.*, 2018). From these treatment groups, more insight can be obtained with regards to 20-HETE receptor-mediated actions to alter VSMC remodeling.

Future experiments can be done to determine if AAA can reverse vascular remodeling. Twelve-day AAA treatment was not able to decrease RIA media thickness and cross-sectional area. One reason for AAA's inability to reverse vascular remodeling is that the duration of treatment was too short to produce an effect. Vascular remodeling is a complex process that involves the production of new proteins to form a viable cell. These changes may take longer periods of time to produce a measurable effect. In addition, the VSMC that are present may take time to undergo apoptosis to reduce the number of cells within the vessel wall. There may be several mechanisms by which 20-HETE receptor antagonism can change signaling to inhibit VSMC proliferation.

Another explanation in which AAA was unable to reverse the vascular remodeling phenotype may be due to 20-HETE promoting hypertrophy in addition to or rather than proliferation. 20-HETE has been documented to

promote hypertrophy in cardiomyocytes that contributes to heart failure in experimental animals (El-Kadi and Zordoky, 2008; Zordoky *et al.*, 2008). There are no reports to suggest that 20-HETE can contribute to hypertrophy in resistant vessels. It is possible that 20-HETE can promote hypertrophy due to its ability to increase ACE expression and activity followed by increased Ang II (Cheng *et al.*, 2012; Garcia *et al.*, 2016). Furthermore, 20-HETE has been documented to activate mitogenic signaling that can also contribute to VSMC hypertrophy (Uddin *et al.*, 1998; Muthalif *et al.*, 2001). Further experimentation can be performed to assess 20-HETE action to promote hypertrophy and to determine if AAA is able to prevent it.

Perspective and Significance

Hypertension is a global burden of which approximately one fourth of the world population is diagnosed. Hypertension is a risk factor for several diseases including myocardial infarction, stroke, and renal failure. Although therapies are present such as ACE inhibitors/ARBs, diuretics and beta-blockers to control blood pressure there is a percentage of the population that do not respond to these therapies. Thus, there is a need to identify novel mechanisms that can be probed to improve blood pressure.

20-HETE has been extensively studied and consistently shows its role in blood pressure regulation. Actions include: 1) endothelial dysfunction, 2) elevated sodium reuptake; 3) VSMC contraction and proliferation. The multifaceted actions of 20-HETE on blood pressure make it an ideal target for blood pressure control. The use of pharmacological tools to either reduce the synthesis or inhibit the action of 20-HETE have shown positive effects on blood pressure and vascular function. What was not known until recently was how 20-HETE was able to initiate its downstream effects in the cell. The work of Garcia and colleagues (2017) was the first report to identify GPR75 as the receptor for 20-HETE. Identification of a novel GPCR for 20-HETE make it an attractive target for pharmacological manipulations. Future studies will be performed to fully characterize the actions of 20-HETE on blood pressure and vascular function through GPR75.

References

- Aird WC (2007) Phenotypic heterogeneity of the endothelium: II. Representative vascular beds. *Circ Res* **100**:174–190.
- Amlal H, Legoff C, Vernimmen C, Paillard M, and Bichara M (1996) Na⁺-K⁺(NH₄⁺)-2Cl⁻ cotransport in medullary thick ascending limb: Control by PKA, PKC, and 20-HETE. *Am J Physiol - Cell Physiol* **271**:C455–C463.
- Amlal H, Legoff C, Vernimmen C, Soleimani M, Paillard M, and Bichara M (1998) ANG II controls Na-K (NH₄⁺)-2Cl⁻ cotransport via 20-HETE and PKC in medullary thick ascending limb. *Am J Physiol - Cell Physiol* **274**:C1047–C1056.
- Capdevila JH, and Falck JR (2000) Biochemical and molecular characteristics of the cytochrome P450 arachidonic acid monooxygenase. *Prostaglandins Other Lipid Mediat* **62**:271–292.
- Cárdenas S, Colombero C, Panelo L, Dakarapu R, Falck JR, Costas MA, and Nowicki S (2020) GPR75 receptor mediates 20-HETE-signaling and metastatic features of androgen-insensitive prostate cancer cells. *Biochim Biophys Acta - Mol Cell Biol Lipids* **1865**:1–14.
- Carroll, M. A., Sala, A., Dunn, C.E., McGiff, J.C. and MRC (1991) Structural identification of cytochrome P450-dependent arachidonate metabolites formed by rabbit medullary thick ascending limb cells. *J Biol Chem* **226**:12306–12312.
- CDC (2020) High Blood Pressure Symptoms and Causes | cdc.gov.
- Chen L, Ackerman R, Saleh M, Gotlinger KH, Kessler M, Mendelowitz LG, Falck JR, Arbab AS, Scicli AG, Schwartzman ML, Yang J, and Guo AM (2014) 20-HETE regulates the angiogenic functions of human endothelial progenitor cells and contributes to angiogenesis in vivo. *J Pharmacol Exp Ther* **348**:442–451.
- Chen L, Joseph G, Zhang FF, Nguyen H, Jiang H, Gotlinger KH, Falck JR, Yang J, Schwartzman ML, and Guo AM (2016) 20-HETE contributes to ischemia-induced angiogenesis. *Vascul Pharmacol* **83**:57–65.
- Cheng J, Edin ML, Hoopes SL, Li H, Bradbury JA, Graves JP, DeGraff LM, Lih FB, Garcia V, Shaik JSB, Tomer KB, Flake GP, Falck JR, Lee CR, Poloyac SM, Schwartzman ML, and Zeldin DC (2014) Vascular characterization of mice with endothelial expression of cytochrome P450 4F2. *FASEB J* **28**:2915–2931.

- Cheng J, Garcia V, Ding Y, Wu C-C, Thakar K, Falck JR, Ramu E, and Schwartzman ML (2012) Induction of angiotensin-converting enzyme and activation of the renin-angiotensin system contribute to 20-hydroxyeicosatetraenoic acid-mediated endothelial dysfunction. *Arterioscler Thromb Vasc Biol* **32**:1917–24.
- Cheng J, Ou J-S, Singh H, Falck JR, Narsimhaswamy D, Pritchard KA, and Schwartzman ML (2008) 20-Hydroxyeicosatetraenoic acid causes endothelial dysfunction via eNOS uncoupling. *Am J Physiol - Circ Physiol* **294**:H1018–H1026.
- Cheng J, Wu C-C, Gotlinger KH, Zhang F, Falck JR, Narsimhaswamy D, and Schwartzman ML (2010) 20-hydroxy-5,8,11,14-eicosatetraenoic acid mediates endothelial dysfunction via I κ B kinase-dependent endothelial nitric-oxide synthase uncoupling. *J Pharmacol Exp Ther* **332**:57–65.
- Christmas P, Jones JP, Patten CJ, Rock DA, Zheng Y, Cheng S-M, Weber BM, Carlesso N, Scadden DT, Rettie AE, and Soberman RJ (2001) Alternative Splicing Determines the Function of CYP4F3 by Switching Substrate Specificity*. *J Biol Chem* **276**:38166–72.
- Chuang SS, Helvig C, Taimi M, Ramshaw HA, Collop AH, Amad M, White JA, Petkovich M, Jones G, and Korczak B (2004) CYP2U1, a Novel Human Thymus- and Brain-specific Cytochrome P450, Catalyzes ω - and (ω -1)-Hydroxylation of Fatty Acids. *J Biol Chem* **279**:6305–6314.
- Costa TJ, Ceravolo GS, Echem C, Hashimoto CM, Costa BP, Santos-Eichler RA, Oliveira MA, Jiménez-Altayó F, Akamine EH, Dantas AP, and Carvalho MHC (2018) Detrimental effects of testosterone addition to estrogen therapy involve cytochrome P-450-induced 20-HETE synthesis in aorta of ovariectomized spontaneously hypertensive rat (SHR), a model of postmenopausal hypertension. *Front Physiol* **9**:1–13.
- Croft KD, McGiff JC, Sanchez-Mendoza A, and Carroll MA (2000) Angiotensin II releases 20-HETE from rat renal microvessels. *Am J Physiol - Renal Physiol* **279**:F544–F551.
- Cushman WC, Ford CE, Cutler JA, Margolis KL, Davis BR, Grimm RH, Black HR, Hamilton BP, Holland J, Nwachuku C, Papademetriou V, Probstfield J, Wright JT, Alderman MH, Weiss RJ, Piller L, Bettencourt J, and Walsh SM (2002) Success and predictors of blood pressure control in diverse North American settings: The antihypertensive and lipid-lowering treatment to prevent heart attack trial (ALLHAT). *J Clin Hypertens* **4**:393–404.

- Davis MJ, Meininger GA, and Zawieja DC (1992) Stretch-induced increases in intracellular calcium of isolated vascular smooth muscle cells. *Am J Physiol - Hear Circ Physiol* **263**:32–4.
- Dedoni S, Campbell LA, Harvey BK, Avdoshina V, and Mocchetti I (2018) The orphan G-protein-coupled receptor 75 signaling is activated by the chemokine CCL5. *J Neurochem* **146**:526–539.
- Ding Y, Wu C-C, Garcia V, Dimitrova I, Weidenhammer A, Joseph G, Zhang F, Manthati VL, Falck JR, Capdevila JH, and Schwartzman ML (2013) 20-HETE induces remodeling of renal resistance arteries independent of blood pressure elevation in hypertension. *Am J Physiol - Renal Physiol* **305**:F753–F763.
- Driska SP, Aksoy MO, and Murphy RA (1981) Myosin light chain phosphorylation associated with contraction in arterial smooth muscle. *Am J Physiol - Cell Physiol* **9**:C222-233.
- Dunn KM, Renic M, Flasch AK, Harder DR, Falck J, Roman Richard J, and Roman R J (2008) Elevated production of 20-HETE in the cerebral vasculature contributes to severity of ischemic stroke and oxidative stress in spontaneously hypertensive rats. *Am J Physiol - Hear Circ Physiol* **295**:2455–2465.
- El-Kadi A, and Zordoky B (2008) Modulation of Cardiac and Hepatic Cytochrome P450 Enzymes During Heart Failure. *Curr Drug Metab* **9**:122–128.
- Escalante B, Erlij D, Falck JR, and McGiff JC (1994) Cytochrome P-450 arachidonate metabolites affect ion fluxes in rabbit medullary thick ascending limb. *Am J Physiol - Cell Physiol* **266**:C1775-1782.
- Escalante B, Erlij D, Falck JR, and McGiff JC (1991) Effect of cytochrome P450 arachidonate metabolites on ion transport in rabbit kidney loop of Henle. *Science* **251**:799–802.
- Fan F, Sun C-W, Maier KG, Williams JM, Pabbidi MR, Didion SP, Falck JR, Zhuo J, and Roman RJ (2013) 20-Hydroxyecosatetraenoic Acid Contributes to the Inhibition of K⁺ Channel Activity and Vasoconstrictor Response to Angiotensin II in Rat Renal Microvessels. *PLoS One* **8**:1–20.
- Fishel RS, Eisenberg S, Shai S-Y, Redden RA, Bernstein KE, and Berk BC (1995) Glucocorticoids Induce Angiotensin-Converting Enzyme Expression in Vascular Smooth Muscle. *Hypertension* **25**:343–349.

- Frismantiene A, Philippova M, Erne P, and Resink TJ (2018) Smooth muscle cell-driven vascular diseases and molecular mechanisms of VSMC plasticity. *Cell Signal* **52**:48–64.
- Garcia V, Cheng J, Weidenhammer A, Ding Y, Wu CC, Zhang F, Gotlinger K, Falck JR, and Schwartzman ML (2015) Androgen-induced hypertension in angiotensinogen deficient mice: Role of 20-HETE and EETS. *Prostaglandins Other Lipid Mediat* **116–117**:124–130.
- Garcia V, Gilani A, Shkolnik B, Pandey V, Zhang FF, Dakarapu R, Gandham SK, Reddy NR, Graves JP, Gruzdev A, Zeldin DC, Capdevila JH, Falck JR, and Schwartzman ML (2017) 20-HETE Signals Through G-Protein–Coupled Receptor GPR75 (G_q) to Affect Vascular Function and Trigger Hypertension. *Circ Res* **120**:1776–1788.
- Garcia V, Joseph G, Shkolnik B, Ding Y, Zhang FF, Gotlinger K, Falck JR, Dakarapu R, Capdevila JH, Bernstein KE, and Schwartzman ML (2015) Angiotensin II receptor blockade or deletion of vascular endothelial ACE does not prevent vascular dysfunction and remodeling in 20-HETE-dependent hypertension. *Am J Physiol - Integr Comp Physiol* **309**:R71–R78.
- Garcia V, Shkolnik B, Milhau L, Falck JR, and Schwartzman ML (2016) 20-HETE Activates the Transcription of Angiotensin-Converting Enzyme via Nuclear Factor-κB Translocation and Promoter Binding. *J Pharmacol Exp Ther* **356**:525–33.
- Gawrys O, Husková Z, Baranowska I, Walkowska A, Sadowski J, Kikerlová S, Vaňourková Z, Honetschlägerová Z, Škaroupková P, Červenka L, Falck JR, Imig JD, and Kompanowska-Jeziarska E (2020) Combined treatment with epoxyeicosatrienoic acid analog and 20-hydroxyeicosatetraenoic acid antagonist provides substantial hypotensive effect in spontaneously hypertensive rats. *J Hypertens* **38**:1802–1810.
- Gebremedhin D, Lange AR, Lowry TF, Taheri MR, Birks EK, Hudetz AG, Narayanan J, Falck JR, Okamoto H, Roman RJ, Nithipatikom K, Campbell WB, and Harder DR (2000) Production of 20-HETE and Its Role in Autoregulation of Cerebral Blood Flow. *Circ Res* **87**:60–65.
- Gebremedhin D, Lange AR, Narayanan J, Aebly MR, Jacobs ER, and Harder DR (1998) Cat cerebral arterial smooth muscle cells express cytochrome P450 4A2 enzyme and produce the vasoconstrictor 20-HETE which enhances L-type Ca²⁺ current. *J Physiol* **507**:771–781.

- Gilani A, Agostinucci K, Hossain S, Pascale J V., Garcia V, Adebessin AM, Falck JR, and Schwartzman ML (2021) 20-HETE Interferes with Insulin Signaling and Contributes to Obesity-Driven Insulin Resistance. *Prostaglandins Other Lipid Mediat* **152**:1–10.
- Gilani A, Agostinucci K, Pascale J V., Hossain S, Kandhi S, Pandey V, Garcia V, Nasjletti A, and Laniado Schwartzman M (2020) Proximal tubule-targeted overexpression of the Cyp4a12-20-HETE synthase promotes salt-sensitive hypertension in male mice. *Am J Physiol - Integr Comp Physiol* **319**:R87–R95.
- Gilani A, Pandey V, Garcia V, Agostinucci K, Singh SP, Schragenheim J, Bellner L, Falck JR, Paudyal MP, Capdevila JH, Abraham NG, and Laniado Schwartzman M (2018) High-fat diet-induced obesity and insulin resistance in CYP4a14 ^{-/-} mice is mediated by 20-HETE. *Am J Physiol - Integr Comp Physiol* **315**:R934–R944.
- Gonzalez-Fernandez E, Staursky D, Lucas K, Nguyen B V., Li M, Liu Y, Washington C, Coolen LM, Fan F, and Roman RJ (2020) 20-HETE Enzymes and Receptors in the Neurovascular Unit: Implications in Cerebrovascular Disease. *Front Neurol* **11**:1–19.
- Gosmanova EO, Mikkelsen MK, Molnar MZ, Lu JL, Yessayan LT, Kalantar-Zadeh K, and Kovesdy CP (2016) Association of Systolic Blood Pressure Variability With Mortality, Coronary Heart Disease, Stroke, and Renal Disease. *J Am Coll Cardiol* **68**:1375–1386.
- Guo AM, Arbab AS, Falck JR, Chen P, Edwards PA, Roman RJ, and Scicli AG (2007) Activation of vascular endothelial growth factor through reactive oxygen species mediates 20-hydroxyeicosatetraenoic acid-induced endothelial cell proliferation. *J Pharmacol Exp Ther* **321**:18–27.
- Guo AM, Scicli G, Sheng J, Falck JC, Edwards PA, and Scicli AG (2009) 20-HETE can act as a nonhypoxic regulator of HIF-1 α in human microvascular endothelial cells. *Am J Physiol - Circ Physiol* **297**:H602–H613.
- Harder DR, Gebremedhin D, Narayanan J, Jefcoat C, Falck JR, Campbell WB, and Roman R (1994) Formation and action of a P-450 4A metabolite of arachidonic acid in cat cerebral microvessels. *Am J Physiol - Hear Circ Physiol* **266**:H2098-2107.
- Hardwick JP (2008) Cytochrome P450 omega hydroxylase (CYP4) function in fatty acid metabolism and metabolic diseases. *Biochem Pharmacol* **75**:2263–2275.

- Hercule HC, and Oyekan AO (2000) Cytochrome P450 */*-1 Hydroxylase-Derived Eicosanoids Contribute to Endothelin A and Endothelin B Receptor-Mediated Vasoconstriction to Endothelin-1 in the Rat Preglomerular Arteriole 1. *J Pharmacol Exp Ther* **292**:1153–1160.
- Holla VR, Adas F, Imig JD, Zhao X, Price E, Olsen N, Kovacs WJ, Magnuson MA, Keeney DS, Breyer MD, Falck JR, Waterman MR, and Capdevila JH (2001) Alterations in the regulation of androgen-sensitive Cyp 4a monooxygenases cause hypertension. *Proc Natl Acad Sci U S A* **98**:5211–5216.
- Huang Z, Jiang Y, and Zhou Y (2020) The role of cytochrome P450 gene rs1126742 polymorphism and risk of hypertension: A systematic review and meta-analysis. *Biosci Rep* **40**:1–10.
- Ignatov A, Robert J, Gregory-Evans C, and Schaller HC (2006) RANTES stimulates Ca²⁺ mobilization and inositol trisphosphate (IP₃) formation in cells transfected with G protein-coupled receptor 75. *Br J Pharmacol* **149**:490–497.
- Inoue K, Sodhi K, Puri N, Gotlinger KH, Cao J, Rezzani R, Falck JR, Abraham NG, and Laniado-Schwartzman M (2009) Endothelial-specific CYP4A2 overexpression leads to renal injury and hypertension via increased production of 20-HETE. *Am J Physiol - Renal Physiol* **297**:F875–F884.
- Ishizuka T, Cheng J, Singh H, Vitto MD, Manthati VL, Falck JR, and Laniado-Schwartzman M (2008) 20-Hydroxyeicosatetraenoic acid stimulates nuclear factor-κB activation and the production of inflammatory cytokines in human endothelial cells. *J Pharmacol Exp Ther* **324**:103–110.
- Ito O, and Roman RJ (1999) Role of 20-HETE in elevating chloride transport in the thick ascending limb of Dahl SS/Jr rats. *Hypertension* **33**:419–423.
- Joseph G, Soler A, Hutcheson R, Hunter I, Bradford C, Hutcheson B, Gotlinger KH, Jiang H, Falck JR, Proctor S, Schwartzman ML, and Rocic P (2017) Elevated 20-HETE impairs coronary collateral growth in metabolic syndrome via endothelial dysfunction. *Am J Physiol - Hear Circ Physiol* **312**:H528–H540.
- Kaide JI, Zhang F, Wei Y, Wang WH, Gopal VR, Falck JR, Laniado-Schwartzman M, and Nasjletti A (2004) Vascular CO counterbalances the sensitizing influence of 20-HETE on agonist-induced vasoconstriction. *Hypertension* **44**:210–216.

- Kalyankrishna S, and Malik KU (2003) Norepinephrine-induced stimulation of p38 mitogen-activated protein kinase is mediated by arachidonic acid metabolites generated by activation of cytosolic phospholipase A2 in vascular smooth muscle cells. *J Pharmacol Exp Ther* **304**:761–772.
- Laffer CL, Gainer J V., Waterman MR, Capdevila JH, Laniado-Schwartzman M, Nasjletti A, Brown NJ, and Elijovich F (2008) The T8590C polymorphism of CYP4A11 and 20-hydroxyeicosatetraenoic acid in essential hypertension. *Hypertension* **51**:767–772.
- Laffer CL, Laniado-Schwartzman M, Wang MH, Nasjletti A, and Elijovich F (2003) Differential regulation of natriuresis by 20-hydroxyeicosatetraenoic acid in human salt-sensitive versus salt-resistant hypertension. *Circulation* **107**:574–578.
- Lai G, Wu J, Liu X, and Zhao Y (2012) 20-HETE Induces Hyperglycemia through the cAMP/PKA-PhK-GP Pathway. *Mol Endocrinol* **26**:1907–1916.
- Lakhkar A, Dhagia V, Joshi SR, Gotlinger K, Patel D, Sun D, Wolin MS, Schwartzman ML, and Gupte SA (2016) 20-HETE-induced mitochondrial superoxide production and inflammatory phenotype in vascular smooth muscle is prevented by glucose-6-phosphate dehydrogenase inhibition. *Am J Physiol - Circ Physiol* **310**:H1107–H1117.
- Lasker JM, Chen WB, Wolf I, Bloswick BP, Wilson PD, and Powell PK (2000) Formation of 20-hydroxyeicosatetraenoic acid, a vasoactive and natriuretic eicosanoid, in human kidney. Role of CYP4F2 and CYP4A11. *J Biol Chem* **275**:4118–4126.
- Lauterbach B, Barbosa-Sicard E, Wang M-H, Honeck H, Kärgel E, Theuer J, Schwartzman ML, Haller H, Luft FC, Gollasch M, and Schunck W-H (2002) Cytochrome P450-Dependent Eicosapentaenoic Acid Metabolites Are Novel BK Channel Activators. *Hypertension* **39**:609–613
- Li JS, Larivière R, and Schiffrin EL (1994) Effect of a nonselective endothelin antagonist on vascular remodeling in deoxycorticosterone acetate-salt hypertensive rats: Evidence for a role of endothelin in vascular hypertrophy. *Hypertension* **24**:183–188.
- Li X, Zhao G, Ma B, Li R, Hong J, Liu S, and Wang DW (2014) 20-Hydroxyeicosatetraenoic acid impairs endothelial insulin signaling by inducing phosphorylation of the insulin receptor substrate-1 at Ser 616. *PLoS One* **9**:1–10.

- Lin F, Rios A, Falck JR, Belosludtsev Y, and Schwartzman ML (1995) 20-hydroxyeicosatetraenoic acid is formed in response to EGF and is a mitogen in rat proximal tubule. *Am J Physiol - Ren Fluid Electrolyte Physiol* **269**:F806–F816.
- Liu B, Hassan Z, Amisten S, King AJ, Bowe JE, Huang GC, Jones PM, and Persaud SJ (2013) The novel chemokine receptor, G-protein-coupled receptor 75, is expressed by islets and is coupled to stimulation of insulin secretion and improved glucose homeostasis. *Diabetologia* **56**:2467–2476.
- Medhora M, Chen Y, Gruenloh S, Harland D, Bodiga S, Zielonka J, Gebremedhin D, Gao Y, Falck JR, Anjaiah S, and Jacobs ER (2008) 20-HETE increases superoxide production and activates NAPDH oxidase in pulmonary artery endothelial cells. *Am J Physiol - Cell Mol Physiol* **294**:L902–L911.
- Muller DN, Schmidt C, Barbosa-Sicard E, Wellner M, Gross V, Hercule H, Markovic M, Honeck H, Luft FC, and Schunck WH (2007) Mouse Cyp4a isoforms: Enzymatic properties, gender- and strain-specific expression, and role in renal 20-hydroxyeicosatetraenoic acid formation. *Biochem J* **403**:109–118.
- Muthalif MM, Benter IF, Uddin MR, and Malik KU (1996) Calcium/calmodulin-dependent protein kinase II α mediates activation of mitogen-activated protein kinase and cytosolic phospholipase A2 in norepinephrine-induced arachidonic acid release in rabbit aortic smooth muscle cells. *J Biol Chem* **271**:30149–30157.
- Muthalif MM, Uddin MR, Fatima S, Parmentier JH, Khandekar Z, and Malik KU (2001) Small GTP binding protein Ras contributes to norepinephrine-induced mitogenesis of vascular smooth muscle cells. *Prostaglandins Other Lipid Mediat* **65**:33–43.
- Nguyen X, Wang M-H, Reddy KM, Falck JR, and Schwartzman ML (1999) Kinetic profile of the rat CYP4A isoforms: arachidonic acid metabolism and isoform-specific inhibitors. *Am J Physiol - Integr Comp Physiol* **276**:R1691–R1700.
- Noma K, Kihara Y, and Higashi Y (2012) Striking crosstalk of ROCK signaling with endothelial function. *J Cardiol* **60**:1–6.
- Nowicki S, Chen SL, Aizman O, Cheng XJ, Li D, Nowicki C, Nairn A, Greengard P, and Aperia A (1997) 20-Hydroxyeicosa-tetraenoic acid (20 HETE) activates protein kinase C. Role in regulation of rat renal Na⁺,K⁺-ATPase. *J Clin Invest* **99**:1224–1230.

- Oelze M, Mollnau H, Hoffmann N, Warnholtz A, Bodenschatz M, Smolenski A, Walter U, Skatchkov M, Meinertz T, and Münzel T (2000) Vasodilator-stimulated phosphoprotein serine 239 phosphorylation as a sensitive monitor of defective nitric oxide/cGMP signaling and endothelial dysfunction. *Circ Res* **87**:999–1005.
- Omata K, Abraham NG, and Schwartzman ML (1992) Renal cytochrome P-450-arachidonic acid metabolism: Localization and hormonal regulation in SHR. *Am J Physiol - Ren Fluid Electrolyte Physiol* **262**:F591–F599.
- Orozco LD, Liu H, Perkins E, Johnson DA, Chen BB, Fan F, Baker RC, and Roman RJ (2013) 20-hydroxyeicosatetraenoic acid inhibition attenuates balloon injury-induced neointima formation and vascular remodeling in rat carotid arteries. *J Pharmacol Exp Ther* **346**:67–74.
- Padmanabhan S, Wallace C, Munroe PB, Dobson R, Brown M, Samani N, Clayton D, Farrall M, Webster J, Lathrop M, Caulfield M, Dominiczak AF, and Connell JM (2006) Chromosome 2p shows significant linkage to antihypertensive response in the British genetics of hypertension study. *Hypertension* **47**:603–608.
- Pandey V, Garcia V, Gilani A, Mishra P, Zhang FF, Paudyal MP, Falck JR, Nasjletti A, Wang W-H, and Schwartzman ML (2017) The Blood Pressure-Lowering Effect of 20-HETE Blockade in Cyp4a14(-/-) Mice Is Associated with Natriuresis. *J Pharmacol Exp Ther* **363**:412–418.
- Parmentier JH, Muthalif MM, Saeed AE, and Malik KU (2001) Phospholipase D activation by norepinephrine is mediated by 12(S)-, 15(S)-, and 20-hydroxyeicosatetraenoic acids generated by stimulation of cytosolic phospholipase A2: Tyrosine phosphorylation of phospholipase D 2 in response to norepinephrine. *J Biol Chem* **276**:15704–15711.
- Pease JE (2006) Tails of the unexpected - an atypical receptor for the chemokine RANTES/CCL5 expressed in brain. *Br J Pharmacol* **149**:460–462.
- Powell PK, Wolf I, Jin R, and Lasker JM (1998) Metabolism of Arachidonic Acid to 20-Hydroxy-5,8,11,14-eicosatetraenoic Acid by P450 Enzymes in Human Liver: Involvement of CYP4F2 and CYP4A11. *J Pharmacol Exp Ther* **285**:1327–1336.
- Quigley R, Chakravarty S, Zhao X, Imig JD, and Capdevila JH (2009) Increased Renal Proximal Convoluted Tubule Transport Contributes to Hypertension in Cyp4a14 Knockout Mice. *Nephron Physiol* **113**:p23–p28.

- Raina H, Zacharia J, Li M, and Wier WG (2009) Activation by Ca²⁺/calmodulin of an exogenous myosin light chain kinase in mouse arteries. *J Physiol* **587**:2599–2612.
- Randriamboavonjy V, Busse R, and Fleming I (2003) 20-HETE-induced contraction of small coronary arteries depends on the activation of Rho-kinase. *Hypertension* **41**:801–806.
- Ribeiro CMP, Dubay GR, Falck JR, and Mandel LJ (1994) Parathyroid hormone inhibits Na⁺-K⁺-ATPase through a cytochrome P-450 pathway. *Am J Physiol - Ren Fluid Electrolyte Physiol* **266**:F497–F505.
- Rocic P, and Schwartzman ML (2018) 20-HETE in the regulation of vascular and cardiac function. *Pharmacol Ther* **192**:74–87.
- Roman RJ (2002) P-450 metabolites of arachidonic acid in the control of cardiovascular function. *Physiol Rev* **82**:131–185.
- Roman RJ, and Kaldunski ML (1991) Enhanced Chloride Reabsorption in the Loop of Henle in Dahl Salt-Sensitive Rats. *Hypertension* **17**:1018–1024.
- Roman RJ, Ma YH, Frohlich B, and Markham B (1993) Clofibrate prevents the development of hypertension in dahl salt-sensitive rats. *Hypertension* **21**:985–9788.
- Rosolowsky M, Falck JR, and Campbell WB (1996) Metabolism of arachidonic acid by canine polymorphonuclear leukocytes synthesis of lipoxygenase and omega-oxidized metabolites. *Biochim Biophys Acta - Lipids Lipid Metab* **1300**:143–150.
- Sacerdoti D, Escalante B, Abraham NG, McGiff JC, Lever RD, and Schwartzman ML (1989) Treatment with tin prevents the development of hypertension in spontaneously hypertensive rats. *Science* **243**:388–390.
- Savas Ü, Wei S, Hsu M-H, Falck JR, Guengerich FP, Capdevila JH, and Johnson EF (2016) 20-Hydroxyeicosatetraenoic acid (HETE)-dependent hypertension in human cytochrome P450 (CYP) 4A11 transgenic mice: Normalization of blood pressure by sodium restriction, hydrochlorothiazide, or blockade of the type 1 angiotensin II receptor. *J Biol Chem* **291**:16904–16919.
- Schwartzman M, Ferreri NR, Carroll MA, Songu-Mize E, and McGiff JC (1985) Renal cytochrome P450-related arachidonate metabolite inhibits (Na⁺ K⁺)ATPase. *Nature* **314**:620–622.

- Sedláková L, Kikerlová S, Husková Z, Červenková L, Chábová VČ, Zicha J, Falck JR, Imig JD, Kompanowska-Jezierska E, Sadowski J, Krátký V, Červenka L, and Kopkan L (2018) 20-Hydroxyeicosatetraenoic acid antagonist attenuates the development of malignant hypertension and reverses it once established: A study in Cyp1a1-Ren-2 transgenic rats. *Biosci Rep* **38**:1–16.
- Silverstein DM, Barac-Nieto M, Falck JR, and Spitzer A (1998) 20-HETE mediates the effect of parathyroid hormone and protein kinase C on renal phosphate transport. *Prostaglandins Leukot Essent Fat Acids* **58**:209–213.
- Singh H, Cheng J, Deng H, Kemp R, Ishizuka T, Nasjletti A, and Schwartzman ML (2007) Vascular cytochrome P450 4A expression and 20-hydroxyeicosatetraenoic acid synthesis contribute to endothelial dysfunction in androgen-induced hypertension. *Hypertens* **50**:123–9.
- Sodhi K, Wu C-C, Cheng J, Gotlinger K, Inoue K, Goli M, Falck JR, Abraham NG, and Schwartzman ML (2010) CYP4A2-induced hypertension is 20-hydroxyeicosatetraenoic acid- and angiotensin II-dependent. *Hypertens* **56**:871–8.
- Soler A, Hunter I, Joseph G, Hutcheson R, Hutcheson B, Yang J, Zhang FF, Joshi SR, Bradford C, Gotlinger KH, Maniyar R, Falck JR, Proctor S, Schwartzman ML, Gupte SA, and Rocic P (2018) Elevated 20-HETE in metabolic syndrome regulates arterial stiffness and systolic hypertension via MMP12 activation. *J Mol Cell Cardiol* **117**:88–99.
- Stec D, Gannon K, Beaird J, and Drummond H (2007) 20-Hydroxyeicosatetraenoic Acid (20-HETE) Stimulates Migration of Vascular Smooth Muscle Cells. *Cell Physiol Biochem* **19**:121–128.
- Stec DE, Deng AY, Rapp JP, and Roman RJ (1996) Cytochrome P4504A genotype cosegregates with hypertension in Dahl S rats. *Hypertension* **27**:564–568.
- Stec DE, Roman RJ, Flasch A, and Rieder MJ (2007) Functional polymorphism in human CYP4F2 decreases 20-HETE production. *Physiol Genomics* **30**:74–81.
- Swärd K, Mita M, Wilson DP, Deng JT, Susnjar M, and Walsh MP (2003) The role of RhoA and Rho-associated kinase in vascular smooth muscle contraction. *Curr Hypertens Rep* **5**:66–72.

- Tansey MG, Luby-Phelps K, Kamm KE, and Stull JT (1994) Ca²⁺-dependent phosphorylation of myosin light chain kinase decreases the Ca²⁺ sensitivity of light chain phosphorylation within smooth muscle cells. *J Biol Chem* **269**:9912–9920.
- Tarttelin EE, Kirschner LS, Bellingham J, Baffi J, Taymans SE, Gregory-Evans K, Csaky K, Stratakis CA, and Gregory-Evans CY (1999) Cloning and characterization of a novel orphan G-protein-coupled receptor localized to human chromosome 2p16. *Biochem Biophys Res Commun* **260**:174–180.
- Toth P, Csiszar A, Tucsek Z, Sosnowska D, Gautam T, Koller A, Schwartzman ML, Sonntag WE, and Ungvari Z (2013) Role of 20-HETE, TRPC channels, and BK_{Ca}²⁺ in dysregulation of pressure-induced Ca²⁺ signaling and myogenic constriction of cerebral arteries in aged hypertensive mice. *Am J Physiol - Circ Physiol* **305**:H1698–H1708.
- Tsai IJ, Croft KD, Puddey IB, Beilin LJ, and Barden A (2011) 20-Hydroxyeicosatetraenoic acid synthesis is increased in human neutrophils and platelets by angiotensin II and endothelin-1. *Am J Physiol - Circ Physiol* **300**:H1194–H1200.
- Tunaru S, Bonnavion R, Brandenburger I, Preussner J, Thomas D, Scholich K, and Offermanns S (2018) 20-HETE promotes glucose-stimulated insulin secretion in an autocrine manner through FFAR1. *Nat Commun* **9**:1–11.
- Uddin MR, Muthalif MM, Karzoun NA, Benter IF, and Malik KU (1998) Cytochrome P-450 Metabolites Mediate Norepinephrine-Induced Mitogenic Signaling. *Hypertension* **31**:242–247.
- Walkowska A, Červenka L, Imig JD, Falck JR, Sadowski J, and Kompanowska-Jeziarska E (2021) Early Renal Vasodilator and Hypotensive Action of Epoxyeicosatrienoic Acid Analog (EET-A) and 20-HETE Receptor Blocker (AAA) in Spontaneously Hypertensive Rats. *Front Physiol* **12**:1–16.
- Wang J-S, Singh H, Zhang F, Ishizuka T, Deng H, Kemp R, Wolin MS, Hintze TH, Abraham NG, Nasjletti A, and Laniado-Schwartzman M (2006) Endothelial Dysfunction and Hypertension in Rats Transduced With CYP4A2 Adenovirus. *Circ Res* **98**:962–969.
- Wang M-H, Wang J, Chang H-H, Zand BA, Jiang M, Nasjletti A, and Laniado-Schwartzman M (2003) Regulation of renal CYP4A expression and 20-HETE synthesis by nitric oxide in pregnant rats. *Am J Physiol - Renal Physiol* **285**:F295–F302.

- Wang Y, Zheng XR, Riddick N, Bryden M, Baur W, Zhang X, and Surks HK (2009) ROCK isoform regulation of myosin phosphatase and contractility in vascular smooth muscle cells. *Circ Res* **104**:531–540.
- Ward NC, Rivera J, Hodgson J, Puddey IB, Beilin LJ, Falck JR, and Croft KD (2004) Urinary 20-hydroxyeicosatetraenoic acid is associated with endothelial dysfunction in humans. *Circulation* **110**:438–443.
- Ward NC, Tsai IJ, Barden A, Van Bockxmeer FM, Puddey IB, Hodgson JM, and Croft KD (2008) A single nucleotide polymorphism in the CYP4F2 but not CYP4A11 gene is associated with increased 20-HETE excretion and blood pressure. *Hypertension* **51**:1393–1398.
- Wirth A, Benyó Z, Lukasova M, Leutgeb B, Wettschureck N, Gorbey S, Orsy P, Horváth B, Maser-Gluth C, Greiner E, Lemmer B, Schütz G, Gutkind S, and Offermanns S (2008) G12-G13-LARG-mediated signaling in vascular smooth muscle is required for salt-induced hypertension. *Nat Med* **14**:64–68.
- Wu CC, Mei S, Cheng J, Ding Y, Weidenhammer A, Garcia V, Zhang F, Gotlinger K, Manthati VL, Falck JR, Capdevila JH, and Schwartzman ML (2013) Androgen-sensitive hypertension associates with upregulated vascular CYP4A12-20-HETE synthase. *J Am Soc Nephrol* **24**:1288–1296.
- Wu J, Liu X, Lai G, Yang X, Wang L, and Zhao Y (2013) Synergistical effect of 20-HETE and high salt on NKCC2 protein and blood pressure via ubiquitin-proteasome pathway. *Hum Genet* **132**:179–187.
- Xin HB, Deng KY, Rishniw M, Ji G, and Kotlikoff MI (2002) Smooth muscle expression of Cre recombinase and eGFP in transgenic mice. *Physiol Genomics* **2002**:211–215.
- Zhang F, Wang M-H, Krishna UM, Falck JR, Laniado-Schwartzman M, and Nasjletti A (2001) Modulation by 20-HETE of Phenylephrine-Induced Mesenteric Artery Contraction in Spontaneously Hypertensive and Wistar-Kyoto Rats. *Hypertension* **38**:1311–1315.
- Zhu D, Zhang C, Medhora M, and Jacobs ER (2002) CYP4A mRNA, protein, and product in rat lungs: novel localization in vascular endothelium. *J Appl Physiol* **93**:330–337.
- Zordoky BNM, Aboutabl ME, and El-Kadi AOS (2008) Modulation of cytochrome P450 gene expression and arachidonic acid metabolism during isoproterenol-induced cardiac hypertrophy in rats. *Drug Metab Dispos* **36**:2277–2286.

Zou AP, Fleming JT, Falck JR, Jacobs ER, Gebremedhin D, Harder DR, and Roman RJ (1996) 20-HETE is an endogenous inhibitor of the large-conductance Ca²⁺-activated K⁺ channel in renal arterioles. *Am J Physiol - Regul Integr Comp Physiol* **270**:R228–R237,.

Zou AP, Imig JD, Kaldunski M, De Montellano PRO, Sui Z, and Roman RJ (1994) Inhibition of renal vascular 20-HETE production impairs autoregulation of renal blood flow. *Am J Physiol - Ren Fluid Electrolyte Physiol* **266**:F275–F282.